TARDEC

--- TECHNICAL REPORT ---

No.

THE NATIONS'S LABORATORY FOR ADVANCED AUTOMOTIVE TECHNOLOGY

WINNER OF THE 1995 PRESIDENTIAL AWARD FOR QUALITY

Dwell, Interface Defeat, and Penetration of Long Rods Impacting Silicon Carbide

Southwest Research Institute®
P.O. Drawer 28510, San Antonio, TX 78238

Contract: W56HZV-06-C-0194
SwRI® Report 18.12544/008

Prepared for:
US Army RDECOM-TARDEC
AMSRD-TAR-R
Warren, MI 43897-5000

April 2009

DISTRIBUTION STATEMENT A:
Approved for public release; distribution is unlimited

U.S. Army Tank Automotive Research,
Development, and Engineering Center
Detroit Arsenal
Warren, Michigan 48397-5000

Dwell, Interface Defeat, and Penetration of Long Rods Impacting Silicon Carbide

Charles E. Anderson, Jr.[1]

Thilo Behner[2]

Timothy J. Holmquist[3]

Dennis L. Orphal[4]

Matthias Wickert[2]

[1]Southwest Research Institute®
P.O. Drawer 28510, San Antonio, TX 78238

[2]Fraunhofer Institut fur Kurzzeitdynamik (Ernst-Mach-Institut)
Eckerstr. 4, 29104 Freiburg, Germany

[3]Southwest Research Institute
5353 Wayzata Blvd., Minneapolis, MN 55416

[4]International Research Associates
4450 Black Ave, Pleasanton, CA 94566

REPORT DOCUMENTATION PAGE	*Form Approved* OMB No. 0704-0188

Public reporting burden for this collection of information is estimated to average 1 hour per response, including the time for reviewing instructions, searching data sources, gathering and maintaining the data needed, and completing and reviewing the collection of information. Send comments regarding this burden estimate or any other aspect of this collection of information, including suggestions for reducing this burden to Washington Headquarters Service, Directorate for Information Operations and Reports, 1215 Jefferson Davis Highway, Suite 1204, Arlington, VA 22202-4302, and to the Office of Management and Budget, Paperwork Reduction Project (0704-0188) Washington, DC 20503.

PLEASE DO NOT RETURN YOUR FORM TO THE ABOVE ADDRESS.

1. REPORT DATE *(DD-MM-YYYY)* 02-04-2009	2. REPORT TYPE Technical	3. DATES COVERED *(From - To)* 11/2007 – 3/2009

4. TITLE AND SUBTITLE	
Dwell, Interface Defeat, and Penetration of Long Rods Impacting Silicon Carbide	**5a. CONTRACT NUMBER** W56HZV-06-C-0194
	5b. GRANT NUMBER
	5c. PROGRAM ELEMENT NUMBER

6. AUTHOR(S)	
Charles E. Anderson, Jr.[1], Thilo Behner[2], Timothy J. Holmquist[3], Dennis L. Orphal[4], and Matthias Wickert[2]	**5d. PROJECT NUMBER** 18.12544
	5e. TASK NUMBER
	5f. WORK UNIT NUMBER

7. PERFORMING ORGANIZATION NAME(S) AND ADDRESS(ES)	8. PERFORMING ORGANIZATION REPORT NUMBER
[1]Southwest Research Institute, P.O. Drawer 28510, San Antonio, TX 78238; [2]Fraunhofer Institut fur Kurzzeitdynamik (Ernst-Mach-Institut) Eckerstr. 4, 29104 Freiburg, Germany; [3]Southwest Research Institute 5353 Wayzata Blvd., Minneapolis, MN 55416; [4]International Research Associates, 4450 Black Ave, Pleasanton, CA 94566	18.12544/008

9. SPONSORING/MONITORING AGENCY NAME(S) AND ADDRESS(ES)	10. SPONSOR/MONITOR'S ACRONYM(S) RDECOM-TARDEC
US Army Tank-Automotive Research, Development, and Engineering Center, Warren, MI 48397-5000	11. SPONSORING/MONITORING AGENCY REPORT NUMBER

12. DISTRIBUTION AVAILABILITY STATEMENT

Approved for Public Release; Unlimited Distribution

13. SUPPLEMENTARY NOTES

The views, opinion, and/or findings contained in this report are those of the authors and should not be construed as an official Department of the Army position, policy, or decision, unless so designated by other documents.

14. ABSTRACT

Test data, analyses, and computed results for gold rods impacting silicon carbide targets are presented. This work focuses on the dwell phenomenon exhibited by silicon carbide, but also investigates the penetration response. Experiments are presented for several target configurations including targets that use a small diameter buffer, targets that use a large diameter buffer, and targets that use no buffer. In-depth analyses of the data are presented. A significant finding is the nonlinear penetration velocity that occurs for impact velocities of 800 - 1500 m/s. The results demonstrate the significant effect a buffer has on interface defeat, and demonstrate that silicon carbide can resist extremely large surface stresses (~25 GPa) without the use of any confinement or prestress. Computations are also presented that identify the critical design parameters of the buffer including the effect of buffer geometry and buffer separation.

15. SUBJECT TERMS

silicon carbide, SiC-N, dwell, interface defeat, buffer, long rods, penetration velocity, numerical simulations, reverse ballistic experiments, dwell-penetration transition velocity, post-dwell penetration

16. SECURITY CLASSIFICATION OF:			17. LIMITATION OF ABSTRACT	18. NUMBER OF PAGES	19a. NAME OF RESPONSIBLE PERSON Dr. Douglas Templeton
a. REPORT Unclassified	**b. ABSTRACT** Unclassified	**c. THIS PAGE** Unclassified	None	106	19b. TELEPONE NUMBER *(Include area code)* 586-574-5325

Table of Contents

Table of Contents (Cont'd)

Page

List of Figures

List of Figures (Cont'd)

List of Figures (Cont'd)

List of Figures (Cont'd)

Page

List of Figures (Cont'd)

Page

x

List of Tables

1.0 Introduction

This report presents recent experimental and computational results investigating ceramic dwell and interface defeat. For completeness, this report also includes some work that has been published over the past several years [1-4]. With regard to this earlier work, some additional results, including penetration-time histories, are included that are not contained in Refs. [1-4]. Further analyses of the experimental work has been conducted and are included here. Additionally, this report contains results from new computational work. Analysis of the results from these new numerical simulations coupled with the experimental results improves our understanding of dwell and dwell transition for long rods impacting thick ceramic targets.

The phenomena of ceramic dwell and interface defeat continue to be of major interest as they may provide significant improvement to armor systems. Ceramic dwell occurs when a high-velocity projectile impacts a ceramic target and flows out radially along the surface of the ceramic with no significant penetration. When the projectile is completely eroded at the ceramic surface it is referred to as interface defeat. As the impact velocity is increased, there is a point at which dwell is not maintained and penetration occurs; this impact velocity is called the dwell-penetration transition velocity, V_t, and is a function of projectile material, projectile configuration, impact velocity, and target configuration. An example of dwell and interface defeat is presented in Fig. 1. Here an APM2 projectile impacts a thick block (300-mm square and 75-mm thick) of AD995 alumina at 850 m/s. This experiment was performed at Southwest Research Institute using high-speed photography to capture the event. Images are presented at approximately $t = 10$ μs, 30 μs, 50 μs and 60 μs after projectile impact. The images clearly show the projectile flowing radially along the surface of the ceramic (dwelling). The post mortem evaluation of the target showed no penetration into the ceramic (interface defeat).

Ceramic dwell was first identified by Mark Wilkins [5] in 1967. Wilkins was primarily interested in light armor where the geometries consisted of thin ceramic front plates backed by thin metal or composite back plates. Wilkins used high-strength steel projectiles with blunt, conical, and hemispherical nose shapes. The projectiles were 7.62 mm in diameter, weighed 8.32 g and were designed to simulate a 30-caliber armor-piercing (AP) projectile. The first documented target that produced interface defeat was presented by Wilkins [5] and is reproduced in Fig. 2. The target consisted of a 8.64-mm-thick AD85 alumina front plate supported by a rigid steel back plate. The target was impacted by a conical projectile at 700 m/s. The post-mortem target (Fig. 2), exhibits the classic fracture patterns typical of targets that have produced interface defeat. In 1988 Hauver, *et al*., began publishing his work on ceramic dwell [6-9]. Hauver, *et al.*'s, work focused on the defeat of long rods by thick, heavily confined targets. Hauver was the first to produce interface defeat of long rods and is attributed with defining the term "interface defeat". One of Hauver's radiographs is reproduced in Fig. 3, where a long, tungsten projectile is dwelling on titanium diboride (TiB_2) confined by a titanium sleeve. A nice summary of Hauver's, *et al*., work is found in Ref. [10].

In 1990, Rosenberg and Tsaliah presented dwell-penetration transition velocities for three different projectile materials (copper, steel and tungsten) impacting very thick (150-mm) alumina targets [11]. The projectiles were right circular cylinders, 8 mm in diameter and 40 mm in length (*L/D* = 5). The results showed that the penetration-transition velocity was very sensitive to the projectile material. P. C. den Reijer presented his doctoral thesis on light weight ceramic armor in 1991 [12]. The den Reijer targets consisted of an 8.1-mm alumina (density = 3.81 g/cm^3)
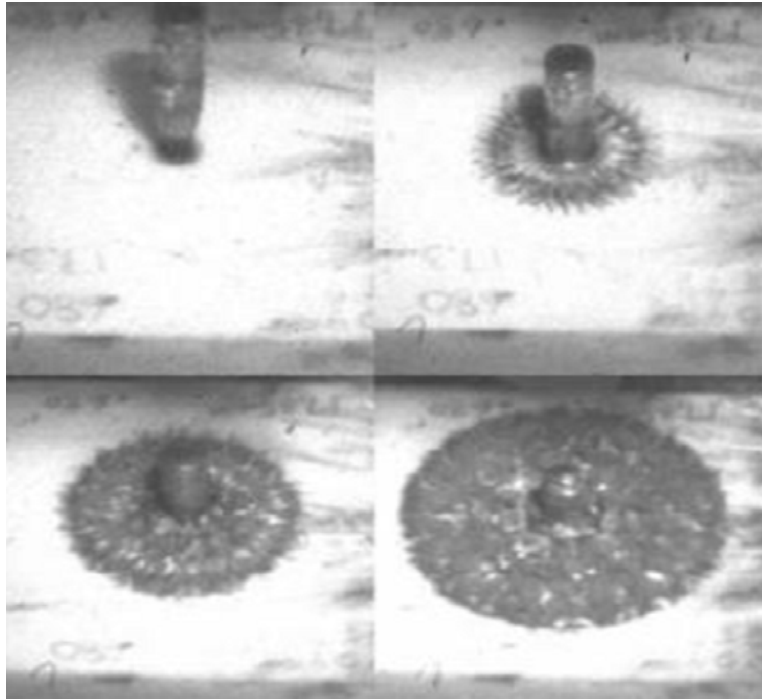
Figure 1. The APM2 projectile impacting a thick AD995 alumina target at 850 m/s showing dwell and interface defeat.
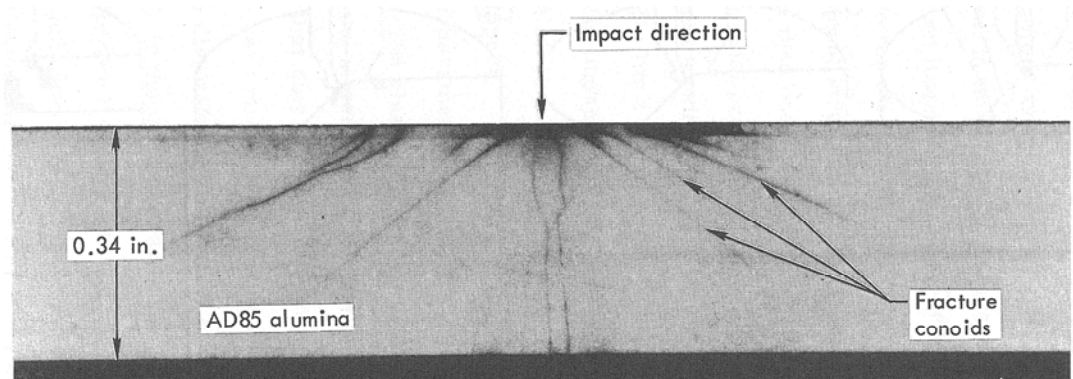
Figure 2. Section view through the center of impact of a recovered AD85 alumina target impacted by a conical projectile at 700 m/s (from Wilkins [5]).

backed by four different 6061-T6 aluminum configurations. The projectile was a 7-g steel cylinder, 6.0 mm in diameter and 31.5-mm long (L/D = 5.3). The experiments used high-speed photography for diagnostics and identified dwell in many of the tests. In 1992, Bless, *et al.*, presented work on the effect of cover plates on the penetration of TiB$_2$ [13]. The penetration into the TiB$_2$ was significantly effected by the type of cover plate used, indicating that dwell was probably occurring.

More recent work by Lundberg, *et al.* (from 1998 to 2007), has made major contributions to the understanding of dwell and interface defeat. His first work was presented in 1998 where the dwell response for a target with boron carbide (B$_4$C) was investigated [14]. Using similar target geometry, the dwell responses for two types of silicon carbide (SiC), Syndie, and TiB$_2$ were investigated in 2000 [15]. In 2001, a SiC target using a specially designed cover plate demonstrated that very long dwell times were possible [16]. In 2005, V_t for four SiC materials
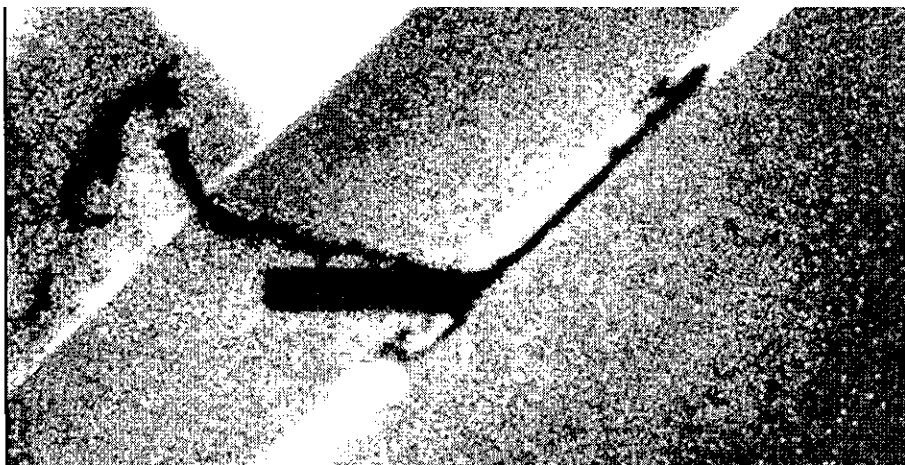
Figure 3. A tungsten long rod impacting and dwelling on the surface of a TiB$_2$ plate (from Hauver, *et al.* [10]).

was determined [17]; the effect of conical projectiles on dwell was investigated in 2006 [18]; and lastly, the influence of confinement was studied in 2007 [19].

Apart from the extensive experimental work performed over the years, there has been a significant effort to develop a computational capability to simulate dwell and interface defeat. In 2003, Johnson, Holmquist, and Beissel (JHB) developed a constitutive model for the response of ceramic materials [20]. This model, along with an algorithm that automatically converts distorted finite elements to meshless particles [21, 22] has produced the capability to simulate dwell and interface defeat [23]. This capability has been used extensively to understand these phenomena [1, 2, 24, 25], and is used in the following sections to help design, evaluate, and understand the response of bare and buffered SiC targets.

The work presented herein focuses only on thick targets. This ensures that the target will fail due to compressive stresses produced from dwell and not from tensile stresses on the back surface of the ceramic. One of the primary objectives of this work is to establish an experimental technique for determining V_t. By establishing the dwell-penetration transition velocity, the maximum surface stress the ceramic can resist can be determined. This maximum stress becomes, in essence, a "material property" of the ceramic (going forward, this stress will be referred to as the *transition stress*, Σ_t). The transition stress is an important material characteristic that can be used to compare one ceramic to another. And because the targets are completely unconfined (no cover, no back plate, no side/radial plate, and no prestress as in much of the work by Lundberg, *et al.*), Σ_t can also be used to evaluate and quantify the effect of confinement and/or prestress. This report presents the experimental technique used to determine Σ_t and the process in which it was developed.

The remainder of this report will present the experimental technique used for this work, experimental and computed results for a bare target, experimental and computed results for a buffered target including the effect of buffer separation, and a summary and conclusions.

2.0 Experimental Set-Up

2.1 Glass Targets and Copper Buffer

The ceramic samples were silicon carbide (SiC-N) cylinders from BAE Systems, Advanced Ceramics Division (formerly CERCOM), with diameter 20 mm and a length of 35 mm. The measured properties of the SiC-N are: density, 3.2 g/cm³; longitudinal velocity, 12.37 km/s; shear wave velocity, 7.83 km/s; and Poisson's ratio, 0.17.

Three different target configurations were examined, as shown in Fig. 4:

- a bare ceramic;

- a ceramic with a small copper (Cu) buffer (E-Cu 57) with a diameter $d = 5$ mm, and height $h = 4$ mm;.

- a ceramic with a full diameter Cu-buffer plate, $d = 20$ mm, $h = 2$ mm.

Both buffer types were glued to the front face with an epoxy resin. The bonding gap was below measuring accuracy (< 10 µm or ½ mil).

Figure 4. Three different target configurations: bare, small Cu buffer, and Cu cover plate.

2.2 Projectiles

The long-rod projectiles were made of pure gold (Au). Because the Au is very weak, any effects of projectile strength are effectively eliminated from these tests. The pure Au rods had a diameter of 1.0 mm and a length of 70 mm (density $\rho_p = 19.3$ g/cm³; hardness 65 HV5; UTS 220 MPa and elongation 30%).

2.3 Reverse Ballistic Test Methodology

The reverse ballistic method was used in conducting the experiments. Figure 5 shows the arrangement for the impact tank. The tests were performed with a powder gun, using a separating sabot to launch the SiC targets. The Au rod was aligned in the trajectory by laser light reflection from the blunt nose of the rod with yaw angles $< \pm 0.1°$. The rear of the rod was inserted in a Styrofoam holder which allowed adjustment in three dimensions. The rod was positioned about
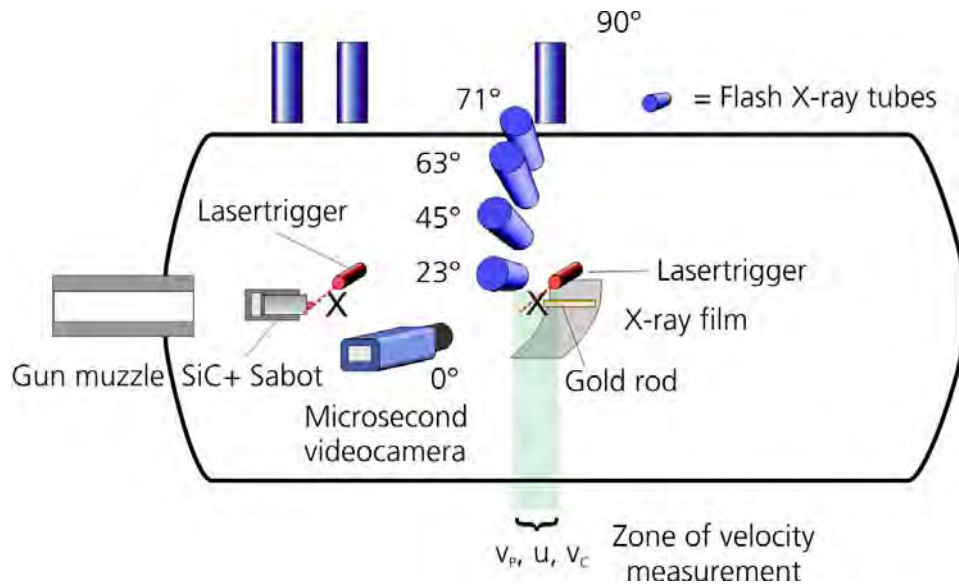
Figure 5. Test set-up.

2 m from the gun muzzle to keep the yaw angle of the glass sample as small as possible, but still permit sabot separation.

Dwell and penetration was observed with five 180-kV flash X-rays. For some experiments, a high-speed video camera (Shimadzu HPV-1) was used to monitor the impact process optically. That camera took a video sequence with an interframe time of 2 µs and an exposure time per frame of 0.5 µs.

The X-ray film was placed 200 mm from the trajectory inside the tank and had the shape of a circular segment. The time measurements for the flash X-ray pictures are very accurate (better than ± 5 ns). Thus, the error for the velocities determined from the X-ray pictures rest in the accuracy of the position measurements, which is in the order of ± 0.10 to 0.15 mm. The X-ray images in this report are digitally enhanced to emphasize the relevant information contained in the images.

3.0 Results and Analysis

3.1 Experimental Data and Analysis Procedures

All experiments are listed by target type in Table 1. Test results are sorted by increasing impact velocity v_p for each group. Sixteen experiments can be rated as successful – four experiments overall missed the attached buffer (labeled "MB"), but can contribute data to the bare target group. Three experiments had excessive yaw, and except for determining the penetration and consumption velocities, these data are not analyzed any further. The various columns are described below.

Table 1. Experimental Results

Exp	Target	yaw [°]	oc [mm]	v_p [m/s]	u [m/s]	v_c [m/s]	h [mm]
11353	bare	0.5	2.1	776±2	0	v_p	-
11354	bare	2.9	1.7	958±4	212±34	676±53	-
11355	bare	1.2	1.7	1212±6	543±43	644±61	-
11358	bare	0.4	1.7	1381±7	662±49	696±35	-
11377[†]	buffer	1.1	0.8	1416±7	645±52	746±38	4.0
11393	buffer	1.0	1.1	1484±5	0	v_p	4.0
11395*[†]	buffer	1.6	1.1	1526±9	0	v_p	4.0
11390*	buffer	1.7	1.1	1550±8	715±20	808±27	4.0
11375	buffer	1.1	1.1	1686±10	824±74	846±88	4.11
11360	plate	1.4	2.7	1382±7	0	v_p	2.04
11389*	plate	1.5	1.7	1571±5	663±105	914±88	2.02
11362	plate	4.9	2.1	1612±6	671±49	934±55	2.04
11359	MB	1.8	3.9	1365±6	578±53	791±49	n/a
11361	MB	2.8	2.7	1538±10	838±3	680±3	n/a
11370	MB	3.0	1.8	1547±9	628±62	906±51	n/a
11369	MB	1.5	2.7	1611±8	765±16	843±2	n/a
11391	yaw	13.1	-	-	-	-	n/a
11366	yaw	7.8	4.7	1546±10	814±27	722±74	n/a
11363	yaw	6.6	4.6	1574±18	817±161	740±13	n/a

[*]Experiments where video camera was available

[†]Experiments where buffer separated before impact

oc: The distance the rod was from the ceramic (and/or Cu buffer) center, determined from the flash X-rays.

yaw: Total yaw (combined pitch and yaw).

An example of the X-ray shadowgraphs is shown in Fig. 6. The X-ray times are measured from impact on the target surface ($t = 0$); which for a bare target is the ceramic surface, but for a buffered target, it is the buffer surface.
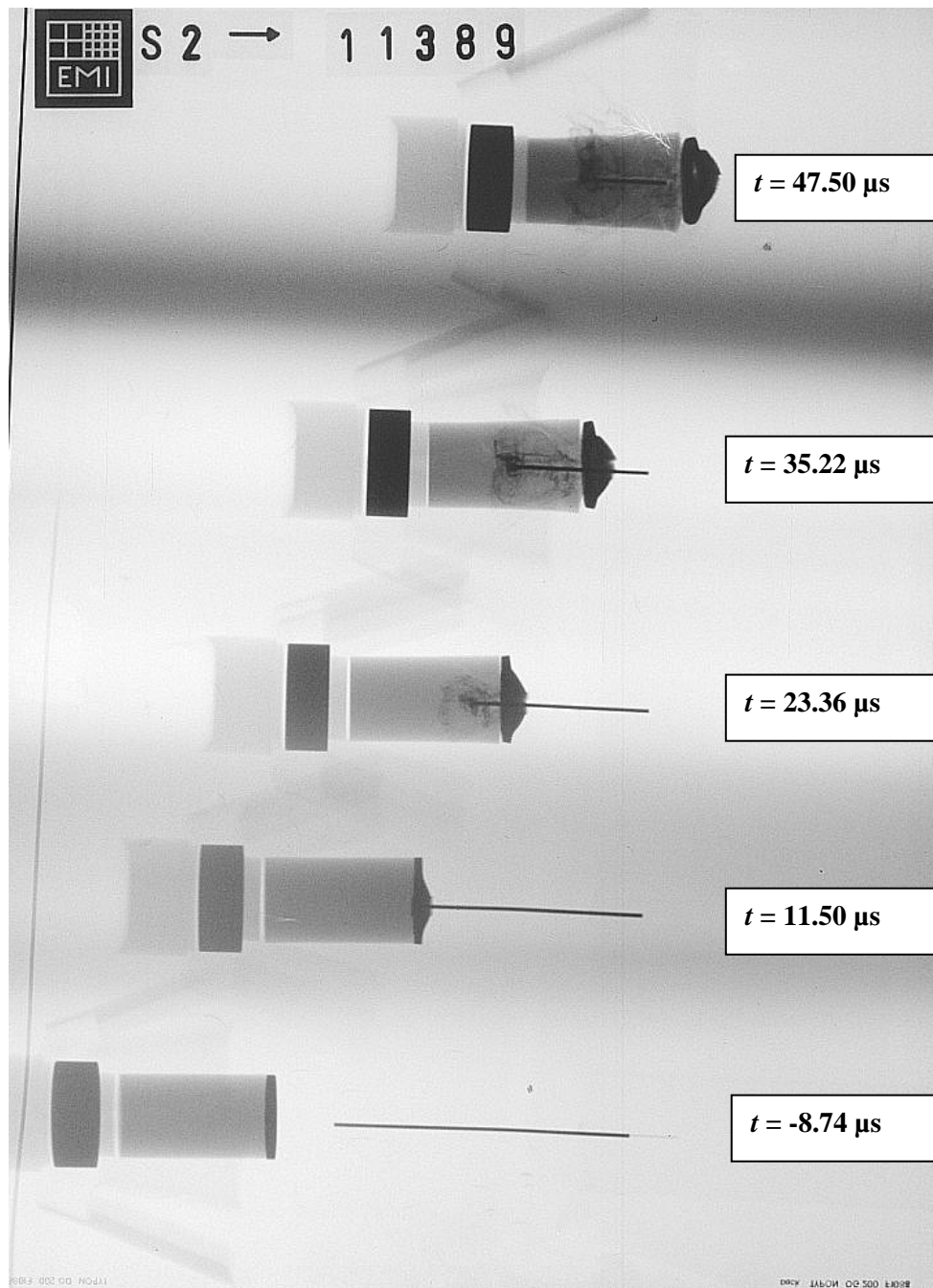
Figure 6. Flash radiographs for Exp. 11389.

The results of the data shown in Fig. 6 are plotted in Fig. 7. The position of the nose and the length of the Au rod were measured from the flash radiographs, and are denoted by the solid circles and triangles, respectively.
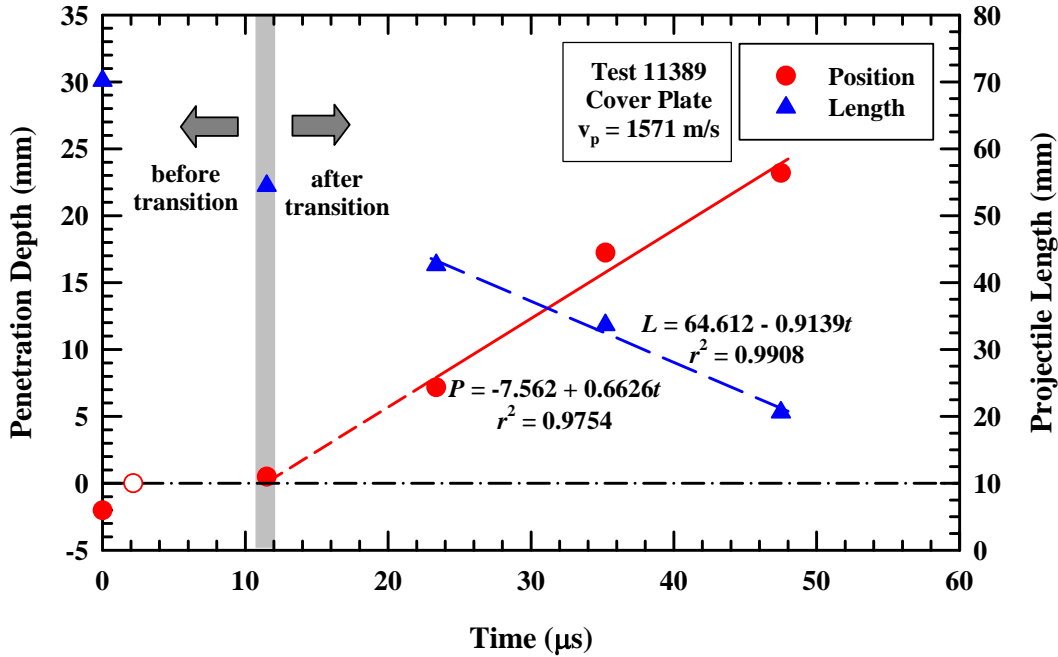
Figure 7. Example of experimental data and analysis (Exp. 11389).

For experiments with a Cu buffer plate, the time for the Au rod to reach the ceramic surface was estimated. If simple hydrodynamic penetration theory (e.g., see Ref. [26]) is used—since the Cu buffer and the Au rod have very low strength—then the time it takes for the projectile to penetrate through the Cu buffer, t_{buf}, and reach the Cu-ceramic interface is given by:

$$u_{hydro} = \frac{v_p}{1 + \sqrt{\rho_t / \rho_p}} \tag{1}$$

$$t_{buf} = \frac{h}{u_{hydro}} \tag{2}$$

where h is the height of the buffer, and ρ_t and ρ_p are the target and projectile densities, respectively. The estimated time for Exp. 11389, 2.2 µs, is denoted by the open circle in Fig. 7. Of course, it is well understood that this is only an estimate since the presence of the ceramic surface can and will affect the penetration velocity when the projectile nose is within a couple of diameters of the interface.[1]

The second penetration data point at 11.5 µs shows little to no penetration, indicating that there was a period of dwell in this experiment. The next data point, at 23.4 µs, indicates that the rod is now penetrating into the ceramic; thus, dwell transitions to penetration. Before transition, the penetration velocity u is 0 (or very, very small); and the consumption velocity v_c, (i.e., the rod erosion rate) is equal to the impact velocity, v_p. After transition, linear regression of the data is used to calculate the penetration position and the rod length as a function of time. The results

---

[1] The initial penetration velocity, because of the shock pressure, will be higher than the hydrodynamic penetration velocity. On the other hand, as the projectile nose nears the very hard ceramic surface, the penetration resistance will increased, thereby decreasing the penetration velocity below that of the hydrodynamic velocity. These two effects are offsetting. Further, the buffer thickness is only a few rod diameters thick. Therefore, it is believed that Eqns. (1) and (2) provide a reasonable estimate for the rod nose to reach the ceramic surface.

of the linear regressions, along with the square of the correlation coefficient, are shown in Fig. 7. The solid line shows the curve fit for the nose position, *P*, and the long dashed line for the rod length, *L*. The slopes of the linear regression provide the penetration and consumption velocities. The *u* and v_c values[2], along with their uncertainties (one standard deviation) are given in Table 1.

The position-time data are also used to extrapolate back to the ceramic surface to estimate the time at which dwell ceased and penetration began, denoted by the shorter dashed line in Fig. 7. This time is estimated from the linear regression, which has the form $P = a + mt$. Thus, the time at which penetration into the ceramic began is given by[3]:

$$t_{pen} = \frac{-a}{m} \tag{3}$$

For Exp. 11389, t_{pen} is 11.4 µs. The dwell time, t_D, is estimated from the difference in t_{pen} and t_{buf}:

$$t_D = t_{pen} - t_{buf}. \tag{4}$$

The dwell time for Exp. 11389 is thus estimated to be 9.6 µs. The calculated values for t_{buf}, t_{pen}, and t_D are given for each test in Table 2.

It is noted that the estimated dwell transition time is almost identical to the time at which the 2nd flash radiograph was taken in Fig. 7. However, in general, it is not known *a priori* when the transition might occur. Thus, the regression fits only include data points that are distinctly past the transition time.

The flash X-rays, with the times of the images relative to impact, and figures analogous to Fig. 7 are provided in the Appendix. The entries in Table 1 and 2 summarize the results of the various analyses in addition to providing information on the impact conditions (velocity, yaw, and distance from a center hit).

3.2 Consumption Velocity and Rod Deceleration

The consumption velocity, as measured here, is the time derivative of the length of the rod; with the rod length measured directly from the flash radiographs. The rod length is also given by the difference in the position of the tail, P_{tail}, and the position of the nose, P_{nose} ($\equiv P$, the projectile-target interface, i.e., depth of penetration). Therefore, the time rate of change of the projectile length is given by:

$$\dot{L} = \dot{P}_{nose} - \dot{P}_{tail} \equiv v_c \approx u - v_p \tag{5}$$

where the dot refers to the time derivative. In Eqn. (5), it has been assumed that the tail velocity is equal to the impact velocity (this assumption will be substantiated below). Thus, a check on the accuracy of the measurements is provided by the sum of *u* and v_c, which should be the impact velocity, i.e.:

$$u + |v_c| = v_p. \tag{6}$$

---

[2] The consumption velocity is by definition negative since the rod is getting shorter. However, the absolute value of v_c is given in Table 1, and the absolute value is often used within the text.
[3] The estimate for the onset of penetration, t_{pen}, is modified slightly for a couple of the bare target tests, as described in Section 3.3.

Table 2. Additional Experimental Results

Exp	Target	Yaw [°]	Oc [mm]	v_p [m/s]	t_{buf} [µs]	t_{pen} [µs]	t_D [µs]	R_t [GPa]
11353	bare	0.5	2.1	776±2	0		sust. dwell	5.81
11354	bare	2.9	1.7	958±4	0		≈ 10	4.48
11355	bare	1.2	1.7	1212±6	0	2.6	≈ 2.6	4.47
11358	bare	0.4	1.7	1381±7	0	3.0	≈ 3.0	5.38
11377[†]	buffer	1.1	0.8	1416±7	4.7	17.0	≈ 12.3	6.03
11393	buffer	1.0	1.1	1484±5	4.5	-	sust. dwell	20.84
11395[†]	buffer	1.6	1.1	1526±9	4.4	-	sust. dwell	20.25
11390	buffer	1.7	1.1	1550±8	4.3	8.9	≈ 4.5	7.11
11375	buffer	1.1	1.1	1686±10	4.1	6.9	≈ 2.8	7.99
11360	plate	1.4	2.7	1382±7	2.5	-	sust. dwell	18.03
11389	plate	1.5	1.7	1571±5	2.2	11.4	≈ 9.3	8.76
11362	plate	4.9	2.1	1612±6	2.1	5.6	≈ 3.5	9.13
11359	MB	1.8	3.9	1365±6	0	4.2	< 4	6.57
11361	MB	2.8	2.7	1538±10	0	2.1	< 2	5.58
11370	MB	3.0	1.8	1547±9	0	3.4	< 3	8.56
11369	MB	1.5	2.7	1611±8	0	2.3	< 2	7.79

[†]Experiments where buffer separated before impact

Of course, measurement uncertainties will result in the equality in Eqn. (6) being an approximation. Using the slopes of the regression fits in Fig. 7, $u + |v_c| = 1.576$ km/s, in excellent agreement with the impact velocity of 1.571 km/s.

It was assumed that the tail velocity could be replaced by the impact velocity in Eqn. (5). This assumption ignores any deceleration of the rod during dwell and/or penetration.[4] For an eroding rod, the incremental decrease in the tail velocity due to elastic waves is given by [27]:

$$\Delta v_{tail} = \frac{2Y_p}{c_L \rho_p} \tag{7}$$

where Y_p is the dynamic flow stress of the rod and c_L is the bar wave speed, $(E/\rho)^{1/2}$, in the rod. For the gold rod, Y_p is 20 MPa,[5] and c_L is 2.03 km/s [28] giving 1.02 m/s for the deceleration of the tail. For an 800-m/s impact velocity, this is only a 0.12% change in the tail velocity, and

---

[4] Technically, since these are reverse ballistic experiments, the rod is not decelerating; rather, there is an acceleration of the rod due to the impact, but the conclusions remain unchanged; therefore, we will often discuss the tests as if the rod is moving.

[5] The initial flow stress is 20 MPa; because of strain hardening, the ultimate strength is 220 MPa, as reported in Section 2.2 and Ref. [28]. There is no strain rate effect reported for Au [28].

even less at the higher impact velocities. For a 70-mm-long Au rod, it takes ~34.5 µs for the first decelerating stress pulse to reach the back of the rod, and the time interval of the experiments is typically less than 50 µs. Thus, it is only near the very end of erosion, where the rod length is quite small, that the effects of deceleration could be measured in the experiments. Numerical simulations confirm the above assumptions. The rod velocity changed by only ~3 m/s with 65 mm of the rod eroded at an impact velocity of 800 m/s (3 elastic transits).

3.3 Bare SiC Experiments

Experiments with a bare target show that dwell is possible for impact velocities near 800 m/s. With higher impact velocities the rod dwells only for a short period, if at all, before it penetrates the ceramic. An example is shown in Fig. 8 for the two lowest impact velocities of the test series. In the left-hand set of images, the rod does not penetrate the SiC, but is diverted at the front surface, presumably due to a chipped or cracked edge. The right-hand images show only a short dwell phase followed by penetration and it can be seen that the ceramic cracks extensively during penetration.

(a) Exp.11353 (v_p = 776 m/s)   (b) Exp. 11354 (v_p = 958 m/s)
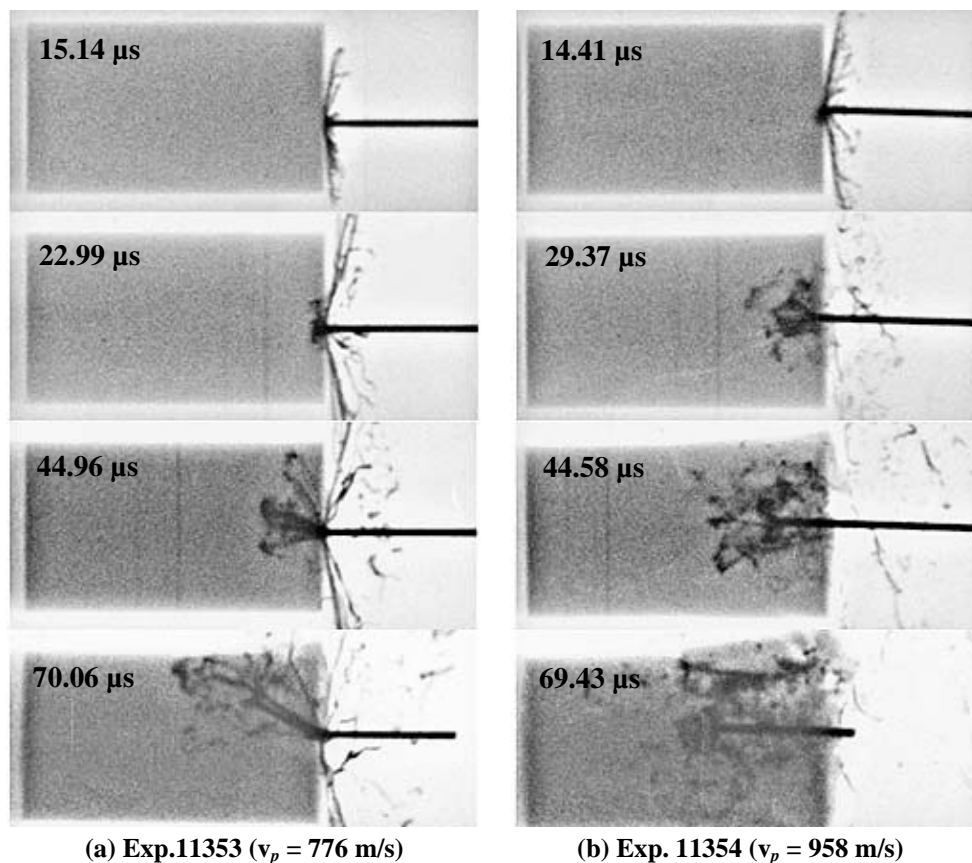
Figure 8. X-ray images for experiments with sustained dwell (Exp. 11353) and a short period of dwell and then penetration (Exp. 11354).

The procedure for estimating the dwell time, Eqns. (3) and (4), was modified for two of the bare-target experiments. There is evidence that the penetration resistance is substantially higher at early times (initial penetration), as pointed out by Hauver, *et al.* [7]. Thus, as already described above, linear regression of the data after dwell transition does not include any data that has a very small penetration value. An example is shown in Fig. 9. Extrapolation of the regression fit

to zero penetration gives 1.3 µs for the start of penetration. This does not appear to be a reasonable estimate given that there is only 1.4 mm of penetration at 14.4 µs. Thus, the extrapolation of the "late-time" data appears to underpredict the time of dwell. Therefore, we have used the two earliest non-zero P-t data to estimate the onset of penetration, denoted by the short dashed line in Fig. 9. The dwell time for Exp. 11354 using the modified method is 10.3 µs, which we believe to be a more accurate estimate.
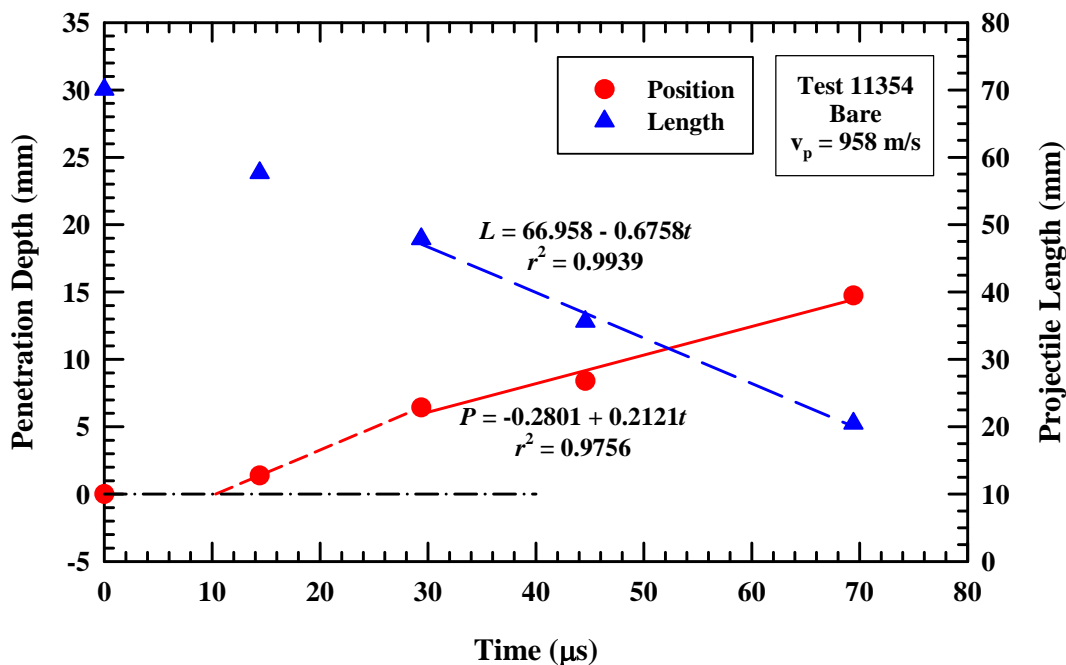
Figure 9. Analysis of Exp. 11354 and the modified estimate for t_D.

Those experiments where the buffer was not hit (MB in Table 1) contribute to the penetration data for bare SiC. The impact velocities were of course too high for a bare target to achieve dwell. Nevertheless, it can be seen that early-time penetration resistance must be quite high since extrapolation of the penetration-time data does not go through the (0,0) coordinate, as shown in Fig. 10. This is true for all the bare target experiments. A t_{pen} is calculated for each of the high-velocity (MB) experiments, and they are given in Table 2. As there are no X-ray shadowgraphs at short times after impact, we cannot differentiate between a very large penetration resistance versus some dwell followed by penetration. Nevertheless, these data are consistent with the interpretation that the penetration resistance of SiC-N is very large immediately after impact, with attendant lower penetration velocities.
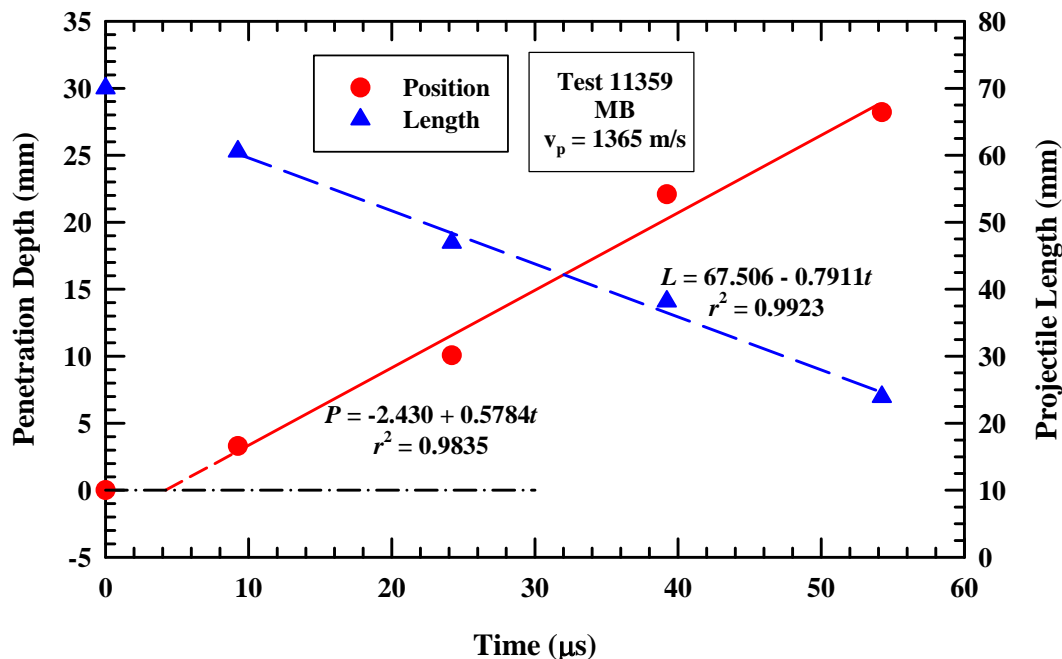
Figure 10. Analysis of Exp. 11359, indicating high penetration resistance at early time.

3.4 Buffered SiC Experiments

Dwell is observed at substantially higher impact velocities for buffered targets than for unbuffered targets. Sustained dwell is possible up to impact velocities of 1530 m/s. Impact velocities above 1550 m/s produce a short dwell period before transitioning to penetration. Targets where the ceramic surface was fully covered by a plate show a similar behavior, although the plate was only half the thickness of the buffers.

The buffer separated from the target before impact in two of the experiments. Figure 11(a) shows, for the relatively low impact velocity of 1416 m/s, a short dwell phase of about 16 µs before penetration begins. With a correctly attached buffer, sustained dwell can be expected at a higher v_p, Fig. 11(b). In the last frame of Fig. 11(b), a conical crack develops at the target surface (similar to findings in [29]), but dwell persists.

For Exp. 11395 in Fig. 12(a), the buffer also separates but only very slightly. Here, at v_p = 1526 m/s, the target shows sustained dwell, although the target surface is clearly more damaged than Exp. 11393, Fig. 11(b). Thus, the distance of buffer separation influences damage and dwell potential. These phenomena are investigated computationally in detail in Section 5.4.

At impact velocities around 1550 m/s, penetration starts after a short dwell phase, Fig. 12(b). Penetration depths versus time for Exps. 11395 and 11390 are shown in Fig. 13. The X-ray images, Fig. 12(b), show that the ceramic is heavily damaged around much of the circumference. It is unclear whether the ceramic is damaged in front of the projectile as the ceramic at the centerline of penetration has the least time to open up and develop cracks for a given X-ray time. Also, the X-rays have to penetrate the full target diameter, which makes it difficult in discerning possible cracks there.

As mentioned previously, a high-speed video camera was available for some of the experiments. Comparing selected frames of the video with the X-ray image reveals some

(a) Exp.11377 (v_p = 1416 m/s)   (b) Exp. 11393 (v_p = 1484 m/s)
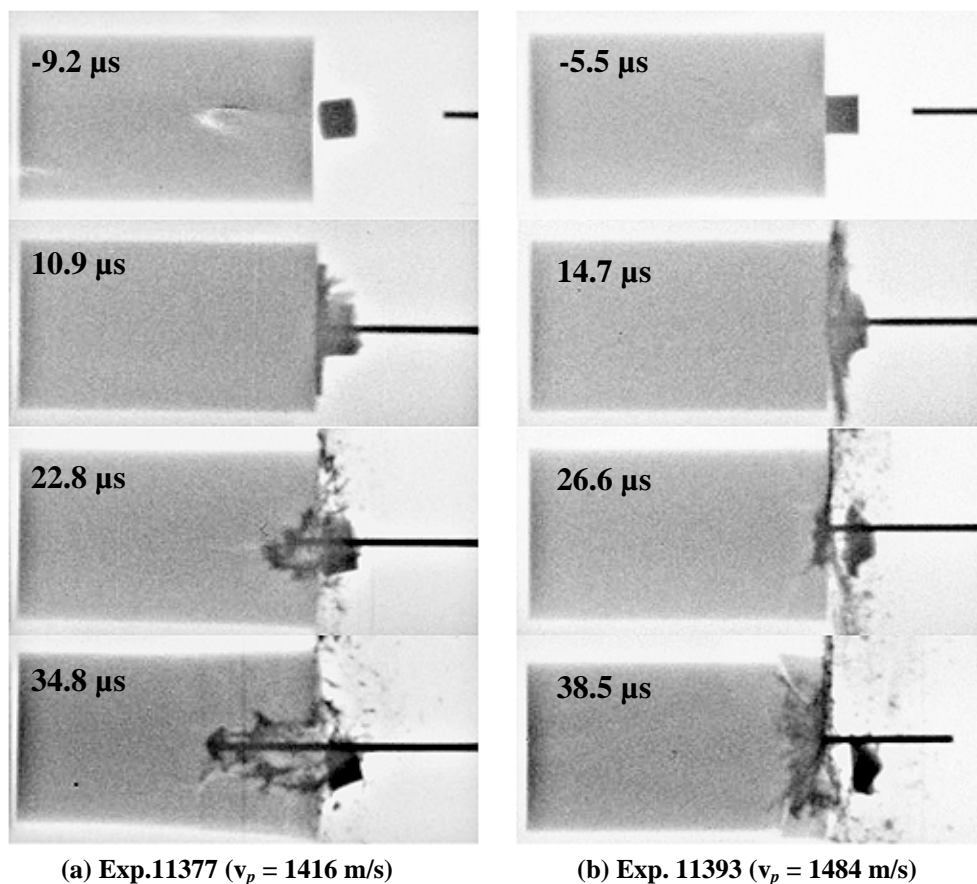
Figure 11. X-ray images for separated and attached buffers.

interesting details. Figure 14 (Exp. 11390) shows early dwell with later penetration in both the X-rays and the still images from the video camera. The early video still shows clearly the disc which is formed by the diverted rod material on the target surface. Also, it can be seen that during penetration (presumably) rod material emerges through cracks in the ceramic to the side surface (arrow), which corresponds to a debris cloud normal to the rod-ceramic interface in the X-ray image (also denoted by an arrow).

3.5 Cover Plate Experiments

Targets with a cover plate behave essentialy the same as bufferd targets. Figure 15 shows sustained dwell at 1367 m/s impact velocity; the rod is completely eroded in the last frame (54.7 µs) of Fig. 15. During the impact process the cover plate bulges but seems to stay at least partially in contact with the ceramic surface; but, because of the cover plate glue bond, the rod material does not flow as freely to the side (radially) as for the buffered targets (see Fig. 11). On the other hand, we observed in experiments with borosilicate glass with a copper cover plate, that the plate completely separated from the glass in the experiments where there was significant dwell, but not in the experiments where there was early-time penetration [30].

When penetration occurs, rod material can flow through side cracks and emerge at the side surface of the ceramic (Fig. 16), similar to the experiments with a buffer. Again, the position of that outflow corresponds both in video still and X-ray images (arrows). The surface cracks can also be seen in the video images.
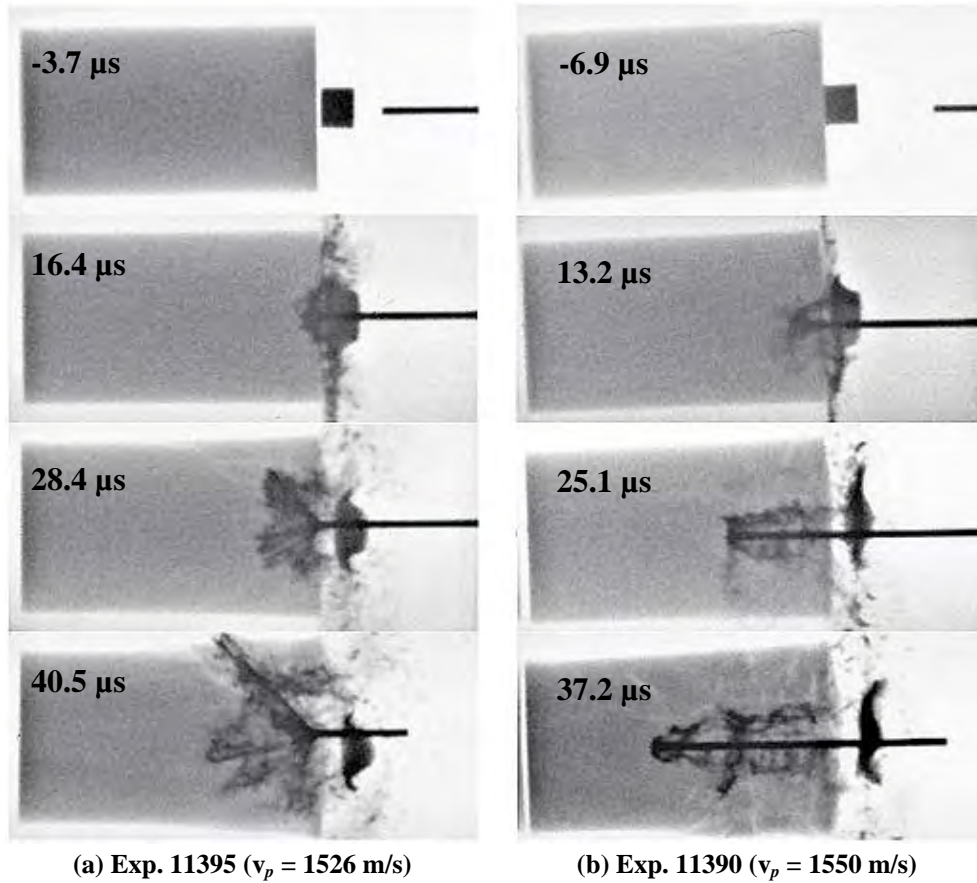
(a) Exp. 11395 (v_p = 1526 m/s) (b) Exp. 11390 (v_p = 1550 m/s)

Figure 12. X-ray images showing extensive cracking of the ceramic.
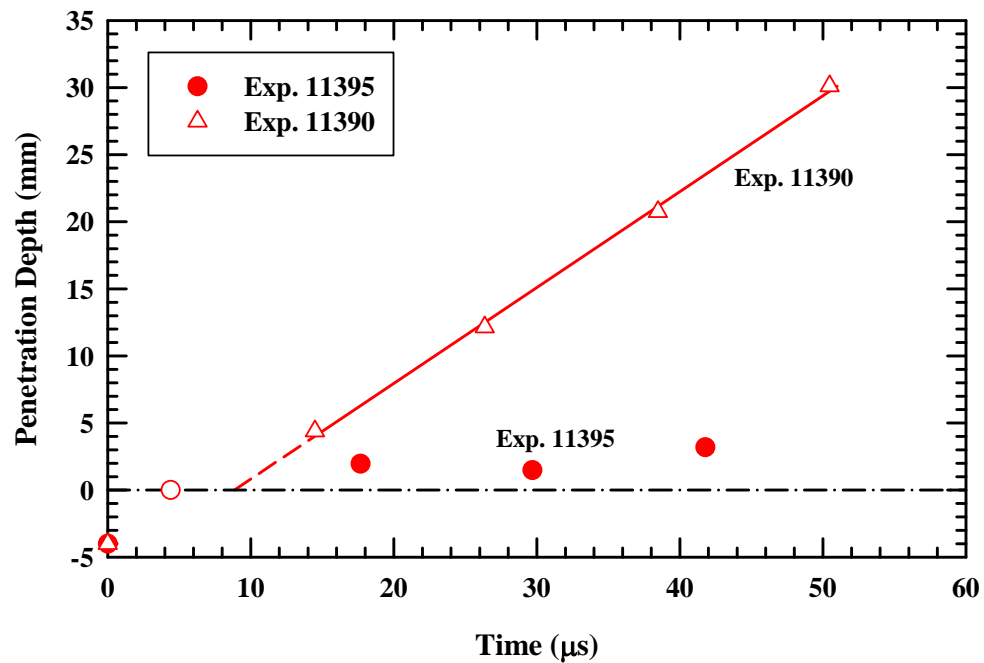
Figure 13. Position vs. time for Exps. 11390 and 11395.

16
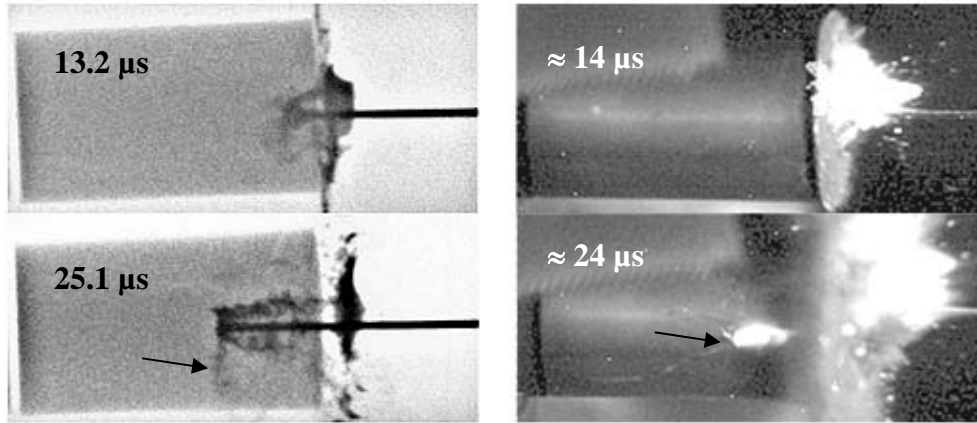
Figure 14. X-ray images (left) and video stills (right) for Exp. 11390 (v_p = 1550 m/s) at nearly the same time after impact.
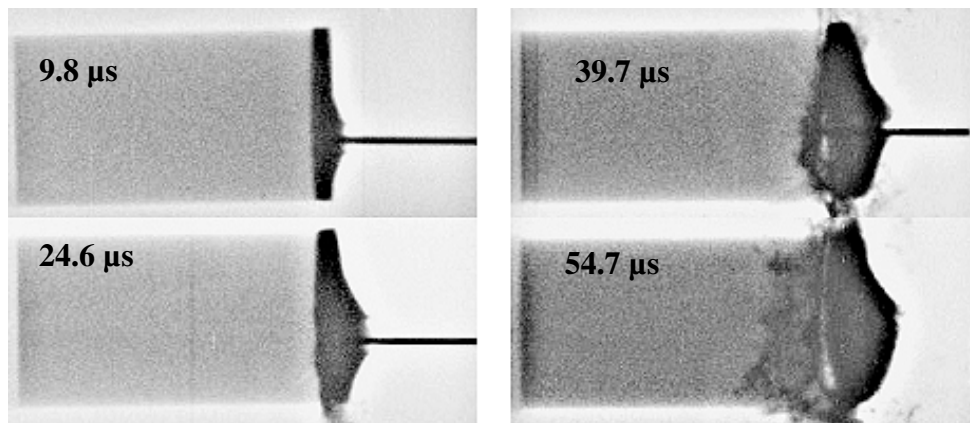
Figure 15. X-ray images for Exp.11360 (v_p = 1382 m/s).
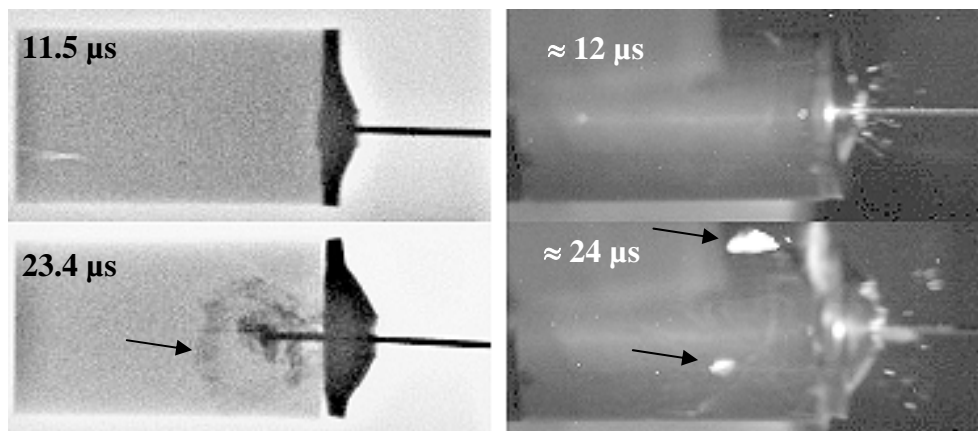
Figure 16. X-ray images (left) and video stills (right) for Exp. 11389 (v_p = 1571 m/s) at nearly the same times after impact.

4.0 Further Analysis of the Data

4.1 Accuracy of Post-Transition Penetration and Consumption Velocities

An assessment of the accuracy of the post-transition penetration measurements can be made by comparing the sum of the penetration and consumption velocities with the original impact velocity, Eqn. (6). This assessment is possible because the rod effectively does not decelerate during the time frame of the experiment, as discussed in Section 3.2. The comparison between $u + v_c$ and v_p is shown in Fig. 17.[6] For a few of the experiments that had sustained dwell, the consumption velocity is plotted (since $u = 0$).
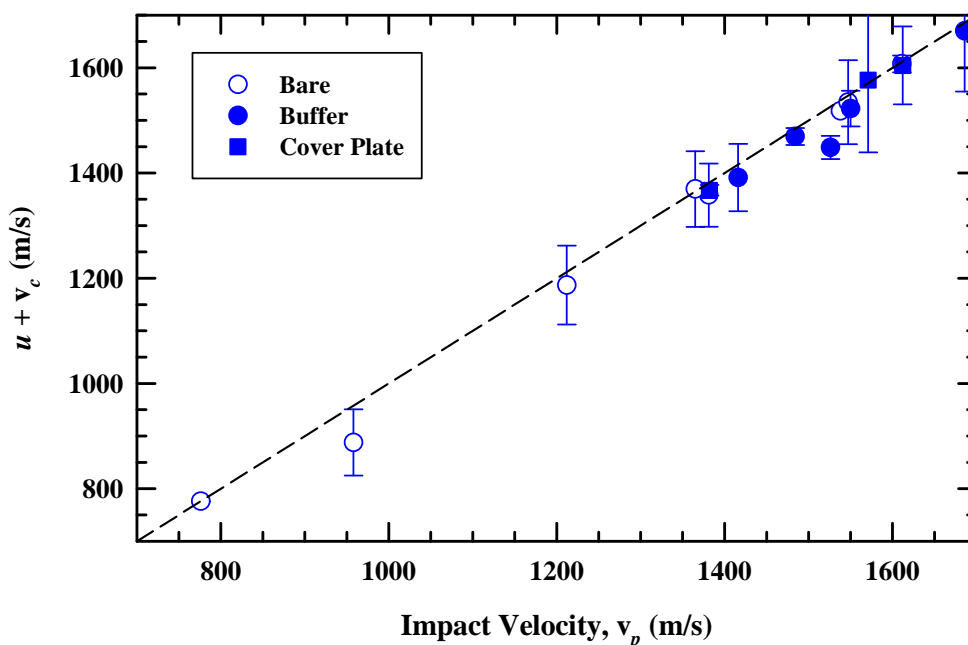
Figure 17. Comparison of the sum of the penetration and consumption velocities with the impact velocity after dwell transition.

The dashed line in Fig. 17 represents the condition where $u + v_c \equiv v_p$. Virtually all the data lie within their experimental uncertainly band[7] of the dashed line. One datum point of particular note at 1526 m/s lies below the dashed line, and with small uncertainty. The position-time data are shown in Fig. 18 for this test. Note that there appears to be a very small amount of penetration, i.e., $u \neq 0$, but a meaningful u is virtually impossible to calculate. The difference between the calculated consumption velocity and the impact velocity is only 77 m/s. A penetration velocity of 77 m/s only gives 1.5 mm of penetration after 20 µs. In general, since the consumption velocity is more reliably estimated for very, very small penetration, the discrepancy in $u + v_c = v_p$ most likely is in the calculation of u for very small depths of penetration. Regardless, the agreement between $u + v_c$ and v_p seen in Fig. 17 attests to the overall accuracy of the data and analysis procedures. Similar findings were found for impact on borosilicate glass [30].

---

[6] For this and subsequent analyses, all the "missed buffer" experiments are analyzed as "bare" experiments.
[7] The uncertainty (or "error bar") is the square root of the sum of the squares of the uncertainties of u and v_c given in Table 1.
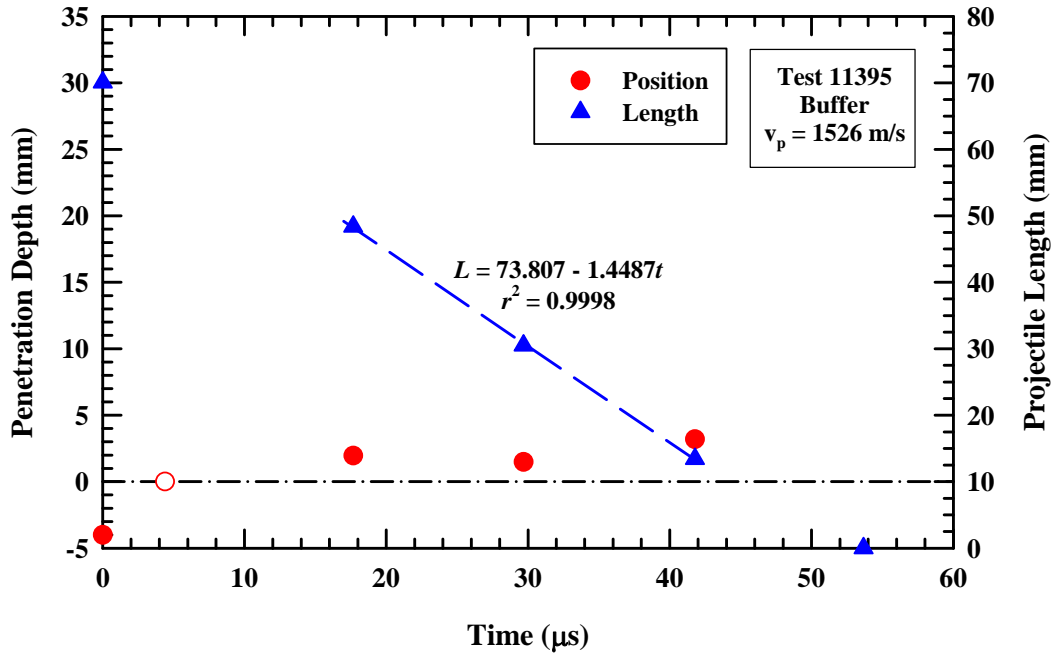
Figure 18. Position-time data for Exp. 11395, depicting a very small, but non-zero penetration velocity.

4.2 Nonlinearity of Penetration Velocity

It was noticed that numerical simulations showed nonlinear penetration for impact velocities a little above the dwell-penetration transition velocity (see Section 5.3.2). These numerical results led us to re-examine the experimental data to determine if we could see nonlinear penetration behavior in the data. Care must be taken that any observed nonlinearity in penetration is greater than the uncertainty in position-time measurements. Statistical procedures permit a determination of whether two slopes are different at some confidence level; but because there are no repeat points, statistical analysis cannot draw any conclusion concerning changes in slope due to uncertainty in measurements.

We therefore conducted an error or uncertainty analysis. The potential errors in the point-to-point penetration velocities can be estimated from the uncertainties in measuring the penetration points and the accuracy of the time measurements. The point-to-point penetration velocity, i.e., the slope of the penetration-time response, is given by:

$$u = \frac{\Delta P}{\Delta t} \tag{8}$$

where ΔP is the difference in the depths of penetration over the time interval Δt. Let the symbol δ represent the uncertainty (or potential error) in a measurement. Thus,

$$\delta u = \left[\left(\frac{\partial\left(\Delta P / \Delta t\right)}{\partial(\Delta P)}\delta P\right)^2 + \left(\frac{\partial\left(\Delta P / \Delta t\right)}{\partial(\Delta t)}\delta t\right)^2\right]^{1/2}$$

$$= \left[\left(\frac{\delta P}{\Delta t}\right)^2 + \left(-\frac{\Delta P}{(\Delta t)^2}\delta t\right)^2\right]^{1/2} = \left[\left(\frac{\delta P}{\Delta t}\right)^2 + \left(-u\frac{\delta t}{\Delta t}\right)^2\right]^{1/2}$$

(9)

The measurement accuracy of a penetration point is ±0.2 mm (rounding up the ±0.10-0.15 mm for a conservative estimate). Since each point has this uncertainty, δP is 0.4 mm. The measurement accuracy of the time of the flash X-rays is 5 ns; thus δt is twice this value, or 10 ns.

We will apply Eqn. (9) to two experiments, Exp. 11370 and 11390. The penetration-time history for Exp. 11370 is shown in Fig. 19, along with the regression fit and the point-to-point slopes. Table 3 provides a summary of the point-to-point δu's for the experiment. Notice that the uncertainty in time has a negligible contribution to the total uncertainty.
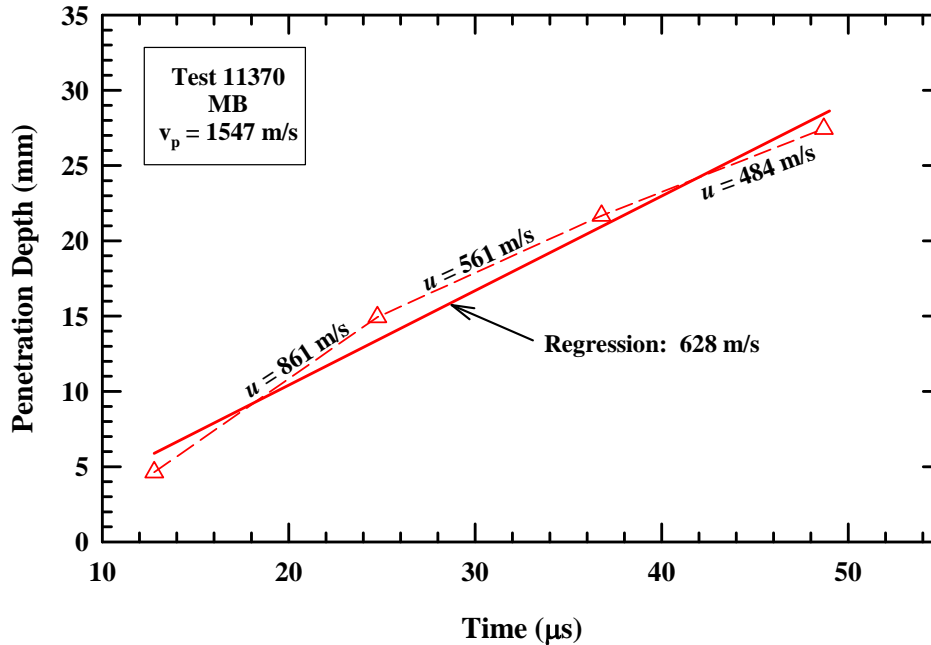
Figure 19. Penetration-time history and point-to-point slopes for Exp. 11370.

It is seen, from Table 3, that the potential error or uncertainty in the point-to-point penetration velocities is associated with the uncertainty in position measurements (the precision of the time measurement results in a very small contribution to δu). It is seen that the possible errors in the point-to-point slopes, for the penetration and time intervals of these experiments, is on the order of 33-34 m/s.

One measure of the nonlinearity of the penetration-time response is the standard error on the slope. For Exp. 11370, the penetration velocity determined from linear regression is 628 ± 62 m/s, where the 62 m/s represents one standard deviation on the slope. 62 m/s is considerably larger than the calculated measurement error of 33-34 m/s. We therefore conclude that the changes in the point-to-point penetration velocities for Exp. 11370 are greater than can be attributed to measurement uncertainties.

Table 3. Computed Uncertainties in Point-to-Point Penetration Velocities

Exp	t (μs)	P (mm)	u (m/s)	$\delta P/\Delta t$ (m/s)	$u(\delta t/\Delta t)$ (m/s)	δu (m/s)
11370	12.79	4.63				
	24.75	14.93	861	33.4	0.72	33.4
	36.77	21.67	561	33.3	0.47	33.3
	48.70	27.45	484	34.5	0.41	34.5
	Regression: $u = 628 \pm 62$ m/s					
11390	14.48	4.39				
	26.36	12.14	652	33.7	0.55	33.7
	38.46	20.75	712	33.1	0.59	33.1
	50.47	30.12	780	33.3	0.65	33.3
	Regression: $u = 715 \pm 20$ m/s					

The penetration-time history for Exp. 11390 is shown in Fig. 20, along with the point-to-point penetration velocities (also listed in Table 3). For this experiment, the uncertainty in the point-to-point slopes (~33 m/s) is greater than one standard error (20 m/s) from the regression analysis. Further, the maximum residual error of penetration depth versus time from the regression is 0.4 mm. Therefore, in contrast to the results of Exp. 11370, it is not possible to clearly state for Exp. 11390 that the differences in point-to-point penetration velocities are due to unsteady penetration (i.e., a physical reality); these differences in slopes could be the result of measurement uncertainties.
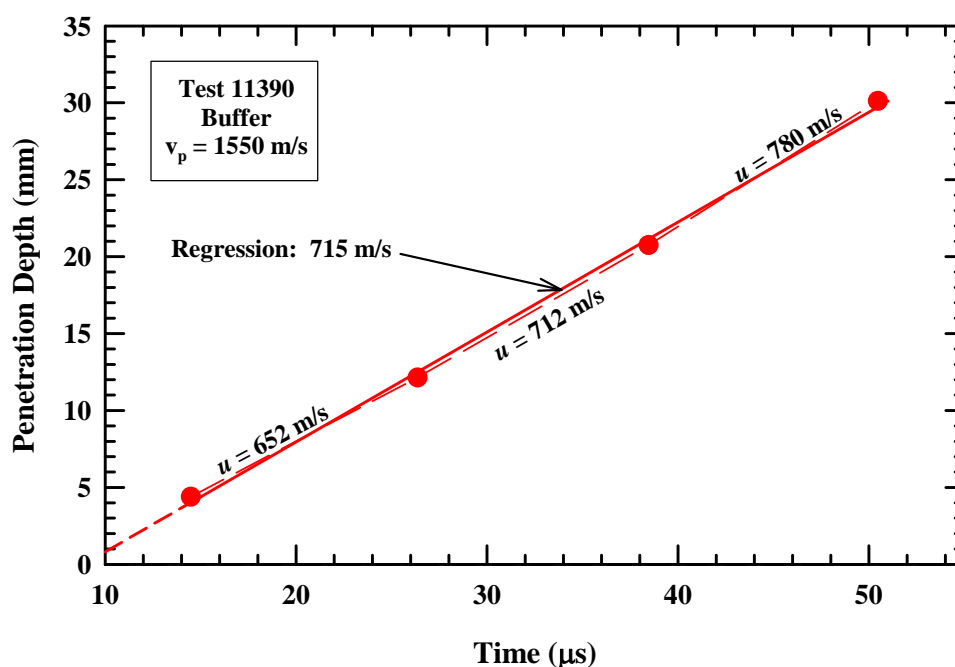
Figure 20. Penetration-time history and point-to-point slopes for Exp. 11390.

Each experiment requires its own uncertainty analysis since the time between flash X-rays were varied during the experiments. For example, the δu's for Exp. 11354 are between 16 and 27 m/s. Nevertheless, for many of the experiments listed in Table 1, a δu of ~30 m/s is typical. Perusing the column of penetration velocities with their standard errors in Table 1, it is seen that most of the penetration velocities computed from linear regression have standard errors greater than the nominal 30 m/s uncertainty associated with measurement errors. We thus conclude that penetration is typically nonsteady for an Au rod into initially intact SiC at impact velocities on the order of 1700 m/s and below. In contrast, the standard deviations associated with linear regression of high-velocity data, i.e., above 3000 m/s, are smaller than the uncertainties due to potential measurement errors [31].

4.3 Target Resistance

Target resistance R_t was calculated from the Tate equation [32-33]:

$$R_t - Y_p = \frac{1}{2} \rho_p \left(v - u\right)^2 - \frac{1}{2} \rho_t u^2 = \frac{1}{2} \rho_p v_c^2 - \frac{1}{2} \rho_t u^2 \tag{10}$$

where u and v_c are used from Table 1. It has been assumed for the purposes here that Y_p is zero for calculating the target resistance.

The target resistance is computed from Eqn. (10) and is plotted as a function of impact velocity in Fig. 21. The solid line is the minimum target resistance, assuming dwell, at the specific impact velocity, which is readily calculated from Eqn. (10) with $u = 0$ and with $v_c = v_p$. The square symbols are calculated from the entries in Table 1, and are listed in Table 2. For all tests that have some dwell, the target resistance starts on the solid line, then transitions to the much lower data point shown (i.e., $R_t \approx$ 4-9 GPa) after dwell transitions to penetration. Only the experiments with sustained dwell lie on or near the solid line. The data points that lie slightly below the theoretical line between approximately 1400 and 1550 m/s are not exactly on the
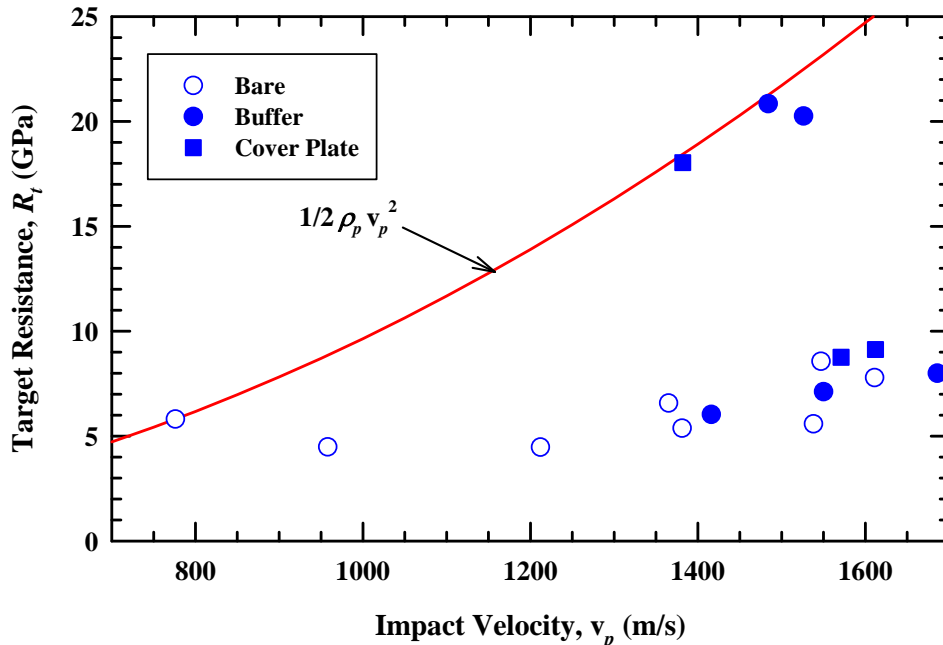
Figure 21. Post-dwell target resistance as a function of impact velocity.

theoretical line since the consumption velocity v_c estimated from the experiments is not identical to the impact velocity v_p. Very large target resistances are realized when dwell occurs[8], but then drops significantly with the onset of penetration.

As observed in other work, the target resistance for ceramic penetration increases with increasing impact velocity [34], going from a value of approximately 4.5 GPa at 1000 m/s to ~9 GPa at 1600 m/s. Once penetration begins, there is no difference in the penetration resistance—within data scatter—for bare or buffered targets.

4.4 Dwell Times and the Dwell-Penetration Transition Velocity

The estimated dwell time as a function of impact velocity for the bare targets is shown in Fig. 22. The last X-ray shadowgraph for the experiment at 776 m/s was at 70 µs, so dwell is shown only to 70 µs. It is noted, though, that the length of the rod remaining at 70 µs is 15.7 mm (initial length of 70 mm). Another 20 µs of dwell would result in complete erosion of the projectile. It is unknown if there is any dwell at impact velocities above 1200 m/s for bare targets because the time of the first X-rays for these experiments was greater than 9 µs. However, the analysis procedure describe in connection with Figs 9 and 10 give a small, but finite dwell time, as shown in Fig. 22.
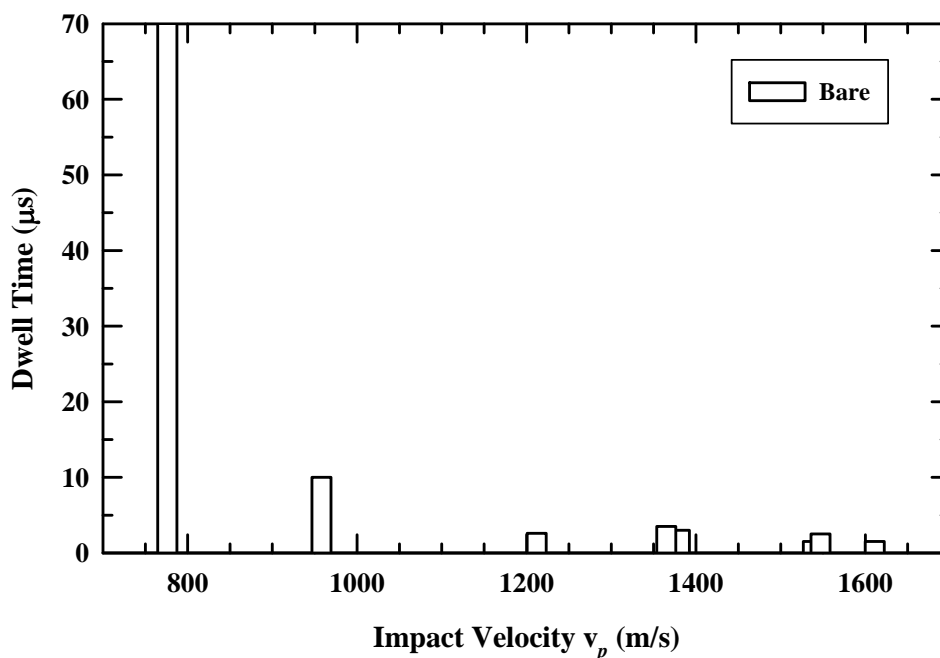
Figure 22. Dwell time vs. impact velocity for bare targets.

The estimated dwell times for the buffered targets (the small-diameter buffer and the cover plate) are shown in Fig. 23 (the higher velocity bare targets are also shown for comparison). The last X-ray shadowgraphs for the experiments that had sustained dwell was ~40 µs, so the dwell time is only shown to 40 µs. For the three experiments that showed sustained dwell, the lengths of the rod in the last X-rays were 17.8 mm (1382 m/s), 15.4 mm (1484 m/s), and 13.4 mm

---

[8] In Ref. [30], it was found that R_t for borosilicate glass (with a buffer) could achieve values during dwell approaching the HEL for the glass (8 GPa) before reaching a surface pressure that could no longer sustain dwell. The HEL for SiC is 12.2 GPa [23], which is significantly lower than the stagnation pressure of about 20 GPa associated with interface defeat observed in the experiments here.

(1526 m/s).[9] It is estimated that an additional 13, 10, and 9 µs of dwell, respectively, would have fully consumed the rods. The results for two preliminary experiments, using 0.75-mm diameter gold rods and 3-mm-high copper buffers, are also shown. Only two X-rays were taken during penetration per experiment (these were preliminary experiments to investigate whether the concept of using a buffer had merit before conducting a more rigorous experimental effort). The last X-ray of these two experiments was taken at 21 and 16 µs, respectively, and are shown in Fig. 24. The dwell times shown in Fig. 23 are adjusted for the time it took for the rod to penetrate the 3-mm copper buffer, Eqns. (1) and (2).
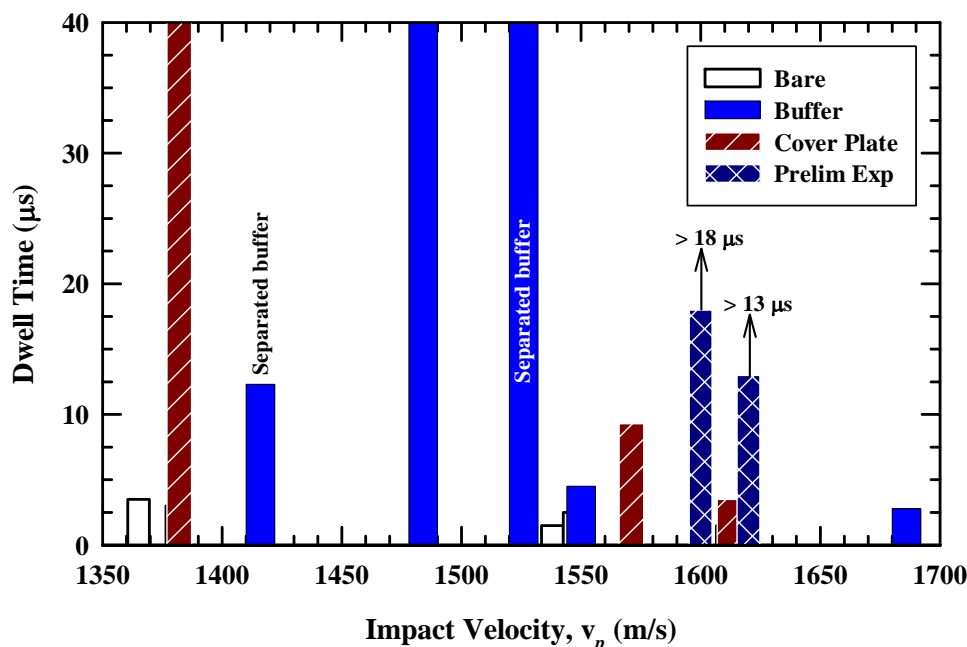
Figure 23. Dwell time vs. impact velocity for buffered targets.

The data in Fig. 23, particularly when combined with the results of the preliminary experiments, are suggestive that a cover plate is somewhat detrimental for sustained dwell; that is, the dwell-penetration transition velocity is somewhat lower for the cover plate configuration than for the smaller diameter buffer. A possible explanation is that the glue bond for the cover plate somewhat impedes the initial radial flow of the rod for a longer period of time since the cover plate has a larger diameter than the buffer. However, there are also some experimental differences between the two preliminary experiments and the experiments with the cover plate. The buffer height for the preliminary experiments—as well as all the other "small" buffer experiments—was 4 projectile diameters ($4D_p$). The thickness of the cover plate was $2D_p$ instead of $4D_p$. Also, the rod used in the preliminary experiments had a diameter of 0.75 mm, whereas all the other experiments reported here had a rod diameter of 1.0 mm. An experimental effort is planned to investigate the effect of different buffer heights and projectile diameters.

An alternative way of displaying dwell time as a function of impact velocity is shown in Fig. 25. The dashed line represents the time it would take a 70-mm-long rod to completely erode as a function of impact velocity.[10] Thus, it is seen that the two buffer experiments at approximately

---

[9] We have defined "sustained dwell" as being any test where the measured penetration is less than ~3 mm.

[10] This calculation ignores any erosion of the rod during penetration of the buffer (complete erosion of the rod ≡ interface defeat of the rod).

(a) v_p = 1600 m/s   (b) v_p = 1620 m/s
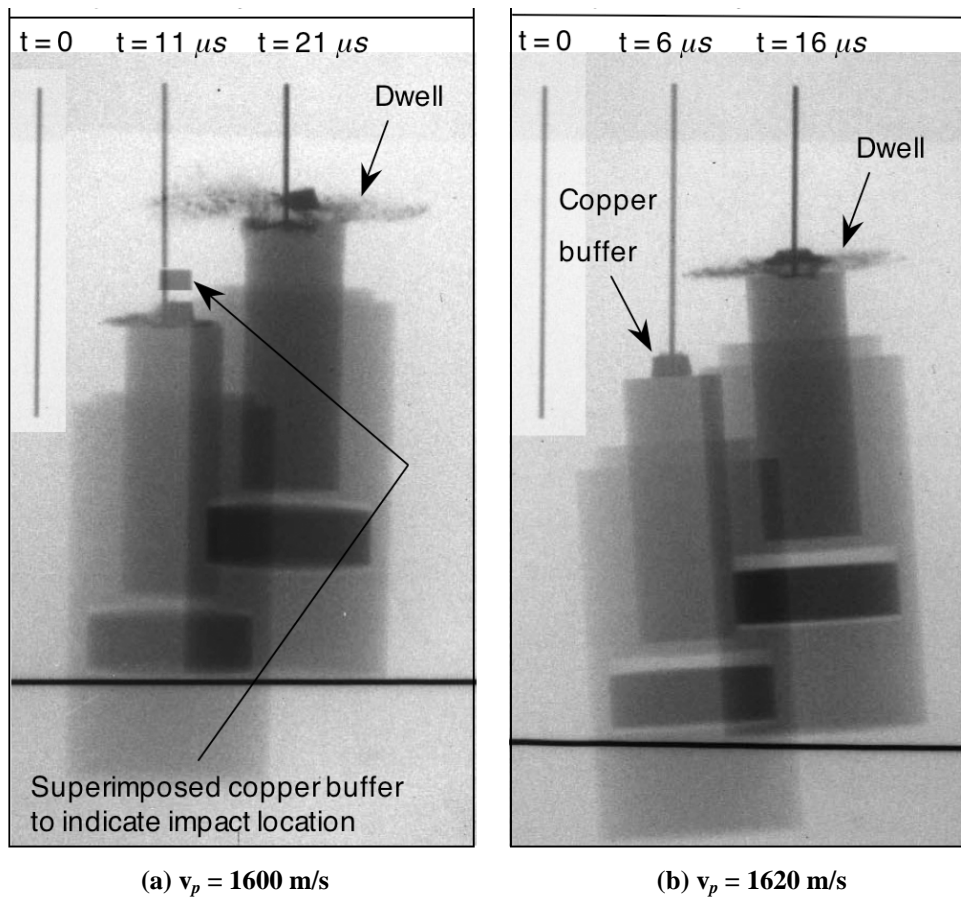
Figure 24. Experimental results for a gold projectile impacting a buffered SiC target at 1600 m/s and 1620 m/s. Three radiographs are shown for each experiment.
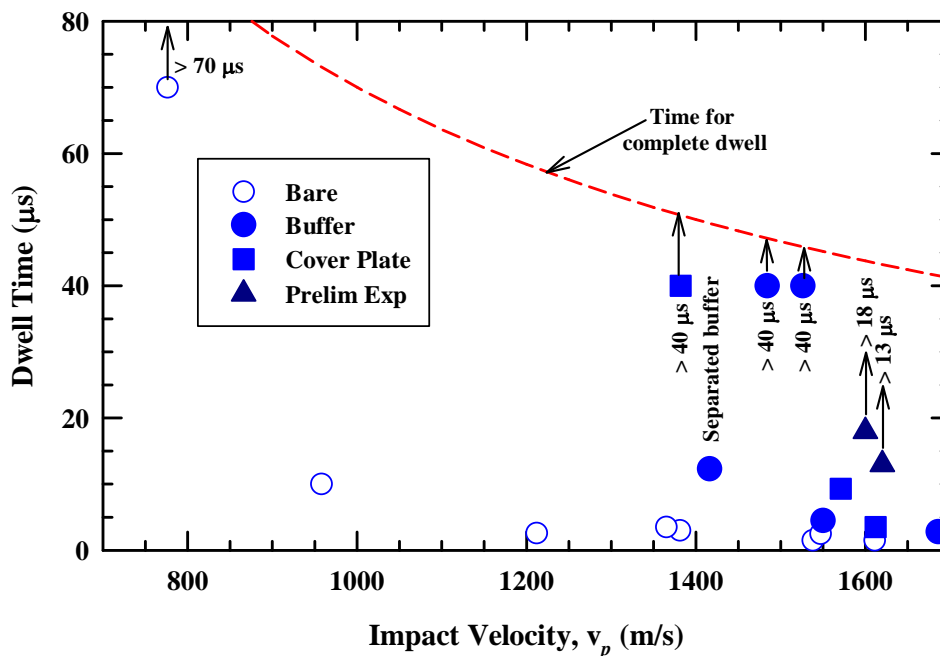
Figure 25. Dwell time vs. impact velocity for all targets.

1500 m/s would only have required a little additional dwell time (after the last observed X-ray) to have fully consumed the rod.

A reasonable estimation of the dwell-penetration transition velocity, V_t, for bare SiC is slighly higher than 800 m/s, but not substantially higher since the dwell time for the impact at 958 m/s is already quite low (~10 µs). An average of the 776-m/s and 958-m/s data points would seem to give too high an estimate since the experiment at 958 m/s had only 10 µs of dwell. Therefore, we estimate the dwell transition velocity to be one-fourth the distance between the two data points, i.e., the dwell-penetration transition velocity, V_t, for an Au rod onto bare SiC is estimated to be 822 ± 46 m/s, Fig. 26.
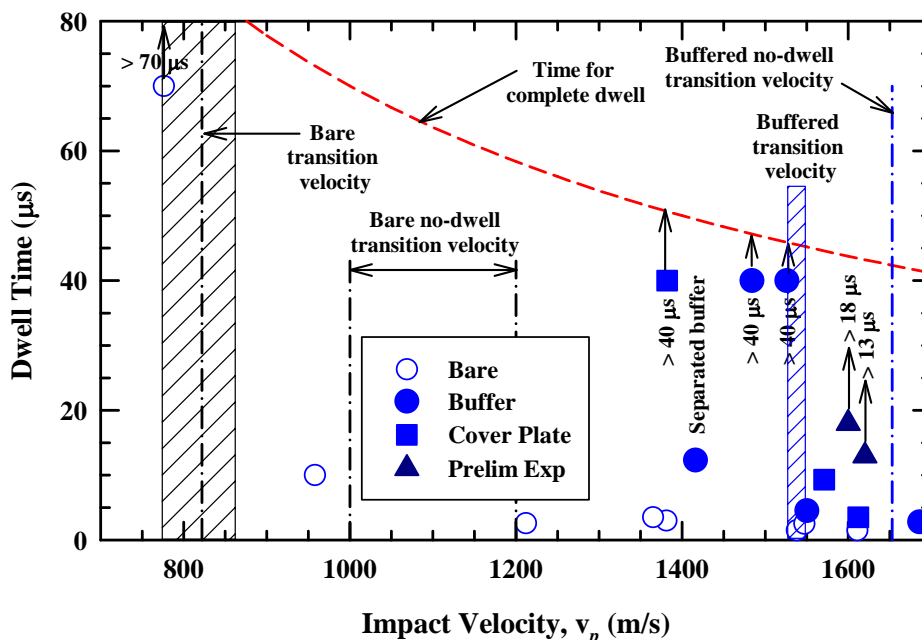
Figure 26. Dwell times with dwell-penetration transition velocities.

The dwell-penetration transition velocity increases to 1538 ± 12 m/s for the buffered targets, denoted by the thin cross-hatched region in Fig. 26. A small amount of dwell (9.3 µs) was estimated for one of the cover plate experiments at an impact velocity of 1571 m/s, and even less dwell at an impact velocity of 1612 m/s. It is noted that the two preliminary experiments (which had differences in experimental parameters, as described in the paragraph above) had appreciable dwell times (> 13 µs). It was found for borosilicate glass [30] that the dwell time generally decreased with increasing impact velocity above the transition velocity. It was also found that there was a zone of mixed results for borosilicate glass [30]; there were instances of prolonged dwell that violated this general trend, that is, there was an uncertainty interval about the dwell-penetration transition velocity (perhaps analogous to V_{50} experiments). It was noted in Ref. [30] that the dwell-penetration transition is inherently an unstable process; small changes in impact conditions result in dwell or penetration. Therefore, it is unknown at this time if the results represented by the two triangles are due to geometric differences of the preliminary experiments (in particular, a smaller diameter rod), or due to inherent scatter about an instability condition.

Similar to glass, there also appears to be a velocity above which there is virtually no or little (< 3 µs) dwell, denoted in Fig. 26 as the "no-dwell transition velocity." For bare SiC, there is a fairly large interval of uncertainty since there exist no data between 958 m/s and 1212 m/s. But

the experiment at 958 m/s had only ~10 μs of dwell, while at 1212 m/s, there was ~ 2.6 μs of dwell. The bare no-dwell transition velocity for an Au rod onto SiC is somewhere between 1000 m/s and 1200 m/s, and probably closer to 1000 m/s. For an Au rod onto buffered SiC, this velocity is estimated to be 1653 ± 23 m/s; although, it might be as low as 1592 ± 20 m/s (the average of the two highest velocity cover plate experiments). The no-dwell transition velocities are denoted by the dot-dashed lines in Fig. 26.

4.5 Post-Dwell Penetration Velocities

The penetration velocities after the transition from dwell to penetration (from Table 1) are shown in Fig. 27. There is considerable variation in the post-transition penetration velocity as a function of impact velocity for 1300 m/s ≤ v_p ≤ 1700 m/s; that is, the penetration velocity falls within a fairly wide band. This is probably a consequence of the nonsteady penetration within individual experiments. The dashed lines bound the penetration velocities for SiC determined in Ref. [35-36].   Thus, the post-transition penetration velocities fall within the band of data observed in previous experiments. Therefore, we conclude, and as observed by Lundberg, *et al.* [15], and for glass [30], that once the rod begins to penetrate, it penetrates at a velocity as if there had been no dwell. The two highly yawed experiments penetrate at slightly higher velocities than do the other experiments.
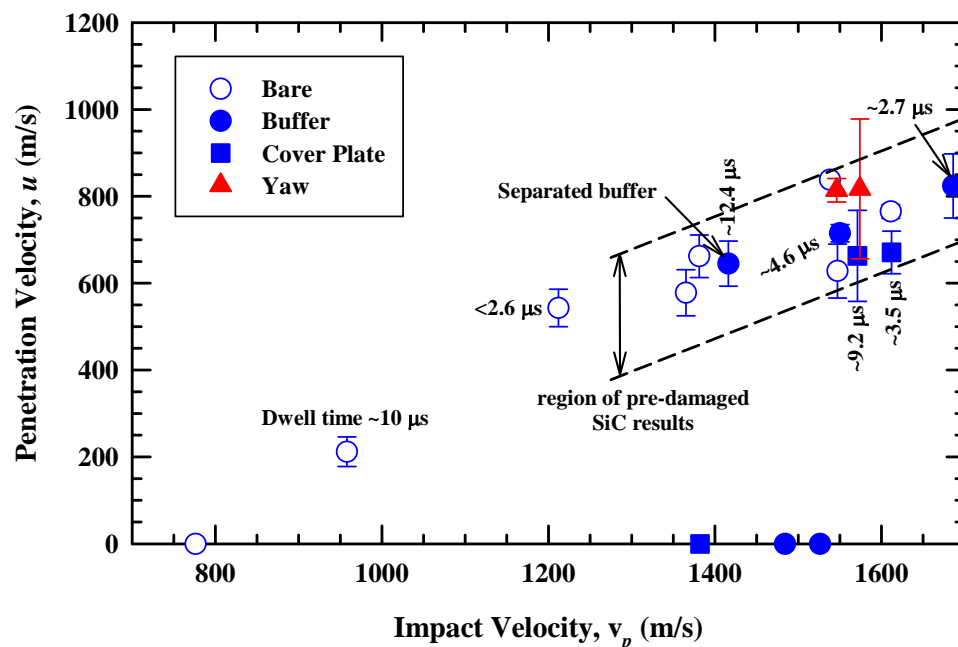

Figure 27. Post-transition penetration velocity vs. impact velocity.

5.0 Simulations

5.1 Introduction

Computations have provided significant input into the design, testing, and analysis of the experiments presented in the previous sections. Computations were performed prior to testing to design the target and the buffer; but, most of the computations were performed after completion of the experiments to analyze and to help understand the experimental results. The majority of the computations used the EPIC [37] code although CTH [38] was also used. The EPIC computations include recent constitutive and algorithm advancements that allow for interface defeat, dwell and penetration. The previously developed JH-1 model [39] and the more recently developed JHB model are used [23], as well as algorithms that automatically convert finite elements into meshless particles during the course of the computation [21, 22]. The following sections will first present a short discussion on bare targets followed by a more in-depth discussion on buffered targets.

5.2 Bare Targets

Computations of the bare target configuration were performed to determine the transition velocity and to compare the computed results to the experimental results. The initial geometry is shown on the left side of Fig. 28 where a long gold projectile, with a diameter of 1.0 mm and a length of 70 mm, impacts a bare SiC target 20 mm in diameter and 35 mm in length. The computed results are also presented in Fig. 28 for impact velocities of 700 m/s, 800 m/s, and 900 m/s, and are shown after the rod has been completely consumed. It is clear that there is no penetration at an impact velocity of 700 m/s (interface defeat). There is penetration at 800 m/s, although the average penetration velocity is very small (~60 m/s). The rod also dwells for approximately 8 μs prior to transitioning to penetration. At 900 m/s, there is significantly more penetration with increased target damage. The penetration velocity is approximately 140 m/s after an initial dwell time of 3 μs. Additional computations were performed between 700 m/s and 800 m/s, at 10 m/s increments (not shown here), to determine more closely the dwell-penetration transition velocity. The results showed interface defeat at 780 m/s and penetration at 790 m/s; thus, an estimate of the dwell-penetration transition velocity is 785 ± 5 m/s. The shock stress is approximately 18 GPa for a gold rod impacting SiC at 780 m/s. This shock stress is compared to the transition stress determined in Section 5.3.2 when the buffered targets are discussed.

5.3 Buffered Targets

The dwell-transition velocity can be greatly increased by attaching a copper buffer to the impact surface of a SiC target. The buffer attenuates the initial impact shock and gradually loads the ceramic during the initial stages of dwell. The buffer ensures that the maximum stress on the ceramic surface occurs from steady-state dwell and not from other stresses that occur during the initial loading process. This ensures that if the ceramic fails, resulting in penetration, it occurs from the stress produced from dwell and allows for the transition stress, Σ_t, to be determined. It should be noted that using a buffer is not new. Hauver, *et al*. [10], used a variety of layers placed between the projectile and top surface of the ceramic. Lundberg *et al*. [16] used a buffer to set up dwell to investigate long interaction times, but the targets were complex, incorporating both confinement and prestress. The difference here is that the targets are simple, and are designed to

Initial geometry
(Bare target)

Computed results showing damage
Rod is completely consumed for all three impact velocities

$v_p = 700$ m/s $v_p = 800$ m/s $v_p = 900$ m/s

Gold Rod
L = 70 mm
D = 1 mm

Silicon
carbide
L = 35 mm
D = 20 mm
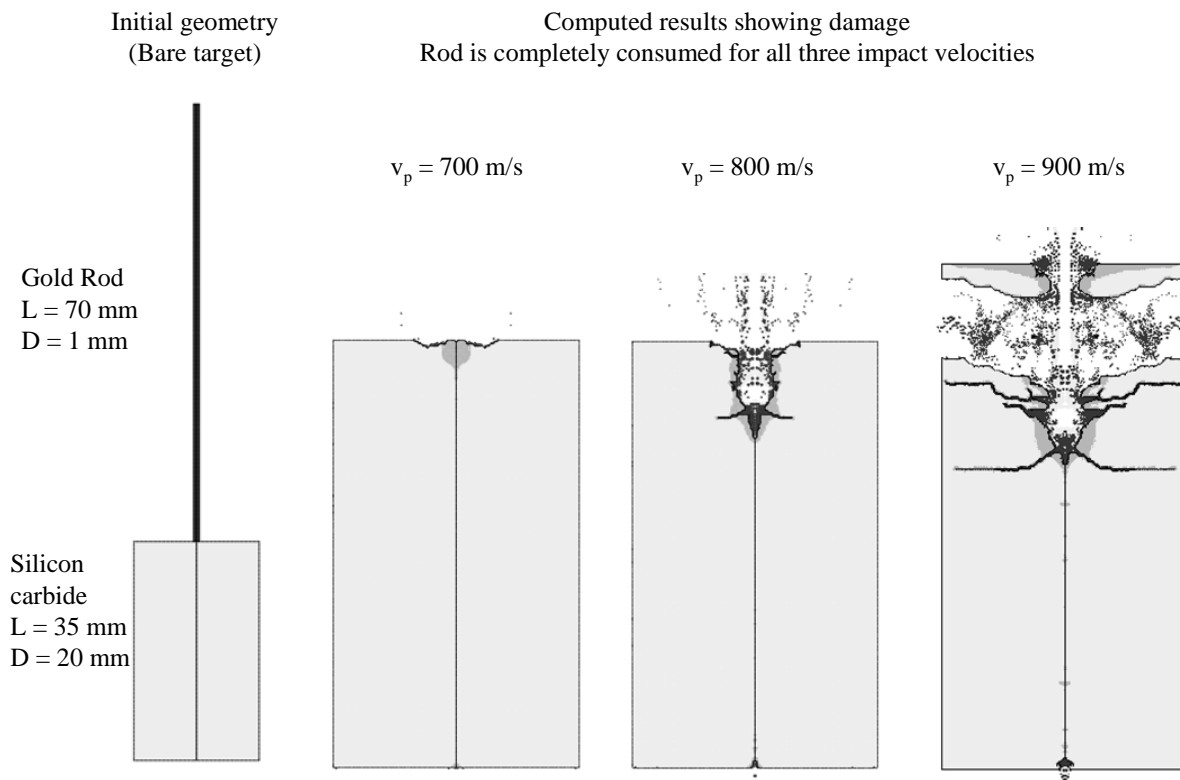
**Figure 28. Initial geometry of the bare target and the computed results
for impact velocities of 700 m/s, 800 m/s, and 900 m/s.**

investigate the maximum resistance of the ceramic alone. The following sections will present how the buffer was designed, the effect of buffer separation, and the effect of a full diameter buffer (plate).

5.3.1 Buffer Design

The initial buffer/target design is presented in Fig. 29. It was designed several years ago [1] and is presented again here for completeness. The target is simply a SiC cylinder (length = 40 mm, diameter = 15 mm) with a copper buffer (height = 3 mm, diameter = 1.5 mm) attached to the impact surface. The work of Lundberg, *et al.* [17] identified the maximum impact velocity for sustained dwell to be approximately 1600 m/s (using a tungsten rod and prestressed target). The work here uses a gold rod and an unconfined target. The gold rod was expected to produce a similar surface stress (because it has slightly higher density, but lower strength then the tungsten rod) for the same impact velocity. The target, being unconfined and without prestress, was expected to be weaker than the configuration used by Lundberg and thus would probably fail at a lower impact velocity. Therefore, 1600 m/s was used as the impact velocity for the buffer design as it was considered an upper bound (meaning that the SiC would fail at this velocity regardless of how the buffer was designed). The steady-state dwell stress, produced from a gold rod dwelling at 1600 m/s, is approximately 26.3 GPa as determined by CTH computations (these computations will be presented later). Hence, the buffer is designed to keep the initial loading stresses below 26.3 GPa.

The buffer is designed using a gold projectile with a diameter of 0.75 mm and a length of 30 mm (the projectile dimensions were chosen to be similar to those used in the anticipated experiments; the rod diameter was subsequently increased in the experiments to facilitate

Figure 29. Unconfined SiC target with copper buffer designed to induce dwell.

handling). The buffer height, diameter, and material are the three design parameters that must be determined. The height, h, must be sufficient to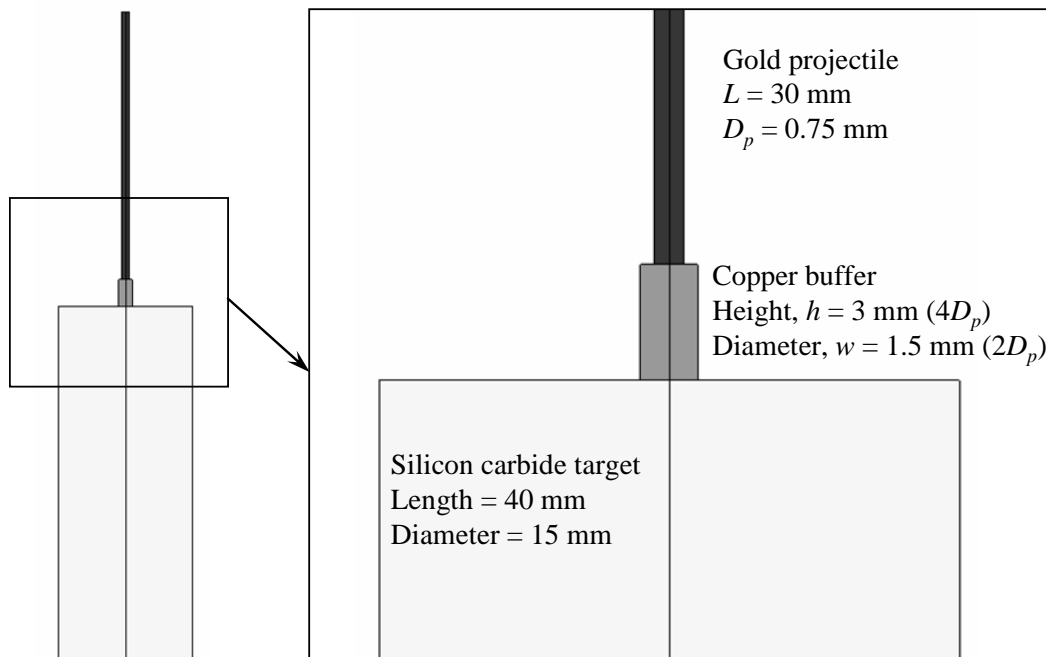 attenuate the initial impact shock and establish steady-state penetration. The diameter, w, must be large enough to ensure steady-state penetration (as the rod penetrates through the buffer), but not so large as to effect steady-state dwell (this will be discuss further in Section 5.5). Lastly, the buffer material must have sufficient density and strength to produce a gradual loading of the ceramic and prevent the impact stresses from exceeding those produced from steady-state dwell.

Figure 30 presents EPIC results that show what effect the buffer material has on the ceramic surface stress during loading. Three materials are investigated: polycarbonate ($\rho = 1.2$ g/cm^3), copper ($\rho = 8.9$ g/cm^3), and a tungsten alloy ($\rho = 17.0$ g/cm^3). The buffer geometry used is the same as shown in Fig. 29. The ceramic is modeled using the JH-1 model, without failure, for SiC [39]. Also shown in Fig. 30 is the maximum surface stress produced from steady-state dwell at an impact velocity of 1600 m/s (26.3 GPa) computed using CTH (the computation used a gold projectile impacting a rigid surface). It is clear that polycarbonate does not have sufficient density/strength, producing a peak stress of approximately 35 GPa, well in excess of the steady-state dwell stress (this occurs because the penetration velocity is too large). In contrast, both the copper and tungsten produce loading conditions that gradually approach the 26.3-GPa dwell stress. Copper was selected as the buffer material because of its ready availability in a variety of diameters.

A parametric study was conducted using CTH to investigate the effect of buffer height and diameter on the stress at the buffer-ceramic interface. The geometry is shown in Fig. 31; the parameter study was generalized to other geometric configurations by normalizing h and w by the projectile diameter, D_p. Figure 32 presents results that show the effect of buffer height h and diameter w (here the SiC is modeled as strictly elastic). It appears that a buffer height of one projectile diameter is sufficient to attenuate the shock and produce loading conditions less then steady-state dwell, although there remains a stress spike of 22 GPa. Increasing the buffer height
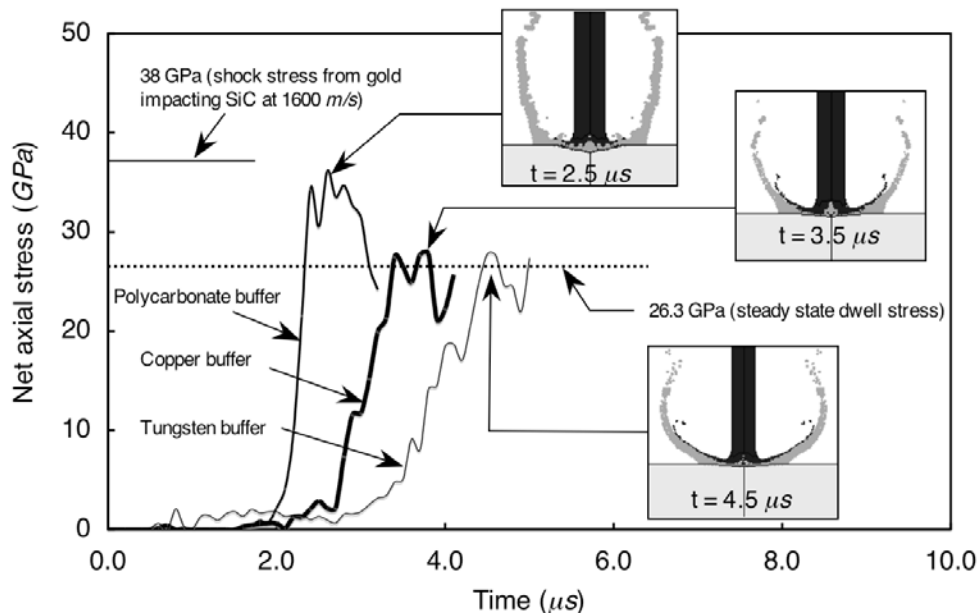
Figure 30. Net axial stress as a function of time for three buffer materials impacted by an Au projectile at v_p = 1600 m/s. Also shown are geometry plots at the time of ceramic impact.
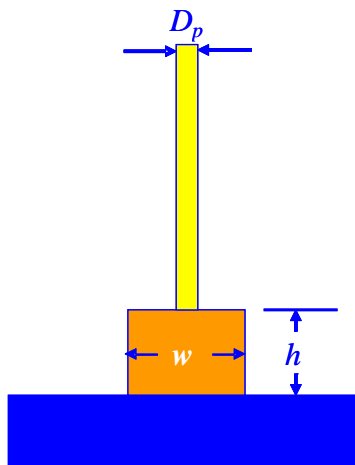
Figure 31. Schematic for parametric study on Cu buffer geometry.

to $2D_p$ attenuates the initial shock stress (at the copper-ceramic interface) to less than 10 GPa and provides ramp (gradual) loading on the ceramic surface. It also appears that a buffer diameter of $2D_p$ is sufficient to keep the impact stress (impact stress is defined here to be when the projectile reaches the ceramic surface after penetrating the copper buffer, examples are shown in the inserts in Fig. 30) below the steady-state dwell stress. From these results a copper buffer of height $2D_p$ and diameter $2D_p$ appears to be an adequate design.

Additional CTH computations were performed to investigate the loading rate and steady-state stress profiles produced for impact velocities near the dwell-penetration transition velocity and are presented in Fig. 33a. As the impact velocity increases, the stress increases. Also, note the stress profiles produced as a function of impact velocity, Fig. 33b. As expected, the peak stress occurs at the center of the projectile and decreases rapidly beyond the projectile radius.

(a) Effect of buffer height

(b) Effect of buffer diameter
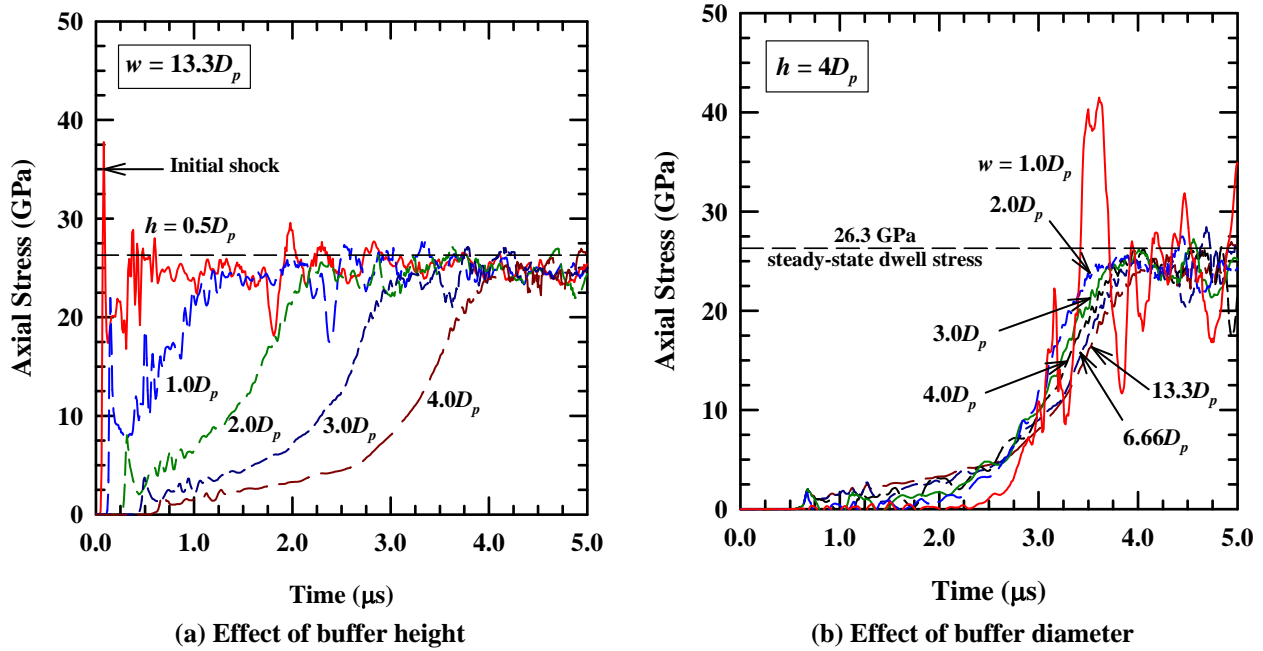
Figure 32. Net axial stress as a function of time for five buffer heights and six diameters at $v_p = 1600$ m/s.

(a) Axial stress vs. time for 5 impact velocities

(b) Axial stress vs. normalized distance from projectile centerline

Figure 33. Computed results showing the a) axial stress as a function of time and b) axial stress as a function of distance from the projectile centerline for five impact velocities.

5.3.2 Computations of a Target with a Buffer

In the previous section it was shown that a copper buffer of height $2D_p$ and diameter $2D_p$ appears to be an adequate design; however, to be somewhat conservative (and also improve the likelihood of impacting the rod on the copper buffer), a height of $4D_p$ and width of $5D_p$ was used. Figure 34 shows the initial geometry of the buffered target including the computed result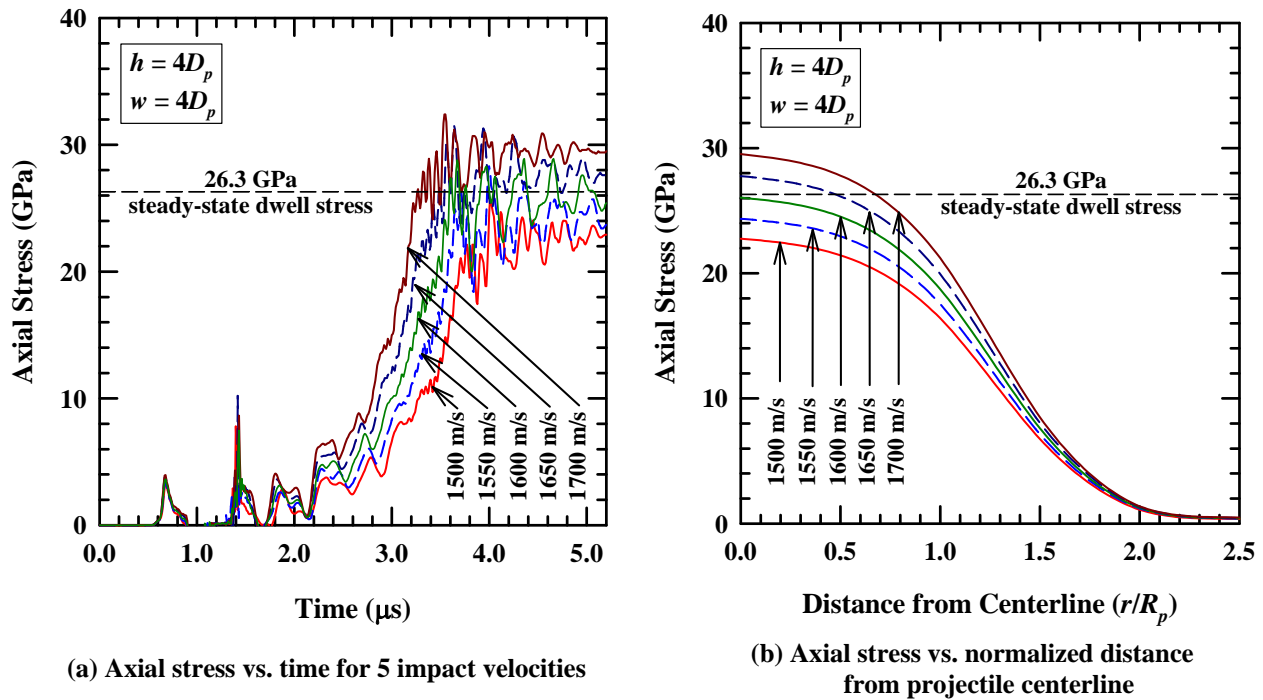s for an impact velocity of 1500 m/s. The target, buffer, and projectile have the same dimensions as the experiments presented in Sections 3 and 4. The EPIC code is used for all the following computations. The computational grid used three sets of crossed triangular elements (four triangles in a quad) across the radius of the projectile. The grid size in the buffer and ceramic is similar to those used in the projectile, and the ceramic is modeled using the JHB model for SiC [23]. The computed result shows that at $t = 5$ µs, the projectile has penetrated the buffer and is beginning to impact the ceramic surface. At $t = 40$ µs, the buffer is perforated and the gold projectile is flowing radially along the ceramic surface (dwell). At $t = 60$ µs, the projectile is completely consumed on the ceramic surface with no ceramic penetration (interface defeat). This result indicates that SiC can resist very high stress levels (for the conditions that occur during dwell) without using a cover plate, rear plate, or lateral confinement.

Initial geometry
(Buffered target)

Computed results showing material

Gold Rod
$v_p = 1500$ m/s
$L = 70$ mm
$D_p = 1$ mm

$t = 0$

Copper buffer
$h = 4$ mm
$w = 5$ mm

$t = 5$ µs

$t = 40$ µs

$t = 60$ µs

Silicon
carbide
$L = 35$ mm
$D = 20$ mm
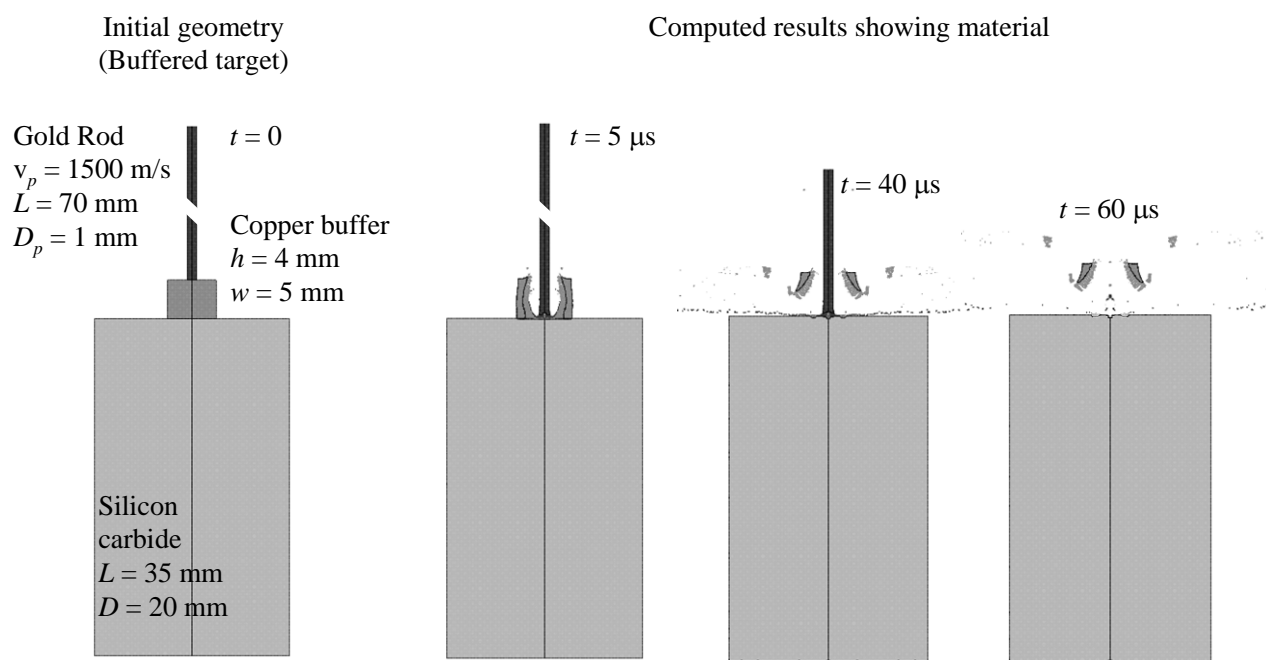
Figure 34. Computed results for an Au projectile impacting a buffered SiC target at 1500 m/s.

It is of interest to determine the computed dwell-penetration transition velocity for this configuration, similar to the bare target (Section 5.2), along with the maximum resisting stress or *transition stress*, Σ_t. Computed results for a bare and buffered target for various impact velocities are shown in Fig. 35. The bare target uses no buffer and the buffered target uses the same buffer as shown in Fig. 34. The bare target is included to show the dramatic effect that occurs by adding a buffer. The computed results show material damage, and are presented 30 µs after impact for the bare targets and after the rod is completely consumed for the buffered targets (except for $v_p = 1600$ m/s, which is shown at 45 µs after impact: 5 µs to penetrate the buffer,

$v_p = 800$ m/s $v_p = 1000$ m/s $v_p = 1200$ m/s $v_p = 1400$ m/s $v_p = 1500$ m/s $v_p = 1600$ m/s

Figure 35. Computed results (showing material damage) for an Au projectile impacting a bare (upper series) and buffered (lower series) SiC target at various impact velocities.

10 µs of dwell and 30 µs of penetration). The results show that penetration begins immediately at an impact velocity above 800 m/s when no buffer is used (as discussed previously). When a buffer is used, no penetration occurs until the impact velocity reaches 1600 m/s. Additional computations were performed between 1500 m/s and 1600 m/s, at 10 m/s increments (not shown here), to determine more closely the dwell-penetration transition velocity. The computational results show penet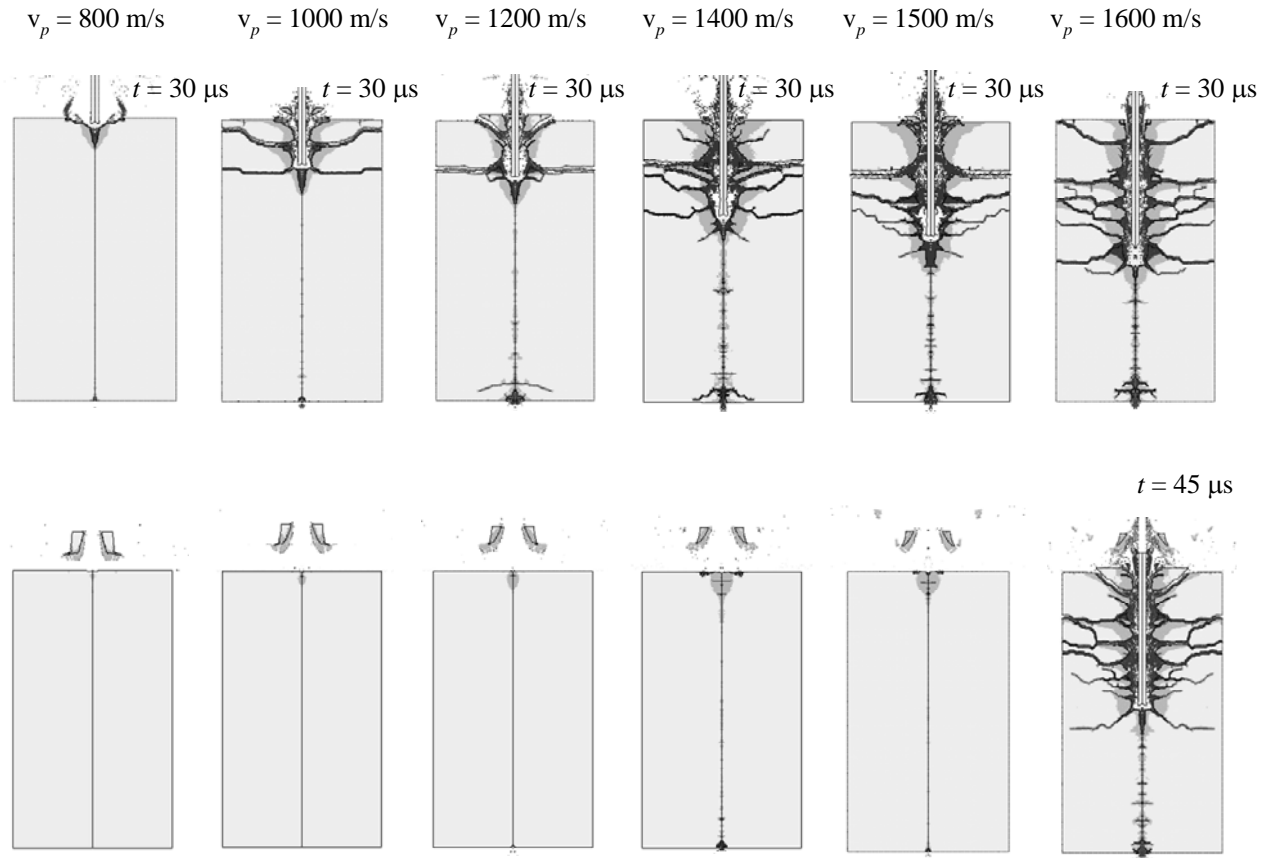ration at 1580 m/s and interface defeat at 1570 m/s; 1580 m/s corresponds to a transition stress of approximately $\Sigma_t = 25$ GPa (estimated from Fig. 33b). It should be noted that the transition velocity presented here (1580 m/s) is slightly lower then was presented in a previous article (1650 m/s) [1]. This is probably because the previous work used the older JH-1 model (with slightly stronger constants), while the work presented here uses the more recent JHB [23] model (there are also minor differences in the target and projectile geometries that could affect the results).

There are several interesting observations that can be made from these results:

1. The shock stress required to fail the target (~18 GPa) is significantly lower then the transition stress required to fail the target ($\Sigma_t = 25$ GPa).

2. The computed dwell-penetration transition velocity (1580 m/s) is slightly higher than the experimental result, Fig. 26 (1538 ± 12 m/s). However, it is noted that there may be a zone of mixed results between 1538 m/s and 1620 m/s. The dwell transition stress for an impact velocity of 1538 m/s is ~23 GPa.

3. The transition stress determined by Lundberg, $\Sigma_t = 26$ GPa, (using a prestressed target) is similar to the transition stress produced using an unconfined target.

The penetration velocities were determined for each of the computations that produced penetration. The technique used to estimate the penetration velocity is presented in Fig. 36 (using the computed result of a bare target impacted at 1200 m/s). The penetration depths are shown at $t = 10$ μs, 20 μs, and 30 μs after impact. A linear regression through the data (including the 0,0 point) produces a penetration velocity of 240 m/s. Also shown are the average penetration velocities calculated between each of the three penetration depths. Note the large non-uniform penetration rate that occurs. From $t = 0$ to 10 μs the average penetration velocity is 400 m/s (there is no dwell for impact velocities over 900 m/s), from 10 μs to 20 μs it drops to 80 m/s and from 20 μs to 30 μs it increases to 280 m/s. This behavior is also observed in the experiments, as discussed in Section 4.2 and shown in Fig. 19. Two more examples are presented in Fig. 37 where the experimental data for Exps. 11354 and 11359 are shown.
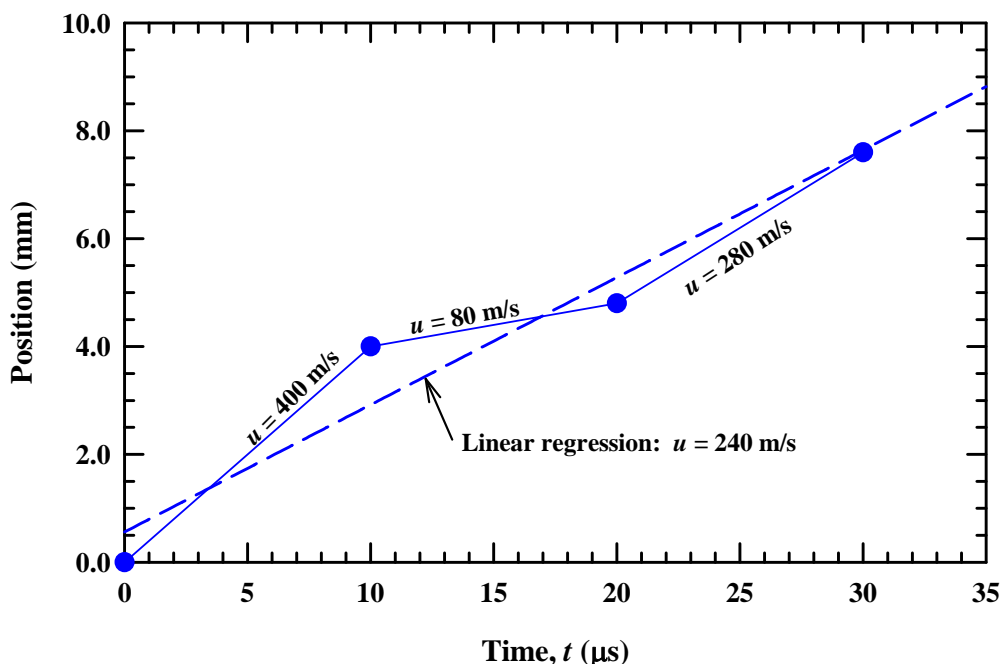
Figure 36. Computed penetration depths measured at $t = 10$ μs, 20 μs and 30 μs after projectile impact ($v_p = 1200$ m/s) with point-to-point penetration velocities (bare target).

This nonlinear penetration behavior is observed for nearly all of the experiments and computed results as shown in Fig. 38. The open and solid symbols represent the penetration velocities determined from linear regression of the penetration-time data. Circles denote bare targets (included "missed buffer" targets) and squares denote buffered targets. Experimental results are represented by solid symbols and computational results by open symbols. Error bars are also included for the test data and denote the standard error associated with the regression analysis (and given in Table 1). Also plotted with each data point are the maximum and minimum point-to-point slopes, such as shown in Figs. 36 and 37. These max and min slopes are denoted by the small "+" signs, which are then connected by a vertical line.
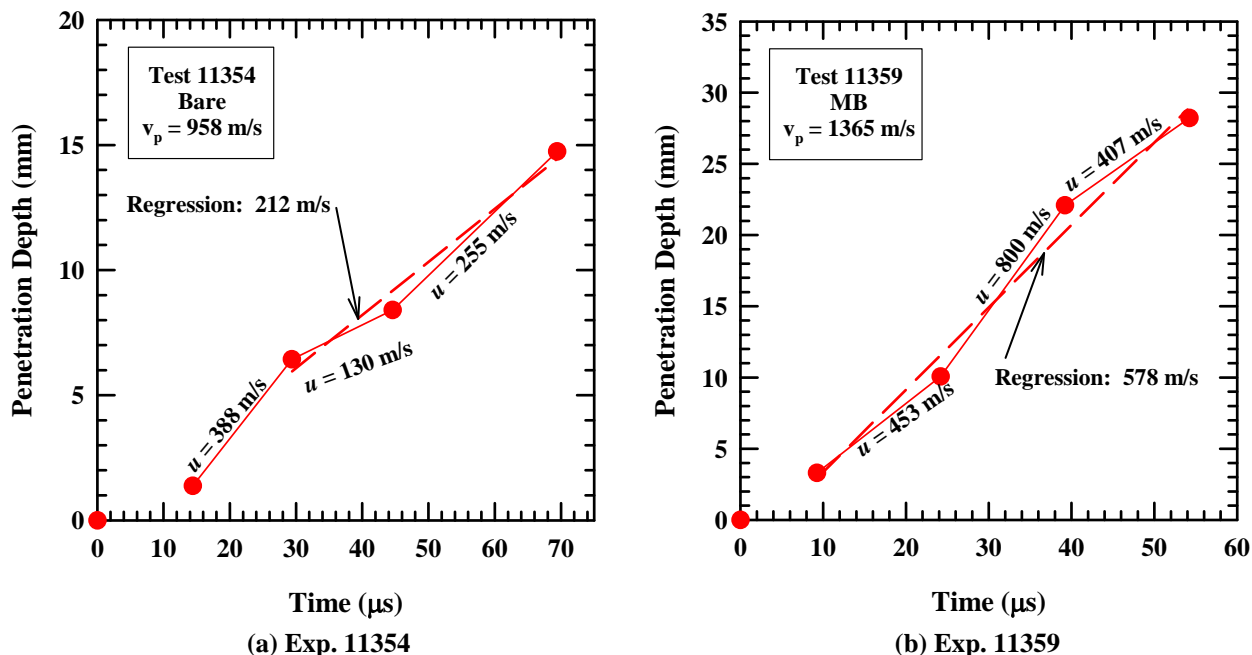
Figure 37. Comparison of experimental point-to-point penetration velocities and penetration velocity computed from linear regression.
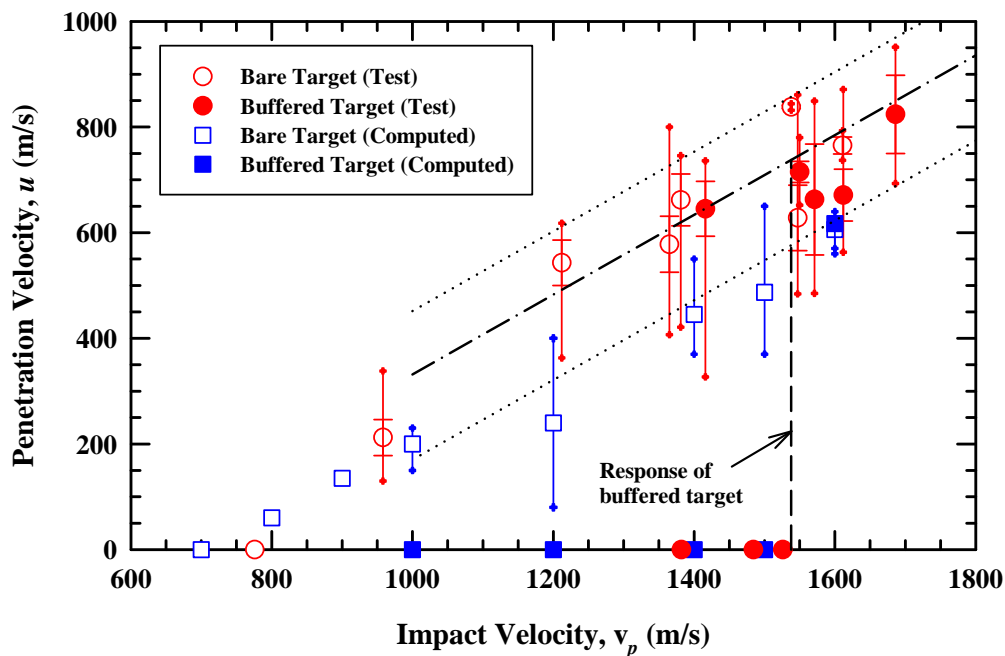
Figure 38. Computed and experimental penetration velocities for a bare and buffered target. Vertical bars indicate the range in penetration velocity.

The dot-dashed line is the average penetration velocity for *in-situ* comminuted SiC [35], and the dotted lines denote the spread in penetration velocities for a series of sleeved and bare SiC penetration experiments [36]. All the experimental penetration velocities from the current study fall within the envelope of data from Ref. [36] (the data in Ref. [36] include the data from Ref. [35]).

Penetration does not begin for the buffered targets until the impact velocity exceeds ~1538 m/s, represented by the vertical dashed line. The one exception is the data point at 1413 m/s, which is the experiment where the buffer separated from the SiC prior to impact by the Au rod.

It is also interesting to note that the maximum and minimum point-to-point slopes generally fall within the band of penetration velocities, although it is more likely that a minimum point-to-point penetration velocity violates this observation. As already discussed, over the range of impact velocities studied here, penetration rate is not a constant. We believe that this is a very important observation. Although the range in the penetration velocities is large for both the computed and experimental results, the computed results are generally lower then that of the tests. However, the experimental and computational results show that once the resisting stress for SiC is exceeded (either by shock or dwell), target response is similar.

It is not known what causes this nonlinear penetration response in the experiments. The computed results suggest it occurs from a series of small penetration events. These events are characterized by the rod first generating a region of failed material (resulting in a lower penetration velocity), and then penetrating the failed material (resulting in a higher penetration velocity) and then repeating the sequence. This process appears to become less pronounced as the impact velocity increases, presumably because the penetration stresses result in a more continuous and homogeneous failing of ceramic.

5.4 Computations of a Separated Buffer

There were two experiments where the buffer separated from the target prior to being impacted by the Au rod. The response of a bare target, a target with a Cu buffer (where the Cu buffer remains attached to the SiC), and a target where the buffer separated from the SiC prior to impact are contrasted in Fig. 39. The top set of images in Fig. 39 presents the results of Exp. 11358, where the bare target is impacted at v_p = 1381 m/s. The X-rays are shown at times relative to projectile impact. There appears to be very little dwell with penetration beginning very soon after impact (t_D is ~3 μs from Table 2). The center row of Fig. 39 presents the results of Exp. 11393 where a buffered target is impacted at v_p = 1484 m/s. At t = −6 μs (before impact), the buffer appears to be securely attached to the ceramic surface. At t = 15 and 27 μs, the projectile is clearly dwelling on the ceramic surface and the projectile and buffer debris are flowing radially. At t = 39 μs the radiograph is more complex, but the authors believe the projectile is still dwelling. It appears that a cone crack, going completely around the circumference of the ceramic has formed. Projectile debris has flowed into the cone crack, removing target material. This has the effect of creating a new ceramic surface and leaving the top surface of the target in the shape of an inverted truncated cone. The apex of the truncated cone is located where the projectile is dwelling. The third row of Fig. 39 presents the results of Exp. 11377 where the buffer separated from the target. The impact velocity is v_p = 1416 m/s. Again, the X-rays are shown at times relative to projectile impact. It is clear that prior to impact (t = -9 μs), the buffer has separated from the ceramic surface (estimated to be approximately 1 to 2 mm). It is also clear that the projectile is dwelling at t = 11 μs and is penetrating at t = 23 and 35 μs. It is estimated that the projectile dwells for approximately 12.3 μs and then begins to penetrate.[11] Experiment 11377, although impacting at a significantly lower impact velocity than

---

[11] The estimate for the dwell time has been adjusted for the time required for the rod to penetrate the copper buffer.

Bare
v_p = 1381 m/s
t = -11 μs

t = 9 μs

t = 24 μs

t = 39 μs

Copper buffer
(no separation)
v_p = 1484 m/s
t = -6 μs

t = 15 μs

t = 27 μs

t = 39 μs

Copper buffer
(~1 mm separation)
v_p = 1416 m/s
t = -9 μs
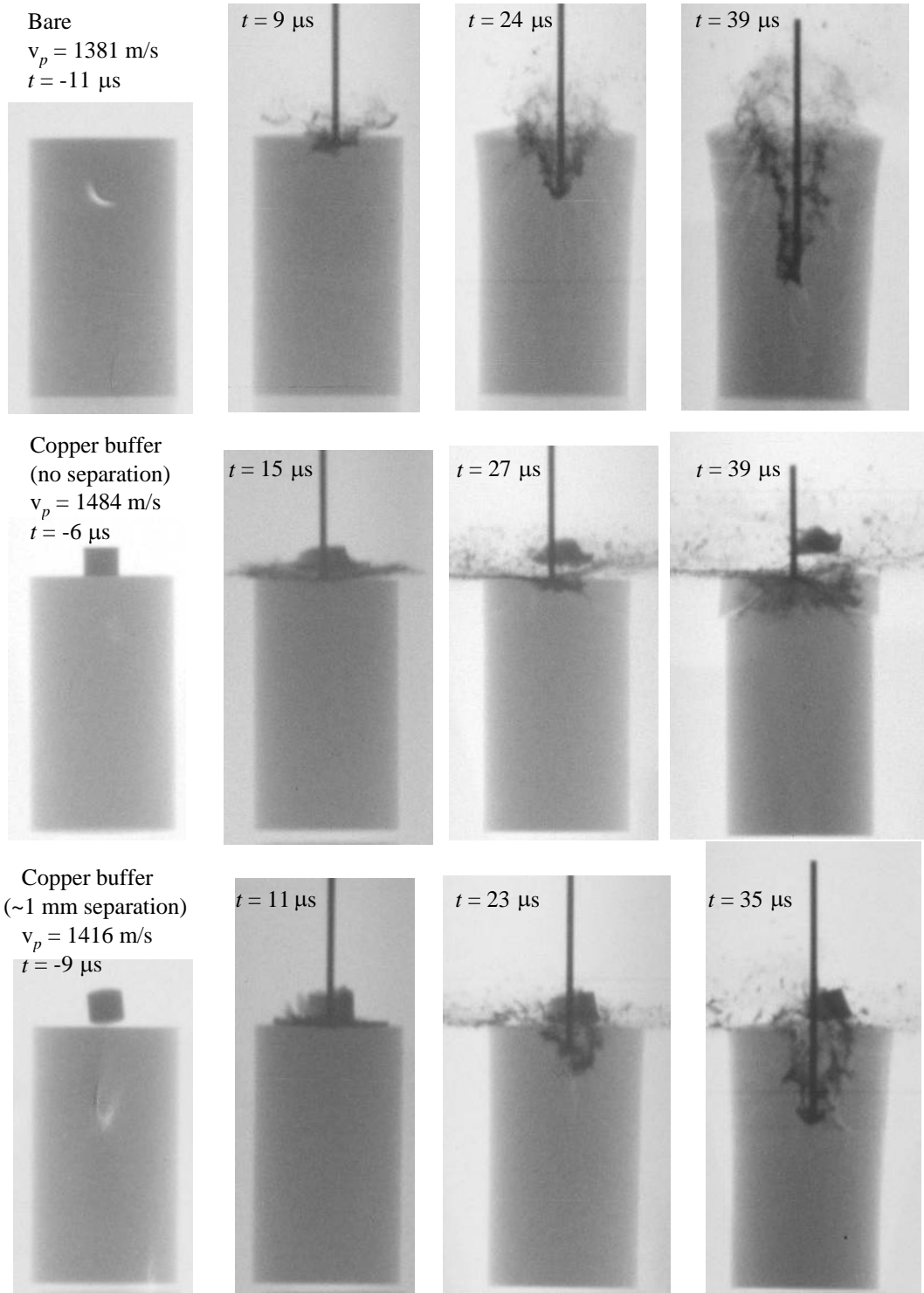
t = 11 μs

t = 23 μs

t = 35 μs

Figure 39. Experimental results for a target with no buffer (Exp. 11358), a target with an attached buffer (Exp. 11393), and a target with a separated buffer (Exp. 11377).

Exp. 11393 (1416 m/s versus 1484 m/s), produced only 12 µs of dwell instead of sustained dwell. In contrast, Exp. 11395 (impacting at 1526 m/s, see Fig. A-13) exhibited slight buffer separation but still produced sustained dwell. Thus, buffer separation can significantly reduce the dwell-penetration transition velocity, but results depend upon the separation distance.

Computations of these three experiments (no buffer, buffer with no separation, and a buffer with separation) were conducted and the results are shown in Fig. 40. The computed results are presented at the same times as the X-rays in Fig. 39 and are in good agreement with the experiments. The bare target does not dwell (penetration begins upon projectile impact), the buffered target with no separation defeats the projectile at the ceramic surface (interface defeat), and the buffered target, with a 1.0-mm separation, results in 19 µs of dwell, then transitions to penetration.

To investigate the effect of buffer separation, four computations were performed with a separation distance of 0 mm, 0.3 mm, 0.5 mm, and 1.0 mm, as displayed in Fig. 41. The results show material damage (D) 10 µs after being impacted by an Au projectile ($v_p = 1400$ m/s). The results show that as the separation distance increases, so does the damaged region. This occurs due to the rear surface of the buffer being accelerated through the air gap (as the projectile approaches the rear of the buffer) impacting the ceramic surface at an elevated velocity.

As the separation distance increases, the velocity of the rear surface of the buffer also increases, which produces a larger impact stress and thus greater damage. Computed impact stresses are presented as a function of time for an attached, and for a buffer with separations of 1.0, 2.0 and 3.0 mm in Fig. 42. The impact stress at the ceramic surface increases with increased separation distance, going from approximately 22 GPa with a 1-mm separation to over 25 GPa with a 2-mm and 3-mm separation. Additionally, instead of the gradual loading that occurs when the buffer is attached, the separated buffer significantly increases the loading rate. As already mentioned, Exp. 11395—where the buffer separated ~1 mm—had sustained dwell (see Figs. A-13 and A-14); however, there was extensive fracture around the periphery of the cylinder (a cone crack and possibly additional fractures formed, nominally originating from the edge of the buffer to the sides of the target). Thus, not only does the impact stress increase significantly as the buffer separates, but the loading rate is much higher. Clearly, the higher impact stress produces more damage, but the higher loading rate may also contribute to the damage accumulation (or perhaps rate of damage accumulation), as seen in Fig. A-13.

5.5 Computations using a Cover Plate

It is desirable experimentally, to make the buffer diameter as large as possible (to make it easier to hit) and to make it as thin as possible (to reduce mass). A desirable buffer geometry has a diameter equal to that of the target ($d = 20$ mm) and a thickness of 2 mm (based on Fig. 32a), but it is important that these changes not affect the original purpose of the buffer (attenuate the shock and gradually load the ceramic). Figure 43 presents computed results for a full-diameter buffer ($h = 2$ mm, $d = 20$ mm) and for the original buffer ($h = 4$ mm, $d = 5$ mm) at an impact velocity of $v_p = 1400$ m/s. The computed results show material damage (D) at $t = 10$ µs after impact for the original buffer and $t = 7$ µs after impact for the full-diameter buffer (the time difference accounts for the difference in buffer thickness). The damaged regions are nearly identical indicating that a buffer thickness of 2 mm is sufficient to attenuate the shock and allow for gradual loading.
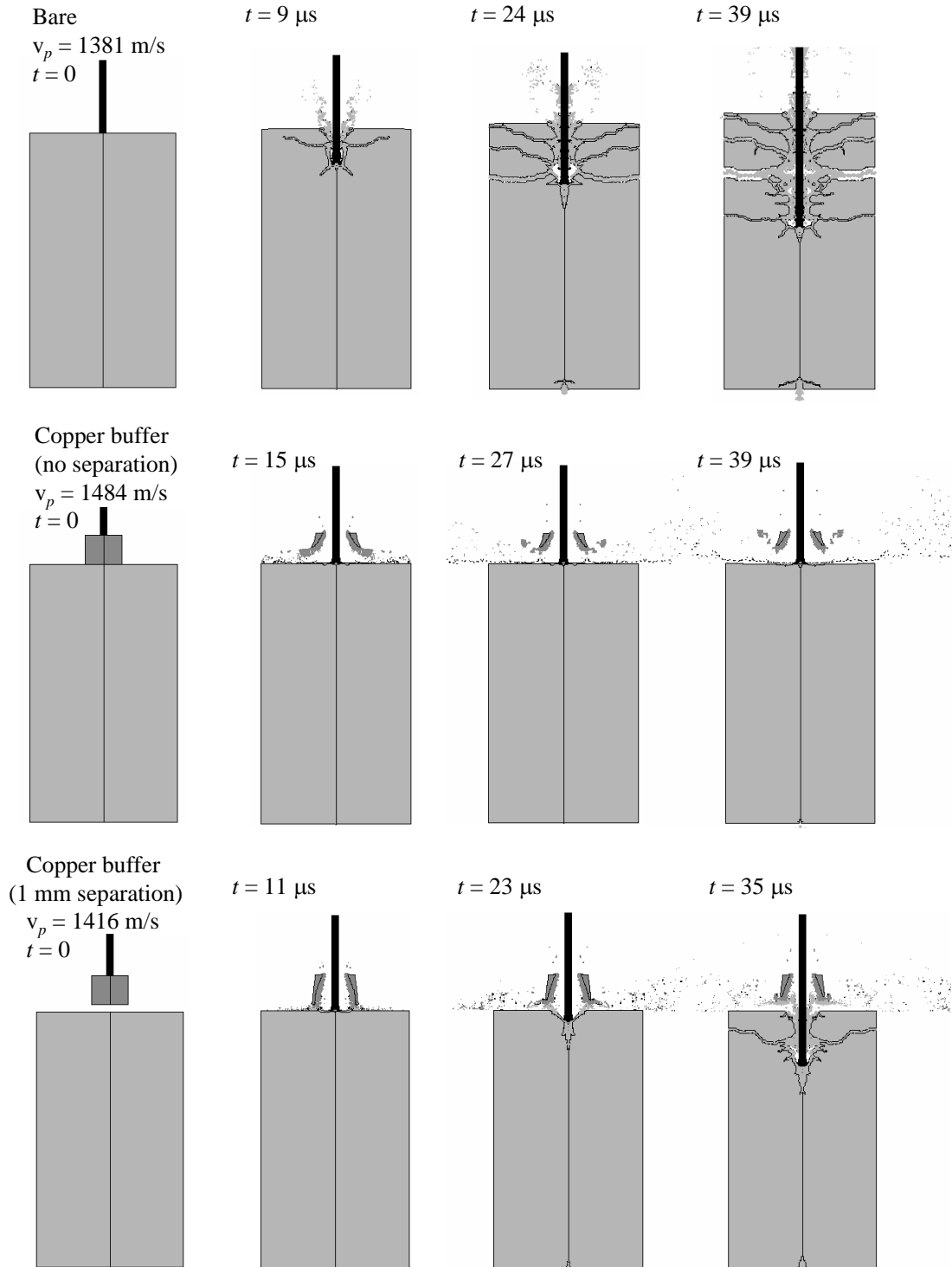
Figure 40.   Computed results showing material, for a target with no buffer, a target with an attached buffer, and a target with a separated buffer.

No separation   Separation = 0.3 mm   Separation = 0.5 mm   Separation = 1.0 mm

v_p = 1400 m/s (t = 0)

Damage (t = 10 µs)

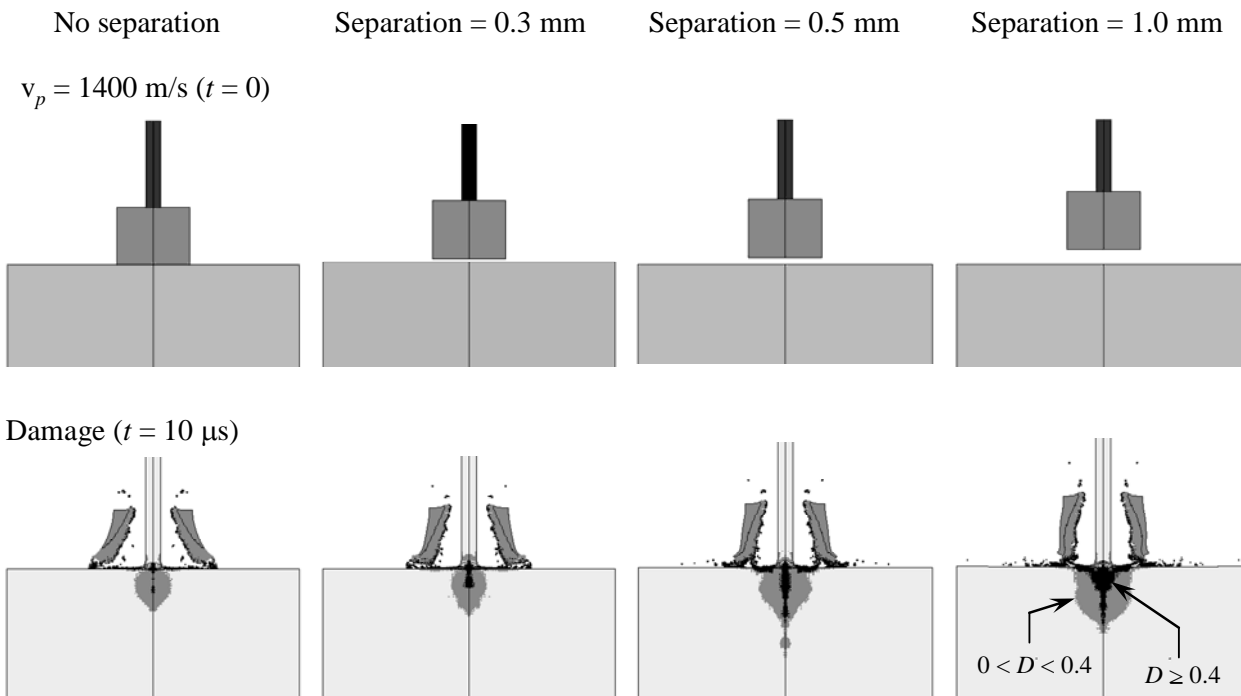$0 < D < 0.4$ $D \geq 0.4$

Figure 41. Computed results of a target with a buffer impacted by an Au rod at 1400 m/s as a function of buffer separation. The results show material damage (D) 10 µs after impact.
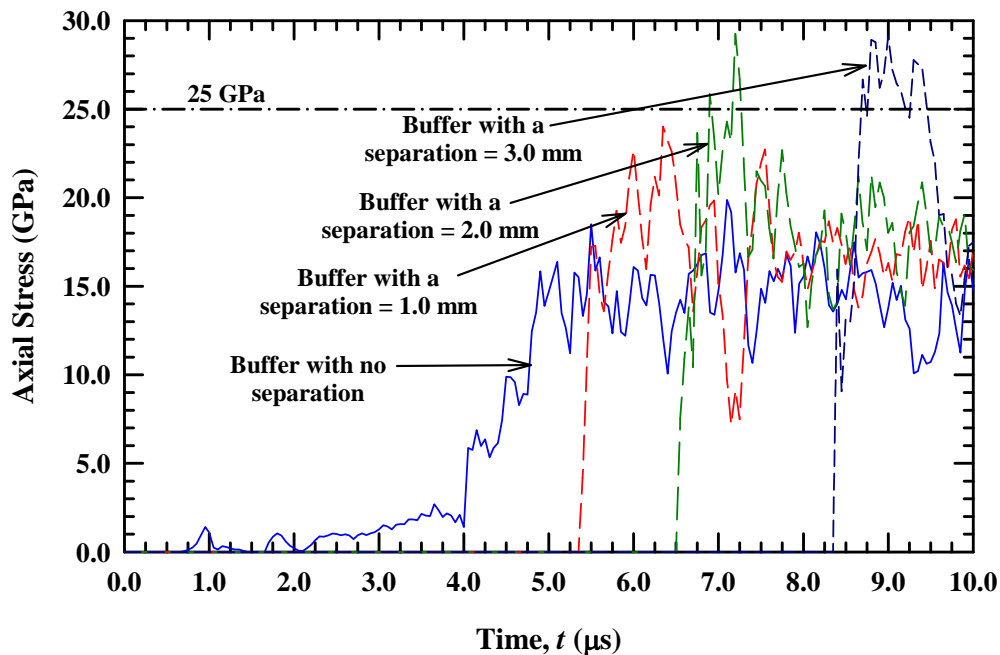
Figure 42. Computed results showing impact stress on ceramic as a function of time for a buffer with no separation and separations of 1.0, 2.0, and 3.0 mm. The impact velocity is 1400 m/s.
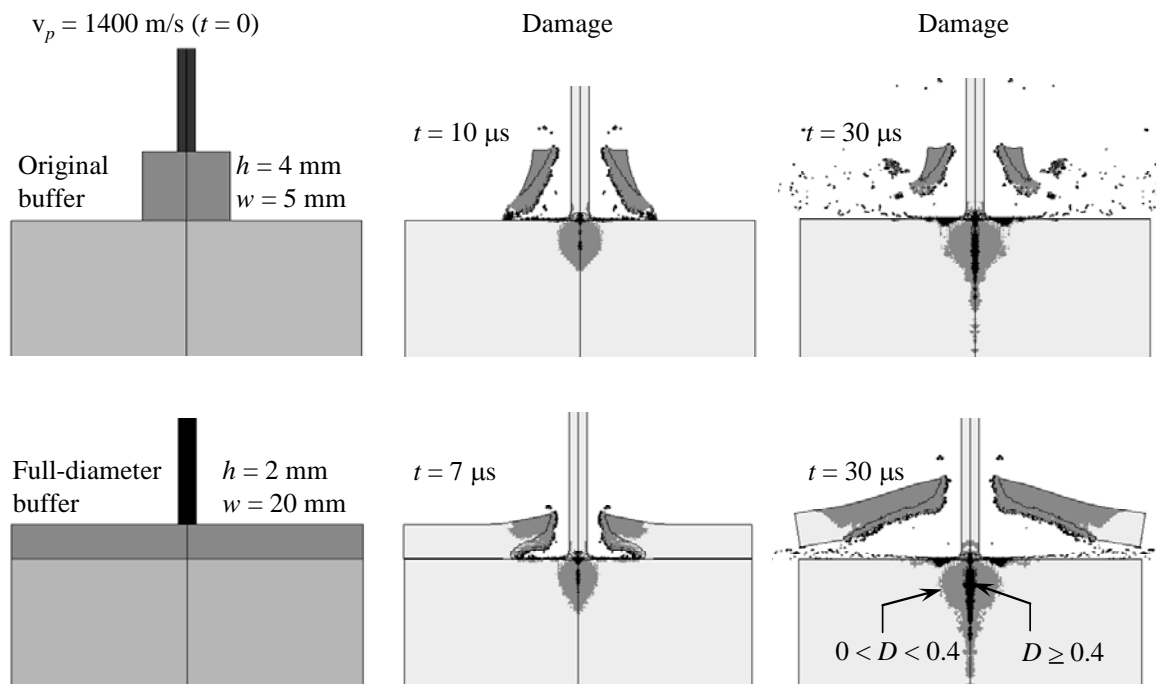
Figure 43. Computed results for an Au rod impacting a small and large diameter buffer at 1400 m/s. The results show material damage (*D*) at early and later times.

The computed results are also presented at $t = 30$ µs in Fig. 43. The damaged regions are again very similar, although there appears to be slightly more damage for the full-diameter configuration. This occurs from additional stresses produced from the projectile debris being channeled between the cover plate and the ceramic surface. Computations using the original buffer and the full diameter buffer, at an impact velocity of 1550 m/s, are compared in Fig. 44. The computed results show interface defeat at 1550 m/s for the original buffer and a long dwell phase (over 40 µs) with slight penetration for the full diameter buffer. These results suggest that using a larger diameter (thinner) buffer will slightly reduce the dwell-penetration velocity by approximately 30 m/s (1550 m/s vs. 1580 m/s).

There is not clear experimental evidence, at this point, that a cover plate is slightly detrimental to dwell and interface defeat, (see Fig. 26). Although there are two "small" buffer experiments that have longer dwell than the two cover plate experiments in the velocity range of 1570 – 1620 m/s, the two preliminary experiments had a slightly different geometry (as already discussed). Further, the cover plate experiment at 1570 m/s had a longer dwell time than the buffered experiment at 1550 m/s. The differences in dwell times observed between 1550 and 1620 m/s may be solely due to a zone of mixed results, and have nothing to do with the dimensions of the buffer and/or difference in geometry.

There are differences and similarities between the simulations and the experiments with the cover plate. The simulations show that the Au debris slides along the Cu plate-ceramic interface and causes the Cu plate to separate from the ceramic. Additionally, there is a bending up of the plate, with plate separation starting near the projectile-target centerline. In the experiments—as seen in Figs. 14 and 15—the Au debris forces a bulging of the cover plate at 24.6 µs. The computational results for the 2-mm-thick cover plate, Fig. 44, indicates a similar response (plate bulging) at 20 µs. The cover plate appears to remain attached to the ceramic in Fig. 14, where it
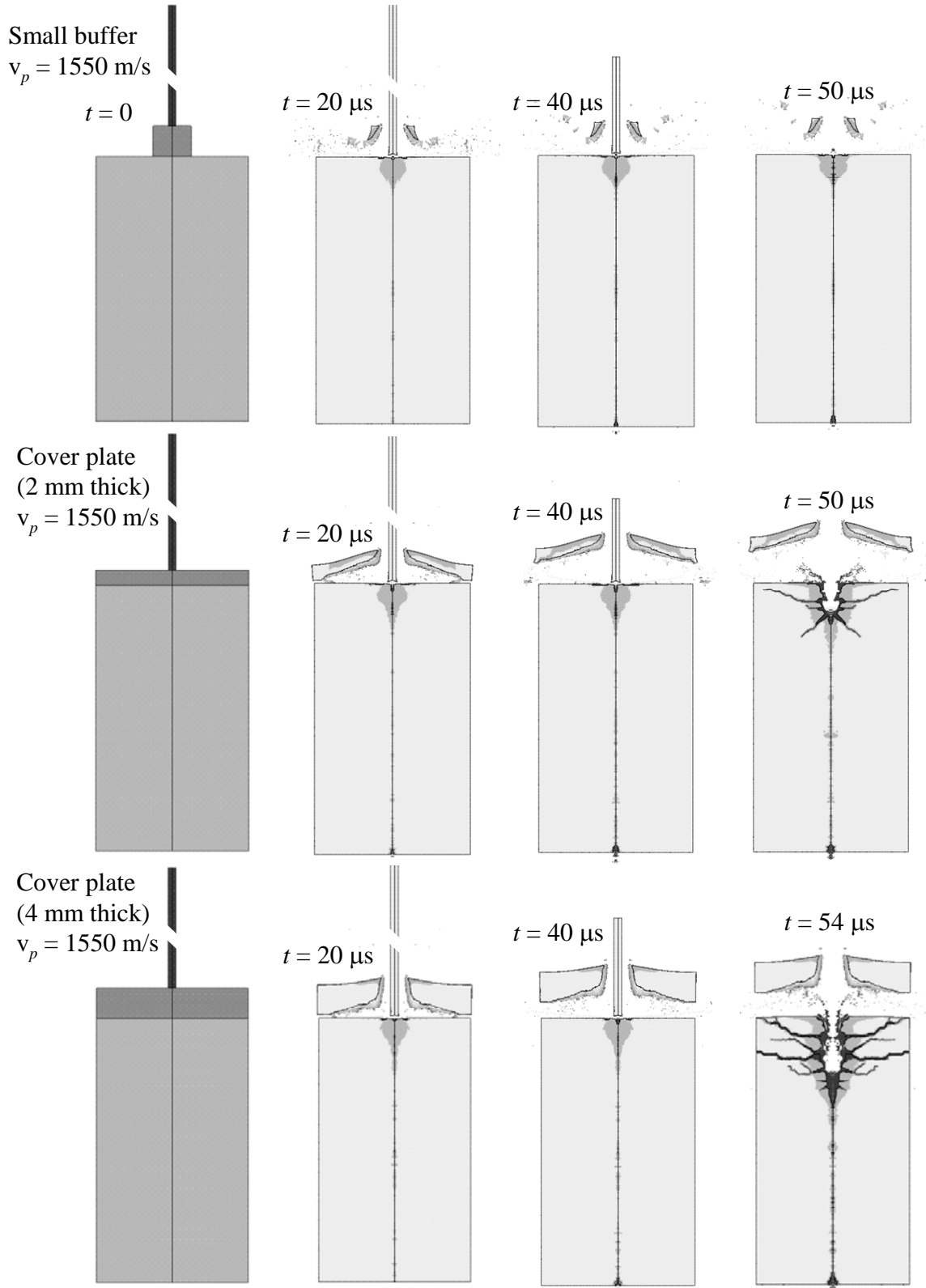
Figure 44. Computed results for an Au rod impacting a small diameter buffer and a cover plate with different thicknesses at 1550 m/s. The results show damage at three times after impact.

has separated in Fig. 44. It can be argued that if the "glue bond" was somewhat stronger in the simulation, than the plate would not have separated as easily. This would result in more local bulging/deformation of the cover plate because the radial flow of the Au debris is impeded by the glue bond. On the other hand, three cover plate experiments were conducted during our investigation of dwell on borosilicate glass [30]. There was a long dwell period in two of these experiments; the cover plate did not bulge, but instead, it was separated from the glass surface by the Au debris, similar to middle row of computational results in Fig. 44. In the third experiment, the impact velocity was sufficiently high that there was little or no dwell and the cover plate remained attached to the glass (with no bulging of the cover plate).

The cover plate thickness was increased to 4 mm in the next simulation. It is seen in the bottom row of Fig. 44 that the increased cover plate thickness results in considerably more damage to the SiC than for the thinner plate. We believe that the increased inertia of the thicker cover plate results in higher stresses on the ceramic (since it is more difficult for the eroding Au rod to move the cover plate material).

The results of these simulations using thicker and thinner cover plates are intriguing, but are too few to be conclusive. We hope to investigate the question of the effects of a buffer or cover plate further in future experiments.

6.0 Summary and Conclusions

Reverse impact experiments were conducted to determine dwell and transition velocities for unconfined SiC ceramic against long gold rods. The targets were either completely bare or had a small copper buffer on the front. Results show that for a bare ceramic stable dwell (interface defeat) is possible for impact velocities up to approximately 800 m/s. With a small Cu-buffer attached to the impact surface, the transition velocity is increased to around 1550 m/s. X-ray images and high-speed videos reveal that once penetration is initiated the ceramic is damaged around much of the circumference. It is noted that the penetration velocities correspond well with experiments done with pre-damaged ceramics [35-36].

The transition velocities determined for the buffered experiments conducted here are 50 m/s to 100 m/s lower than determined in a similar test arrangement where the rod diameter was 25% smaller [1]. There maybe a scaling or size effect involving the rod diameter. Additional experiments are being planned to investigate this possible scaling effect.

Numerous computations were performed to provide insight into the design, testing and analysis of the experiments. Most of the computations used the EPIC [37] code although CTH [38] was also used. The computations investigated the response of both bare and buffered targets including the effects of buffer separation, buffer diameter, and buffer thickness.

Numerous observations of the experimental and computational results were made and are listed below.

1. The gold rod penetrates with essentially no deceleration (except for the last few diameters, e.g., during dwell); thus, the sum of the penetration and consumption velocities is the impact velocity, i.e., $u + v_c = v_p$.

2. In some experiments with sustained dwell, $v_c \neq v_p$; v_c is slightly less than v_p, implying that there is a very low penetration velocity and/or slight erosion of the surface.

3. It was shown that the penetration velocity, although quasi-linear with time, is not steady state for most of the experiments at impact velocities $v_p \leq$ ~1.6 km/s.

4. Penetration resistance, R_t, could achieve values on the order of 20 GPa (using a copper buffer to achieve dwell), but after transition to penetration, R_t decreases to ~5 GPa to ~9 GPa, depending upon the impact velocity.

5. The penetration resistance of bare and initially buffered SiC are the same once penetration is initiated.

6. The experimental dwell-penetration transition velocity for an Au rod onto bare SiC was found to be $V_t = 822 \pm 46$ m/s; the associated Bernoulli stress is 6.52 GPa. It is acknowledged that the uncertainty in the dwell-penetration transition velocity may, in fact, be larger since the transition is inherently an instability.

7. The experimental dwell-penetration transition velocity for a Cu-buffered target is $V_t = 1538 \pm 12$ m/s resulting in a transition stress of $\Sigma_t \sim 24$ GPa. Again, the number of tests was limited, so the ± 12 m/s is itself uncertain.

8. Analogous to the findings for dwell on borosilicate glass [30], there exists a mixed region of dwell-penetration response for buffered SiC targets: $1550 \leq v_p \leq 1653$ m/s. In this velocity regime the time extent of dwell appears to be varying (shorter versus longer dwell times). However, it could be these results are due to differences in the geometry (small diameter Au rod) in two of the experiments.

9. For bare targets, there is less than 3 μs of dwell for impact velocities above 1200 m/s. This "no-dwell" transition velocity is probably closer to 1000 m/s, but there are no experimental data between 958 m/s and 1200 m/s to provide a better estimate on the no-dwell transition velocity for bare SiC.

10. The no-dwell transition velocity for an Au gold rod onto a Cu-buffered target is 1653 ± 23 m/s, although it could be somewhat lower, 1592 ± 20 m/s. This uncertainty is because it is unknown whether the long dwell times of the two preliminary experiments are due to differences in projectile diameters or the existence of a zone of mixed results.

11. After dwell-penetration transition, the rod penetrates at the same velocity as if there had been no dwell. Similar results were seen with borosilicate glass [30].

12. It was observed, as with previous penetration data into SiC [35-36], that there is considerable variation in the penetration velocity as a function of impact velocity for 1300 m/s $\leq v_p \leq 1700$ m/s; that is, the penetration velocity falls within a fairly wide band. This is probably a consequence of nonsteady penetration within individual experiments.

13. The computed transition velocity for a bare target was 785 ± 5 m/s; and while a little lower than the experimental value, it is within the uncertainty band of the experimental value.

14. The shock stress is approximately 18 GPa at the dwell-penetration transition velocity (780 m/s).

15. A copper buffer of height $2D_p$ and diameter $2D_p$ attenuates the initial impact shock and gradually loads the ceramic.

16. When the buffer is used, the computational dwell-penetration transition velocity is 1575 ± 5 m/s ($\Sigma_t \sim 25$ GPa), slightly higher than the experimental value of 1538 ± 12 m/s ($\Sigma_t \sim 24$ GPa).

17. There is a significant difference between the shock stress (no buffer) that results in penetration (18 GPa) and the transition stress ($\Sigma_t = 24 - 25$ GPa) that results in penetration.

18. The penetration velocity is significantly nonlinear (for both the computed and experimental result) over the impacted velocities investigated. The computed results suggest a series of time-varying penetration events characterized by generating failed material (slower penetration) followed by the penetration of the failed material (faster penetration), and then repeating this sequence.

19. Buffer separation (prior to projectile impact) produces a higher loading rate on the ceramic surface, a higher impact stress, and greater damage, resulting in a reduction in the transition velocity.

20. Computationally, a full diameter buffer plate ($h/D_p = 2$, $w = 20$ mm) slightly reduces the transition velocity (by approximately 30 m/s) compared to the thicker/smaller buffer ($h/D_p = 4$, $w = 5$ mm).

21. Computationally, a thick cover plate ($h/D_p = 4$) results in more damage to the ceramic than a thinner ($h/D_p = 2$) cover plate, probably because the inertia of the thicker plate results in larger stresses at the plate/ceramic interface as projectile debris tries to flow radially. Thus, although the cover plate is necessary to attenuate the shock, too thick of a cover plate is detrimental to potential performance.

7.0 Acknowledgements

52

8.0 References

1. Holmquist T. J., C. E. Anderson, Jr. and T. Behner. 2005. "Design, Analysis and Testing of an Unconfined Ceramic Target to Induce Dwell," *Proc. 22nd Int. Symp. Ballistics*, **2**, 860-868, DES*tech* Publications, Inc., Lancaster, PA.

2. Behner, T., C. E. Anderson, Jr., T. J. Holmquist, M. Wickert and D. W. Templeton. 2008. "Interface Defeat for Unconfined SiC Ceramics," *Proc. 24th Int. Symp. on Ballistics*, **1**, 35-42, DES*tech* Publications, Inc., Lancaster, PA.

3. Holmquist T. J., C. E. Anderson, Jr. and T. Behner. 2008. "The Effect of a Copper Buffer on Interface Defeat," *Proc. 24th Int. Symp. on Ballistics*, **2**, 721-728, DES*tech* Publications, Inc., Lancaster, PA.

4. Anderson C. E., Jr., T. Behner, D. L. Orphal, A. E. Nicholls, T. J. Holmquist and M. Wickert. 2008. "Long-Rod Penetration into Intact and Pre-damaged SiC Ceramic," *Proc. 24th Int. Symp. on Ballistics*, **2**, 822-829, DES*tech* Publications, Inc., Lancaster, PA.

5. Wilkins M. L., 1967. "Second Progress Report of Light Armor Program," Report No. UCRL-50349, Lawrence Livermore National Laboratory.

6. Hauver G. E., and A. Melani. 1988. "Behavior During Penetration by Long Rods," *Proceedings of the Second BRL Topical Symposium: Experimental Research and Modeling Support*, pp. 149-160, U. S. Army Ballistic Research Laboratory, Aberdeen Proving Ground, MD.

7. Hauver G. E., P. H. Netherwood, R. F. Benck, W. A. Gooch, W. J. Perciballi and M. S. Burkins. 1992. "Variation of Target Resistance During Long-Rod Penetration into Ceramics," *Proc. 13th Int. Symp. on Ballistics*, **3**, 257-264, National Defence Establishment, Sundyberg, Sweden;.

8. Hauver G. E., P. H. Netherwood, R. F. Benck, and L. J. Kecskes. 1993. "Ballistic Performance of Ceramics," *Proc. 13th Army Symp. on Solid Mechanics*, Plymouth, MA.

9. Hauver G. E., P. H. Netherwood, R. F. Benck, and L. J. Kecskes. 1994. "Enhanced Ballistic Performance of Ceramics," *Proc. 19th Army Science Conf.*, Orlando, FL.

10. Hauver G. E., E. J. Rapacki, Jr., P. H. Netherwood, and R. F. Benck. 2005. "Interface Defeat of Long-Rod Projectiles by Ceramic Armor," Army Research Laboratory Report, ARL-TR-3590, Aberdeen Proving Ground, MD.

11. Rosenberg Z. and J. Tsaliah. 1990. "Applying Tate's Model for the Interaction of Long Rod Projectiles with Ceramic Targets," *Int. J. Impact Eng*. **9**(2), 247-251.

12. den Reijer, P. C. 1991. "Impact on Ceramic Faced Armor," PhD dissertation, Delft University of Technology, The Netherlands.

13. Bless S. J., M. Benyami, L. S. Apgar, and D. Eylon. 1990. "Impenetrable Ceramic Targets Struck by High Velocity Tungsten Long Rods," *Proc. 2nd Int. Conf. on Structures Under Shock and Impact*, 27-38, P. S. Bulson, eds, Computational Mechanics Publication, Southampton, UK.

14. Lundberg P., L. Holmberg and B. Janzon. 1998. "An Experimental Study of Long Rod Penetration into Boron Carbide at Ordnance and Hyper Velocities," *Proc. 17th Int. Symp. on Ballistics,* **3**, 251-258, South Africa Ballistics Organisation, South Africa.

15. Lundberg P., R. Renstrom and B. Lundberg. 2000. "Impact of Metallic projectiles on Ceramic Targets: Transition between Interface Defeat and Penetration," *Int. J. Impact Eng*. **24**(3), 259-275.

16. Lundberg P., R. Renstrom, and L. Holmberg. 2001. "An Experimental Investigation of Interface Defeat at Extended Interaction Time," *Proc. 19th Int. Symp. on Ballistics*, **3**, 1463-1469, RAUG Land Systems, Switzerland.

17. Lundberg P. and B. Lundberg. 2005. "Transition Between Interface Defeat and Penetration for Tungsten Projectiles and Four Silicon Carbide Materials," *Int. J. Impact Eng*., **31**(7), 781-792.

18. Lundberg P., R. Renstrom and B. Lundberg. 2006. "Impact of Conical Tungsten Projectiles on Flat Silicon Carbide Targets: Transition from Interface Defeat to Penetration," *Int. J. Impact Eng*., **32**(11), 1842-1856.

19. Andersson, O., P. Lundberg and R. Renstrom. 2007. "Influence of Confinement on the Transition Velocity of Silicon Carbide," *Proc. 23rd Int. Symp. on Ballistics*, **2**, 1273-1280, Gráficas Couche, Madrid, Spain.

20. Johnson, G. R., T. J. Holmquist and S. R. Beissel. 2003. "Response of Aluminum Nitride (Including a Phase Change) to Large Strains, High Strain Rates, and High Pressures," *J. Appl. Phys.*, **94**(3), 1639-1646.

21. Johnson, G. R., R. A. Stryk, S. R. Beissel and T. J. Holmquist. 2002. "An Algorithm to Automatically Convert Distorted Finite Elements into Meshless Particles during Dynamic Deformation," *Int. J. Impact Eng.*, **27**(10), 997-1013.

22. Johnson, G. R., S. R. Beissel, and R. A. Stryk. 2002. "An Improved Generalized Particle Algorithm that includes Boundaries and Interfaces," *Int. J. Numer. Meth. Eng.,* **53**, 875-904.

23. Holmquist, T. J. and G. R. Johnson. 2005. "Characterization and Evaluation of Silicon Carbide for High-Velocity Impact," *J. Appl. Phys.,* **97**, 093502.

24. Holmquist T. J. and G. R. Johnson. 2002. "Modeling Ceramic Dwell and Interface Defeat," ***Ceramic Armor Materials by Design*** (J. W. McCauley, *et al.*, Eds.), *Ceramic Transactions*, **134**, The American Ceramic Society.

25. Holmquist T. J. and G. R. Johnson. 2002. "A Detailed Computational Analysis of Interface Defeat, Dwell and Penetration for a Variety of Ceramic Targets," *Proc. 20th Int. Symp. on Ballistics*, **2**, 746-753, DES*tech* Publications, Lancaster, PA.

26. Anderson, C. E. Jr. and D. L. Orphal. 2008. "An Examination of Deviations from Hydrodynamic Theory," *Int. J. Impact Engng.*, **35**(12), 1386-1392.

27. Anderson, C. E. Jr. and J. D. Walker. 1991. "An Examination of Long-Rod Penetration," *Int. J. Impact Engng.*, **11**(4), 481-501.

28. Steinberg, D. J. 1996. "Equation of State and Strength Properties of Selected Materials," UCRL-MA-106439, Rev. 1, Lawrence Livermore National Laboratory, Livermore, CA.

29. Anderson, C. E. Jr., Th. Behner, T. J. Holmquist, M. Wickert, V. Hohler and D. Templeton. 2007. "Interface Defeat of Long Rods Impacting Borosilicate Glass," *Proc. 23rd Int. Symp. Ballistics*, **2**, pp. 1049-1056, Gráficas Couche, Madrid, Spain.

30. Anderson, C. E. Jr., T. Behner, D. L. Orphal, T. J. Holmquist, V. Hohler, and M. Wickert. 2008. "Interface Defeat of Long Rods Impacting Borosilicate Glass," SwRI Report 18.12544/009, prepared for RDECOM-TARDEC, AMSRD-TAR-R, Warren, MI, February 2009.

31. Behner, T, D. L. Orphal, V. Hohler, C. E. Anderson, Jr., R. Mason, and D. W. Templeton. 2006. "Hypervelocity Penetration of Gold Rods into SiC-N for Impact Velocities from 2.0 to 6.2 km/s," *Int. J. Impact Engng.*, **33**(1-12), 68-79.

32. Tate, A. 1967. "Theory for the Deceleration of Long Rods after Impact," *J. Mech. Phys. Solids*, **15**, 387-399.

33. Tate, A. 1969. "Further Results in the Theory of Long Rod Penetration," *J. Mech. Phys. Solids*, **17**, 141-150.

34. Orphal, D. L. and R. R. Franzen. 1997. "Penetration of Confined Silicon Carbide Targets by Tungsten Long Rods at Impact Velocities from 1.5 to 4.6 km/s," *Int. J. Impact Engng*., **19**(1), 1-13.

35. Anderson C. E. Jr, T. Behner, D. L. Orphal, A. I. Nicholls, and D. W. Templeton. 2008. "Time-Resolved Penetration into Pre-Damaged Hot-Pressed Silicon Carbide. *Int. J. Impact Eng*., **35**(8), 661-673, 2008.

36. Anderson C. E. Jr., T. Behner, D. L. Orphal, A. E. Nicholls, T. J. Holmquist, and M. Wickert. 2008. "Long-Rod Penetration into Intact and Pre-Damaged SiC Ceramic," *Proc. 24ᵗʰ Int. Symp. Ballistics*, **2**, 822-829, DES*tech* Publications, Inc., Lancaster, PA.

37. Johnson, G. R., R. A. Stryk, T. J. Holmquist and S. R. Beissel. 1997. "Numerical Algorithms in a Lagrangian Hydrocode," Report No. WL-TR-1997-7039, Wright Laboratory.

38. McGlaun, J. M., S. L. Thompson, and M. G. Erlick. 1990. "CTH: A Three-Dimensional Shock Physics Code," *Int. J. Impact Eng*., **10**(1-4):351-360.

39. Holmquist, T. J., and G. R. Johnson. 2002. "Response of Silicon Carbide to High Velocity Impact," *J. App. Phys*., **91**(9): 5858-5866.

A-1

Appendix: Data Plots

The appendix contains the table with the position-time data of the rod penetration in the ceramic as well as the X-ray pictures for each of the experiments. Graphical plots of the data and regression fits are also shown.

Table A-1. Position-Time Data for All Experiments

|	*t* after imp [µs]	pen depth [mm]	rod length [mm]		*t* after imp [µs]	pen depth [mm]	rod length [mm]
		Bare				**Bare**	
11353	70.06	0	20.50	**11358**	54.05	28.70	24.80
	44.96	0	35.60		39.03	20.03	36.17
	22.99	0	47.87		24.02	8.83	45.71
	15.14	0	57.69		9.14	2.57	60.30
	0.00	0	70.04		0.00	0.00	70.07
	-10.08				-11.01		
11354	69.43	14.74	20.50				
	44.58	8.40	35.60			**Buffered**	
	29.37	6.43	47.87	**11377**	48.33	19.85	25.90
	14.41	1.38	57.69		36.25	13.14	35.70
	0.00	0.00	70.04		24.26	4.31	43.85
	-10.67				12.35	0.54	56.86
11355	60.32	27.42	25.32		0.00	-4.00	70.16
	42.35	16.32	34.99		-9.15		
	24.26	7.84	48.54	**11393**	51.97	fully	eroded
	6.44	1.38	63.78		39.87	0.86	15.41
	0.00	0.00	70.12		27.95	0.35	33.25
	-13.74				16.05	0.61	50.41
					0.00	-4.00	70.10
		Cover plate			-5.53		
11360	54.73	fully	eroded	**11395**	53.67	fully	eroded
	39.70	0	17.85		41.78	3.19	13.43
	24.63	0	38.20		29.69	1.48	30.49
	9.76	0	58.78		17.67	1.95	48.36
	0.00	-2.04	70.03		0.00	-4.00	70.06
	-10.40				-3.73		
11389	47.50	23.19	20.60	**11390**	50.47	30.12	26.14
	35.22	17.24	33.65		38.46	20.75	34.83
	23.36	7.17	42.64		26.36	12.14	44.60
	11.50	0.49	54.48		14.48	4.39	55.22
	0.00	-2.02	70.19		0.00	-4.00	69.97
	-8.74				-6.92		
11362	48.25	29.57	23.82	**11375**	50.43	complete	penetration
	36.13	19.01	32.45		38.39	26.47	36.05
	24.21	12.30	44.78		26.34	15.01	44.44
	12.39	5.10	56.92		14.54	6.83	56.24
	0.00	-2.04	70.06		0.00	-4.11	70.15
	-7.71				-6.83		
			Missed Buffer				
11359	54.24	28.21	23.94	**11370**	48.70	27.45	22.27
	39.21	22.09	38.18		36.77	21.67	34.40
	24.19	10.07	46.95		24.75	14.93	46.09
	9.25	3.20	60.57		12.79	4.63	54.56
	0.00	0	70.00		0.00	0	70.00
	-10.92				-7.28		
11361	46.83	complete	penetration	**11369**	47.29	complete	penetration
	34.84	24.97	41.73		35.24	25.10	38.63
	22.71	14.73	49.90		23.18	16.21	48.75
	10.84	4.85	58.04		11.26	6.76	58.84
	0.00	0	69.99		0.00	0	70.11
	-9.24				-8.81		
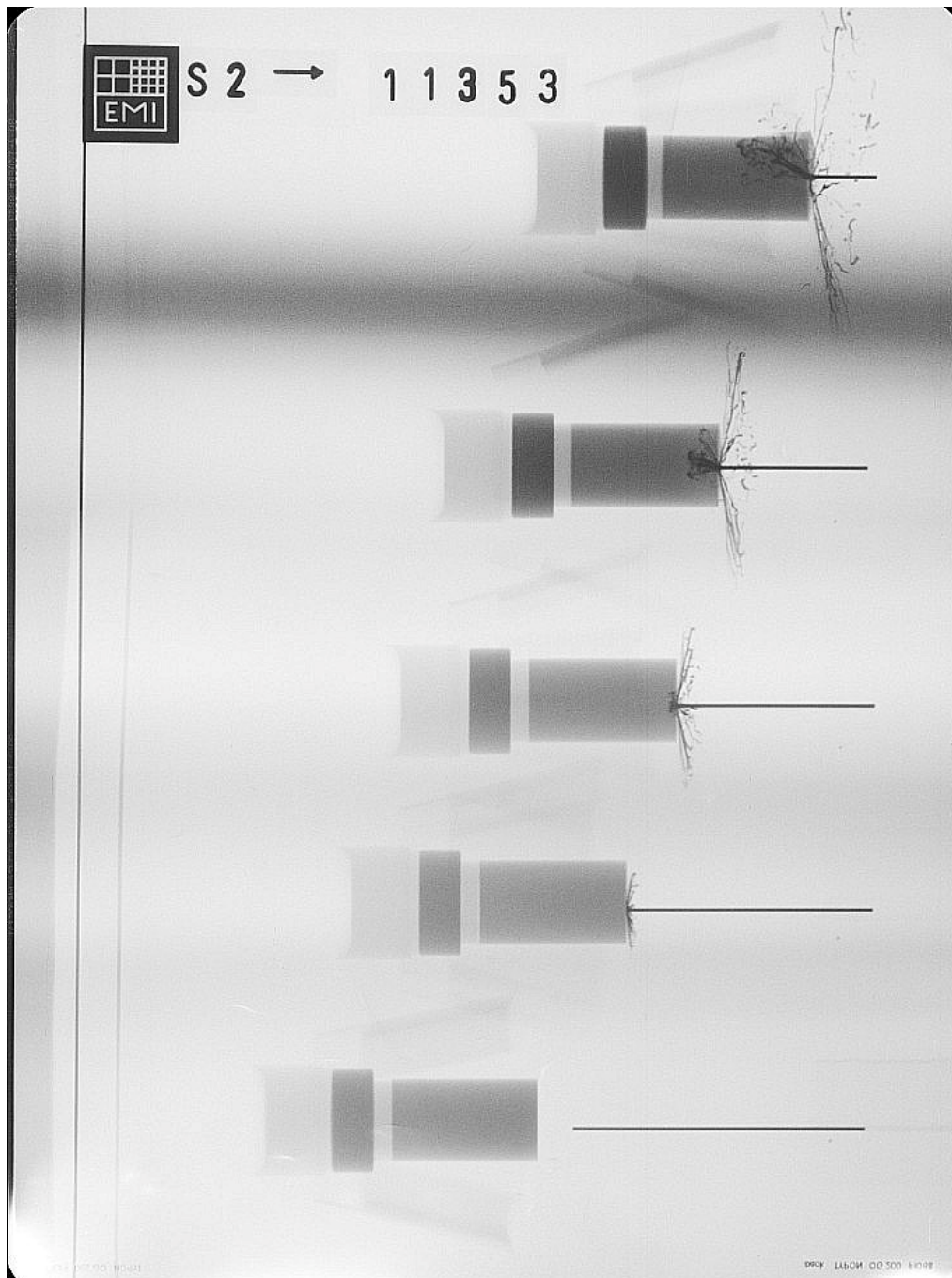
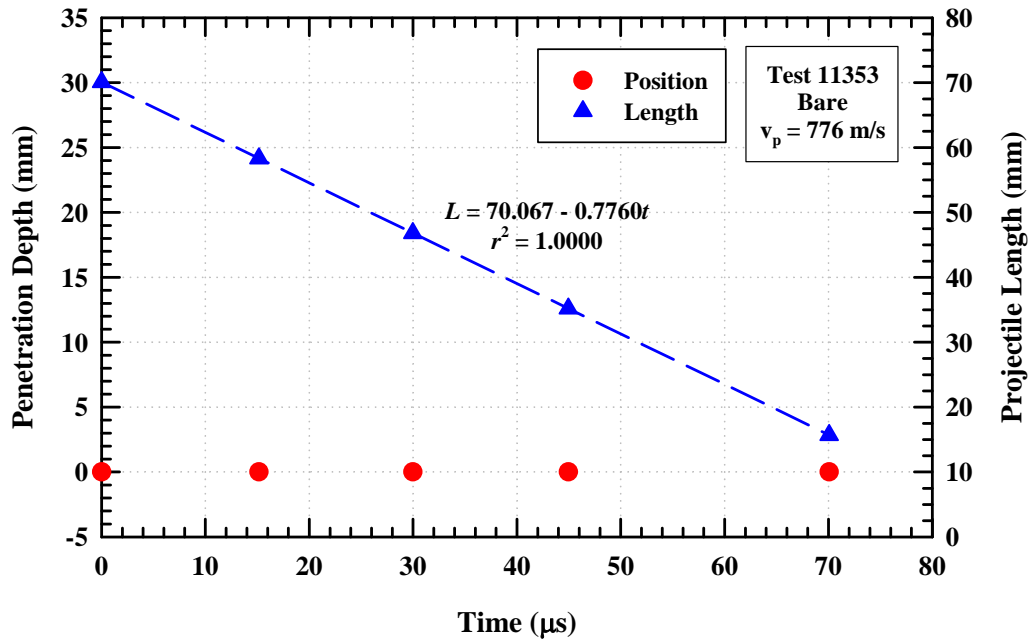**Figure A-1. X-ray picture for Exp. 11353: bare SiC, v_p = 776 m/s.**

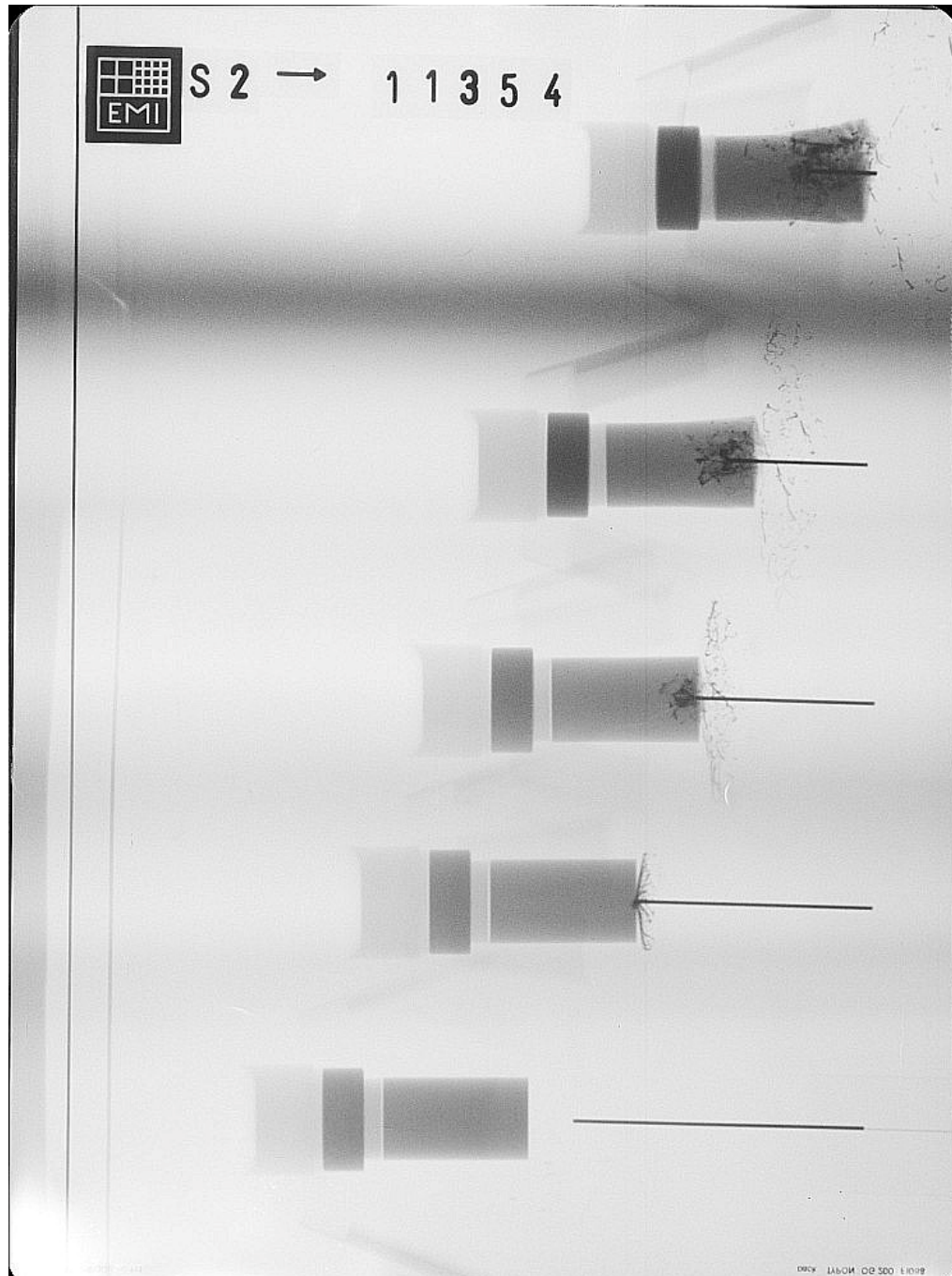**Figure A-2. Plot of test data for Exp. 11353.**

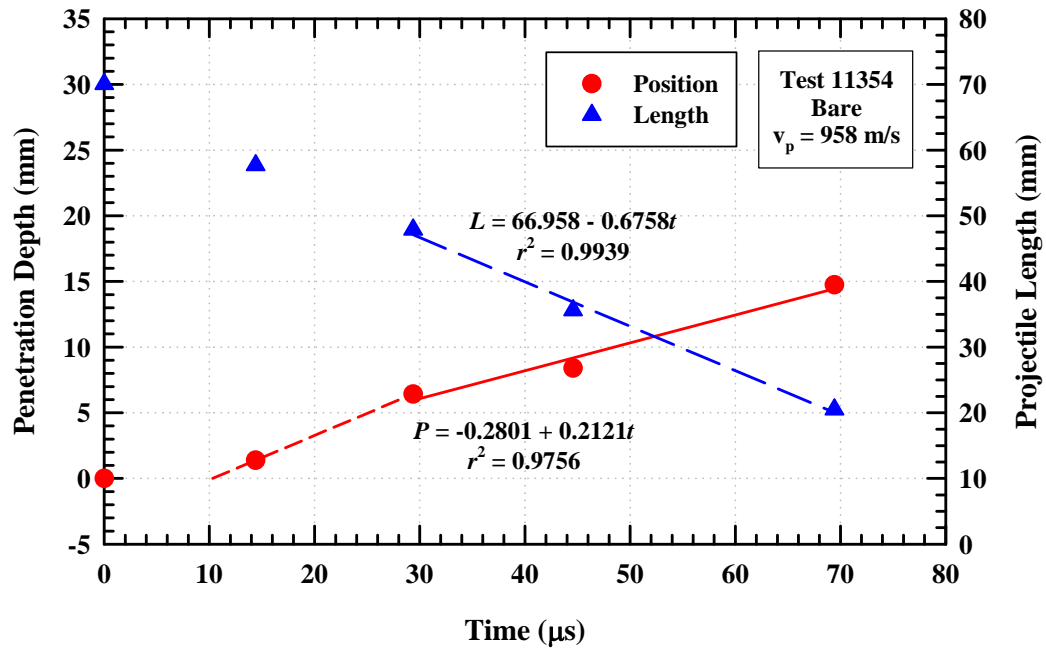**Figure A-3. X-ray picture for Exp. 11354: bare SiC, v_p = 958 m/s.**

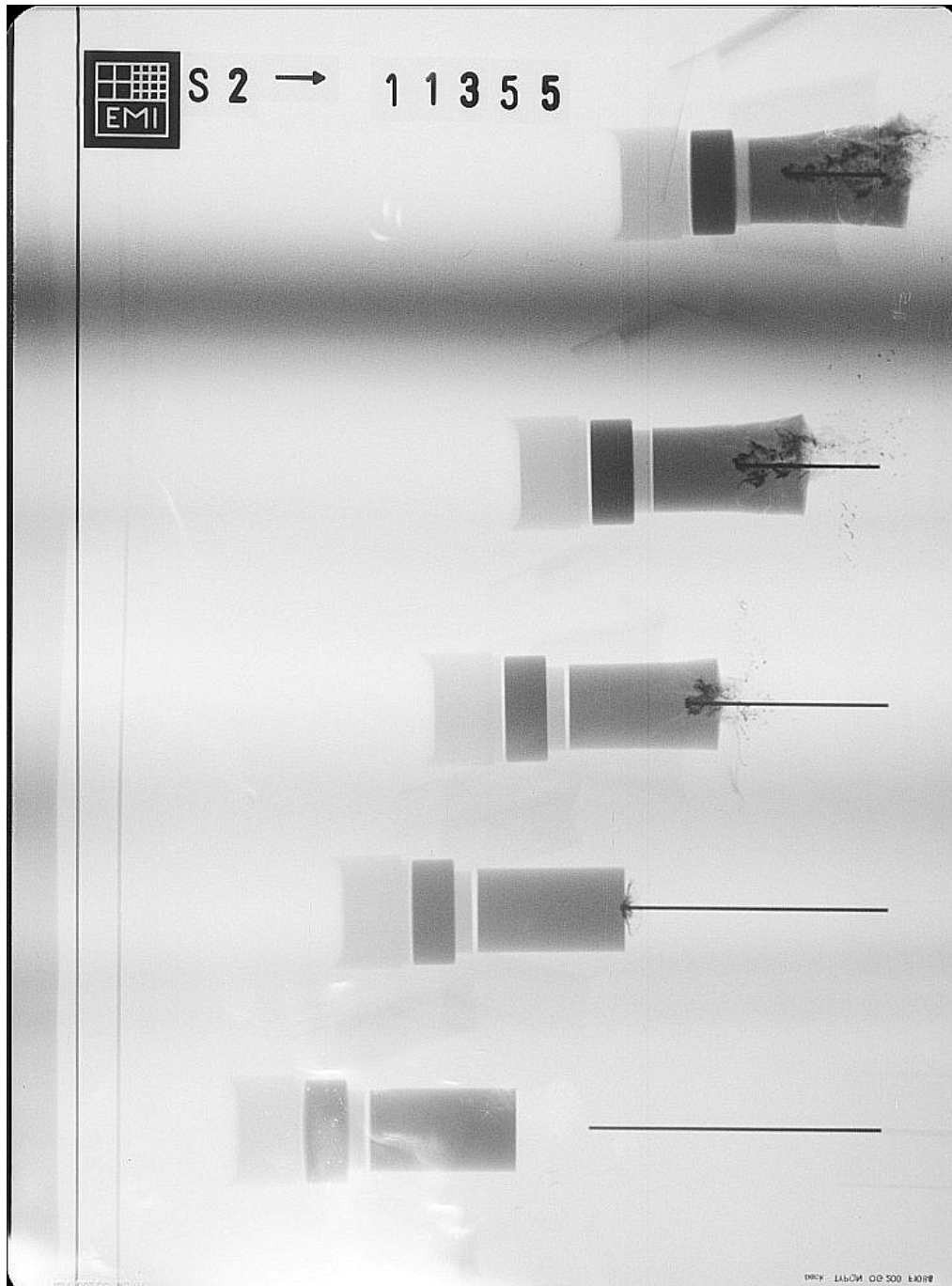**Figure A-4. Plot of test data for Exp. 11354.**

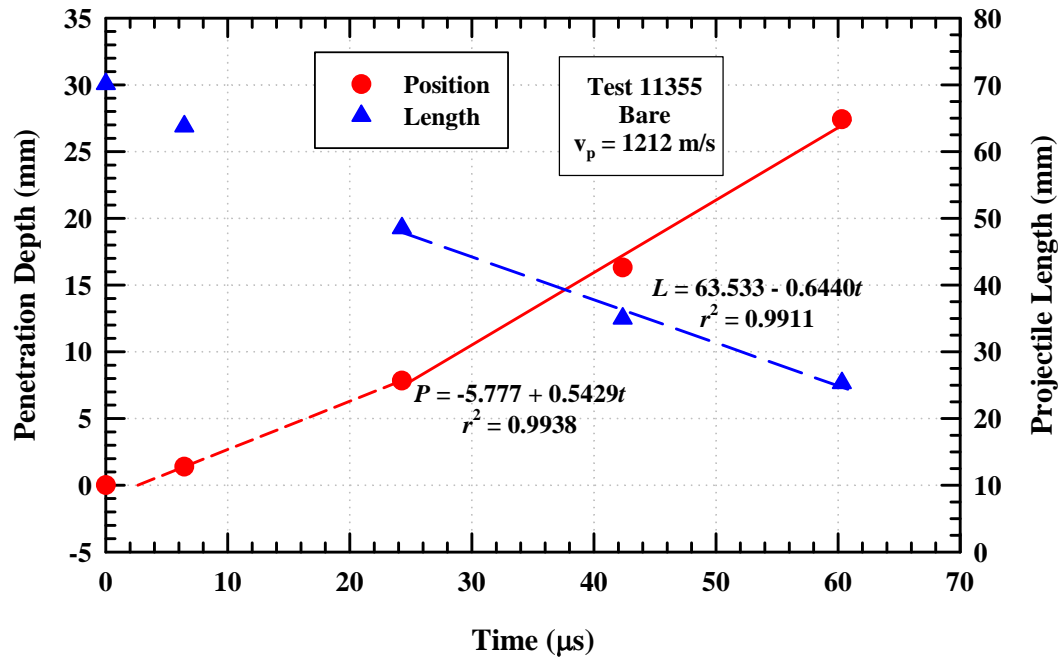**Figure A-5. X-ray picture for Exp. 11355: bare SiC, $v_p = 1212$ m/s.**
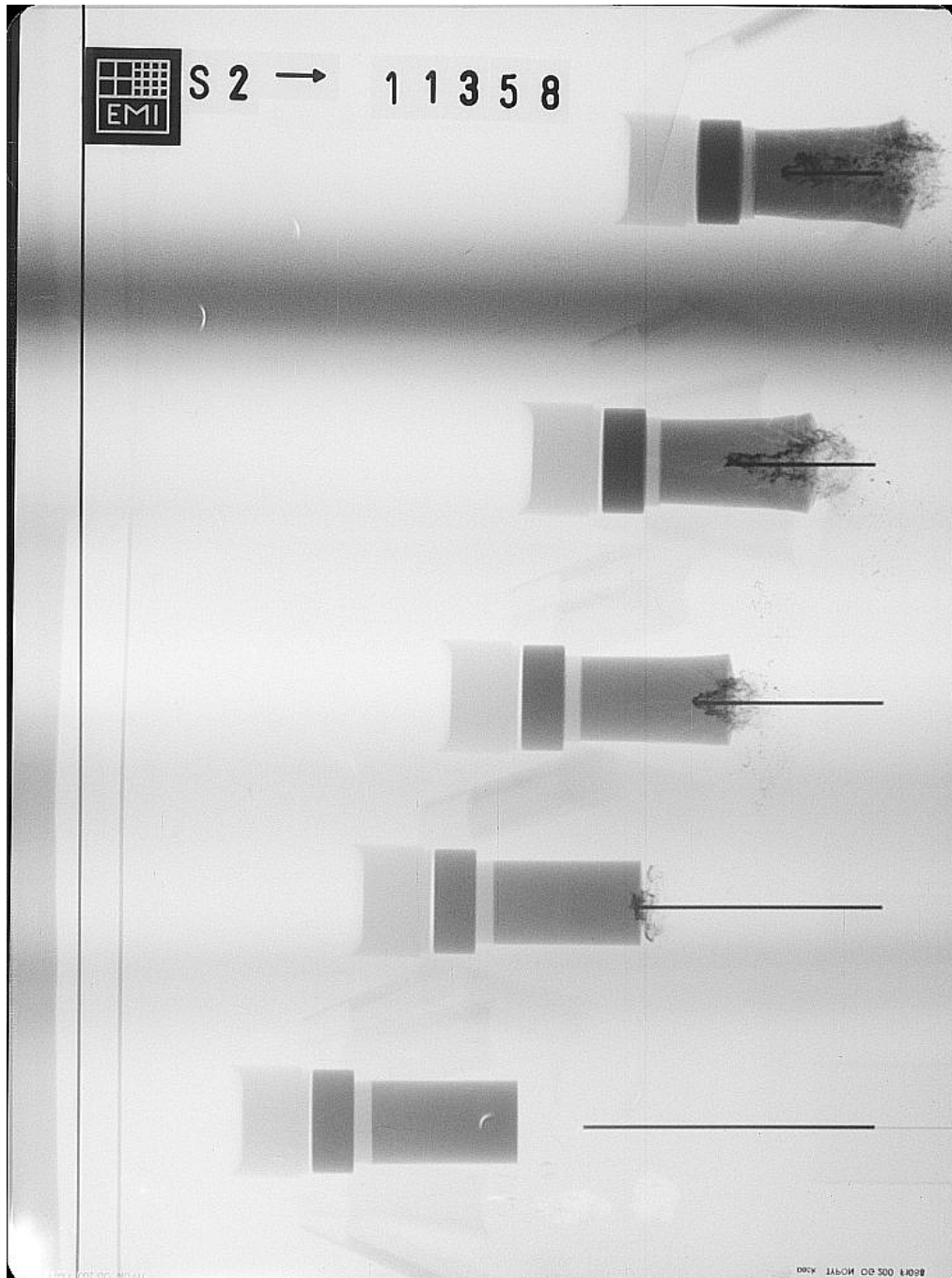
Figure A-6. Plot of test data for Exp. 11355.

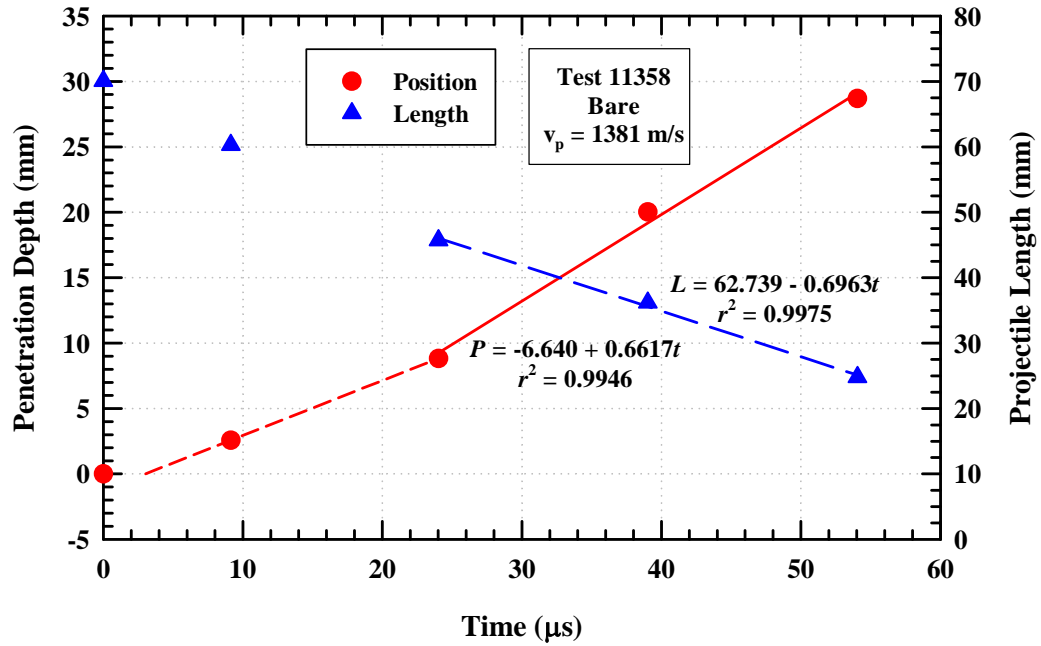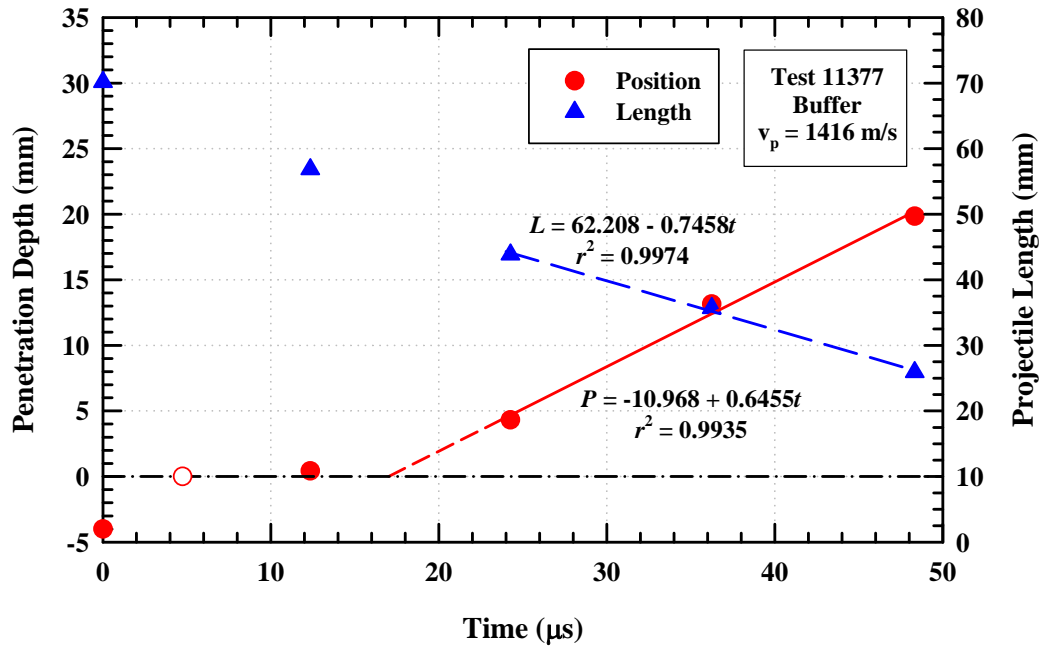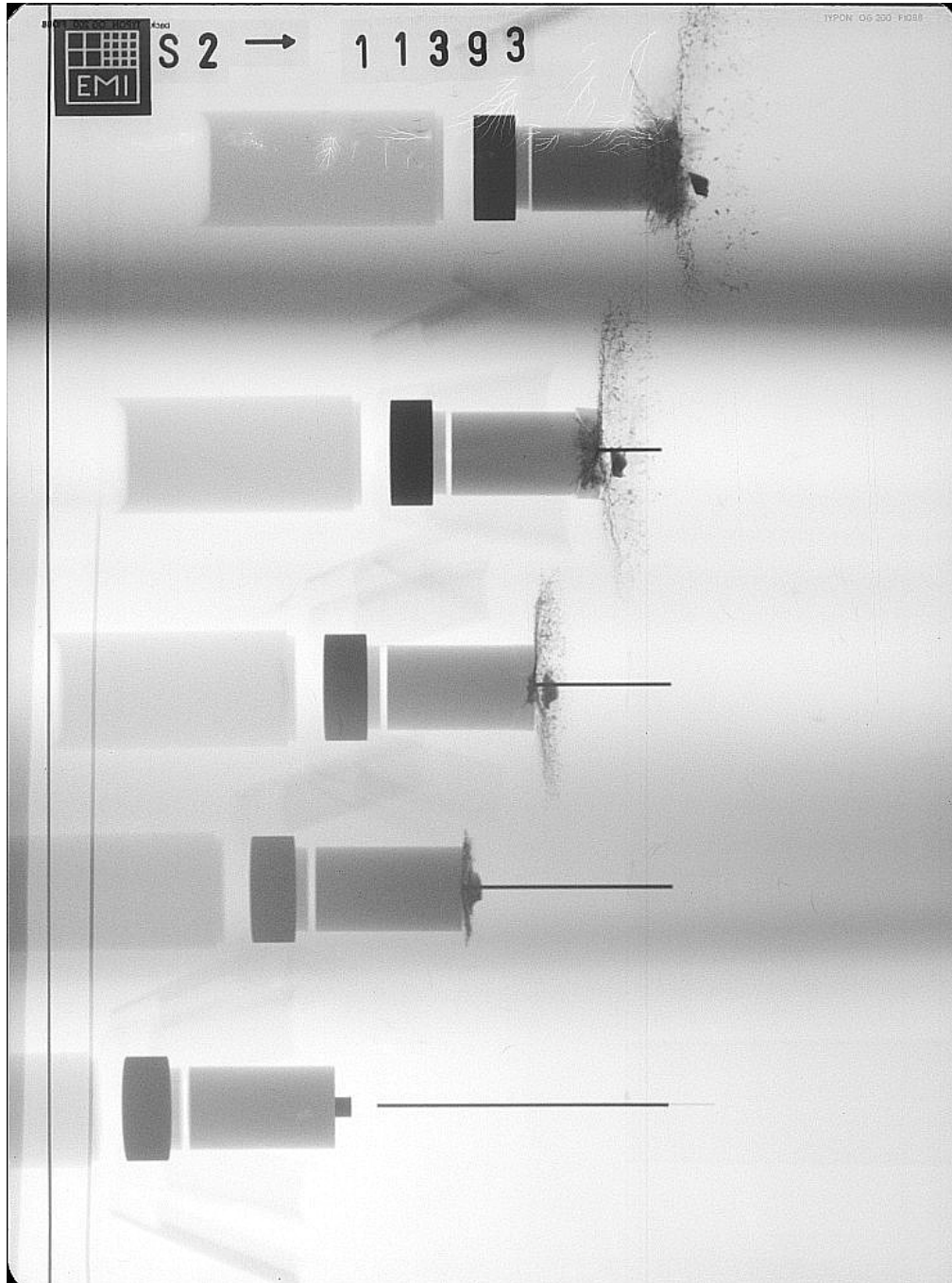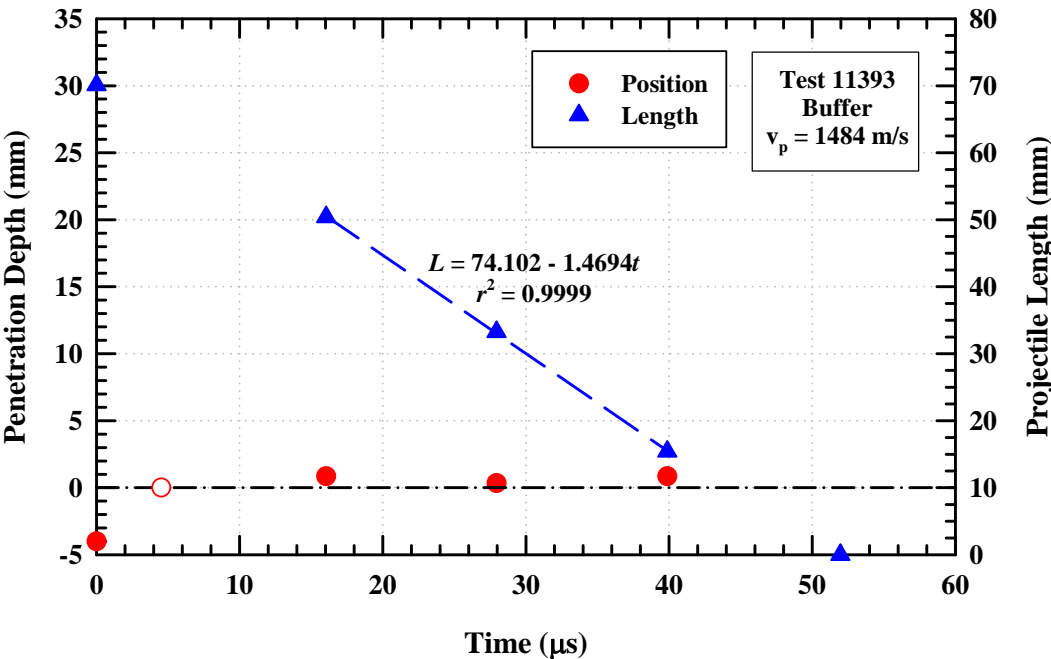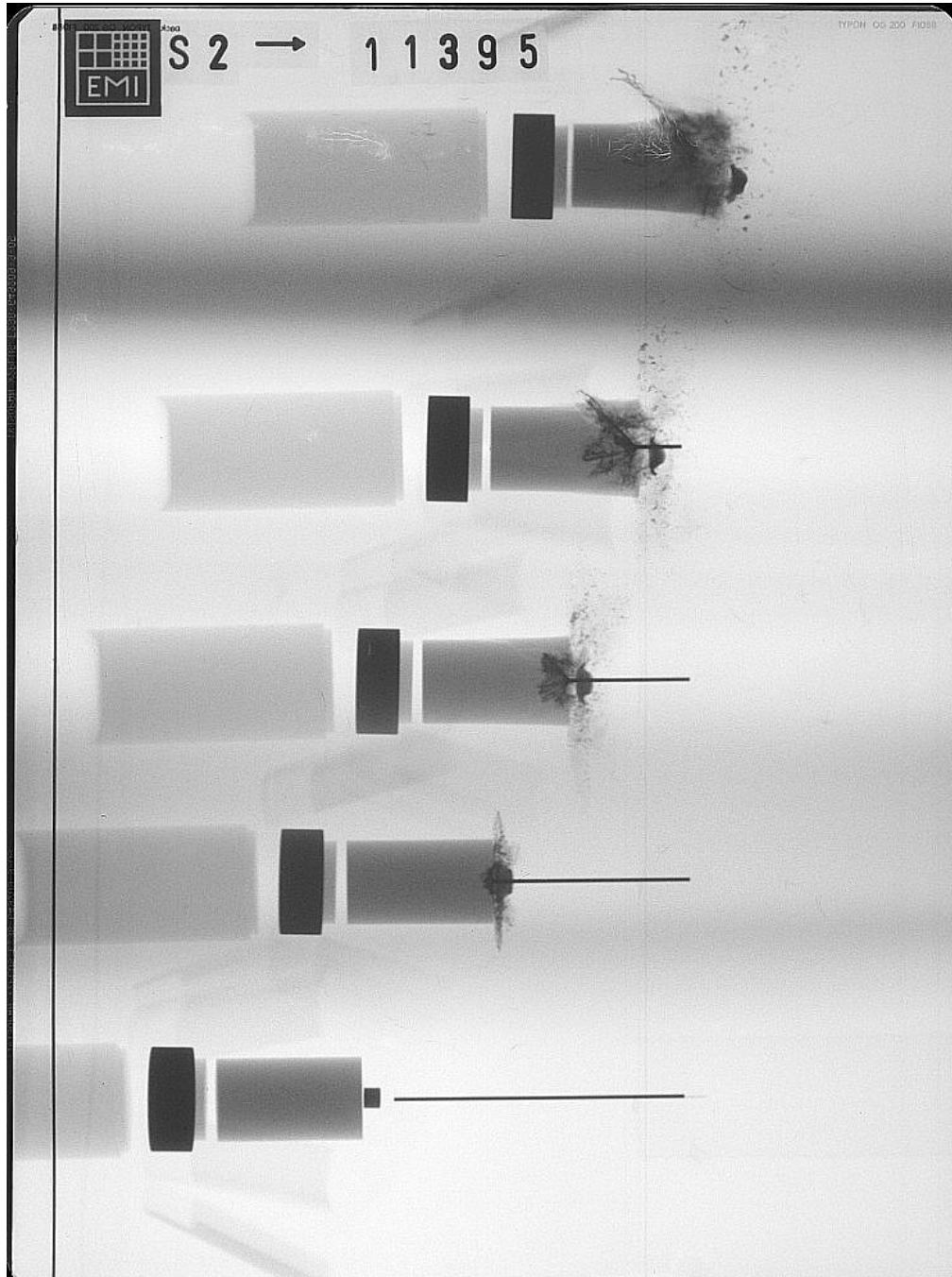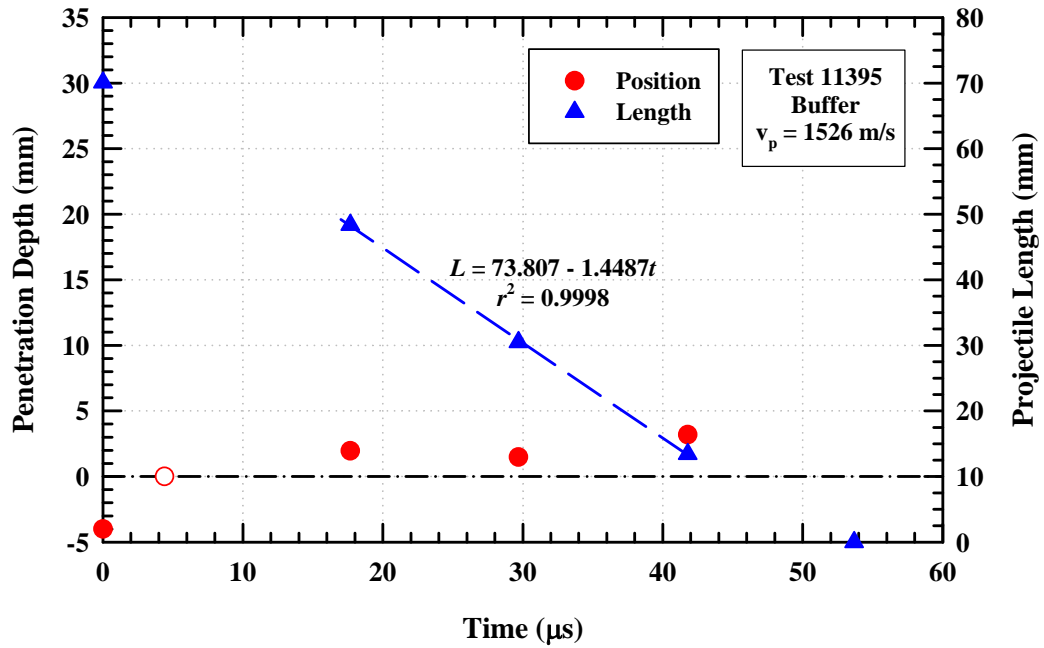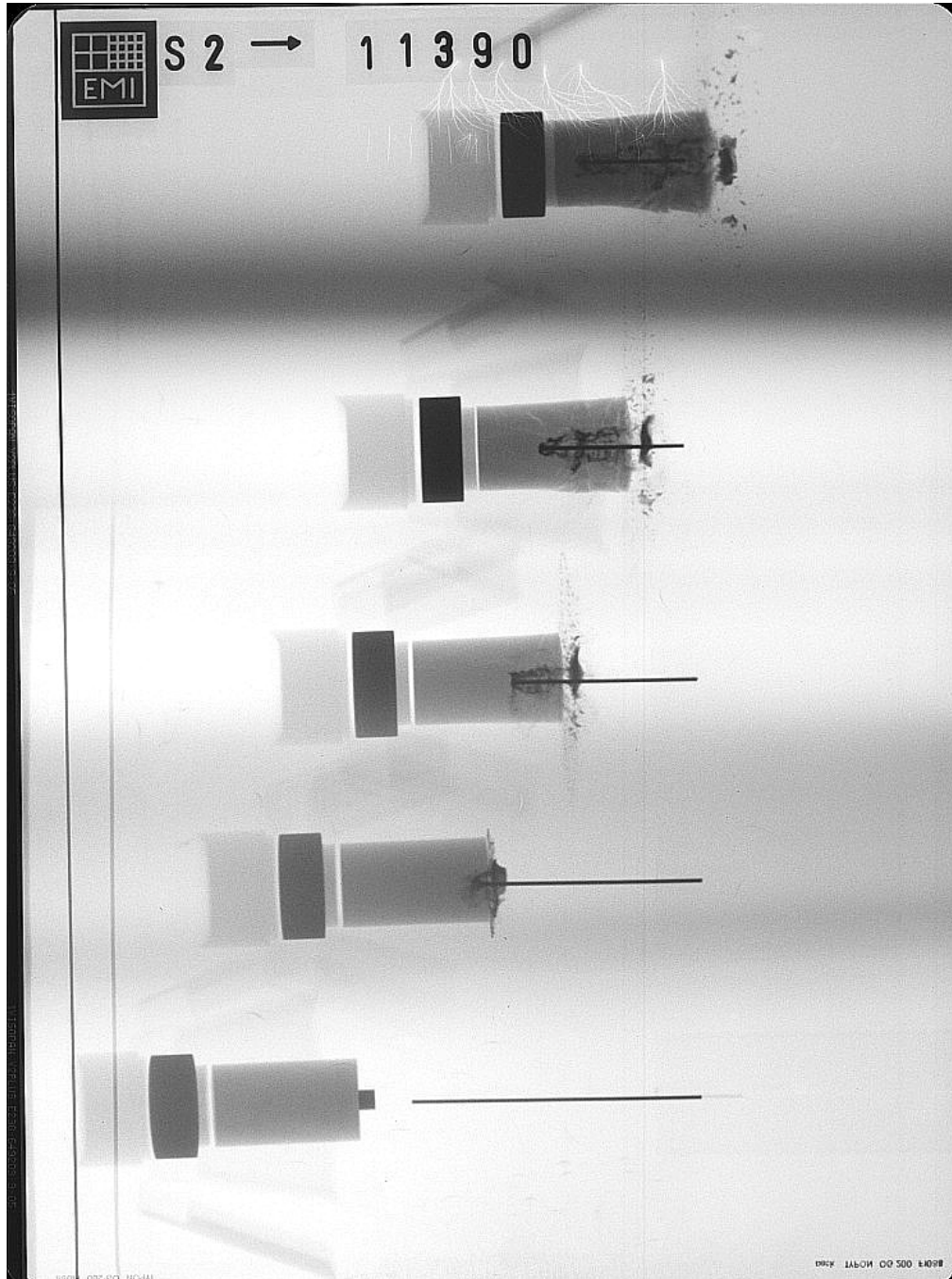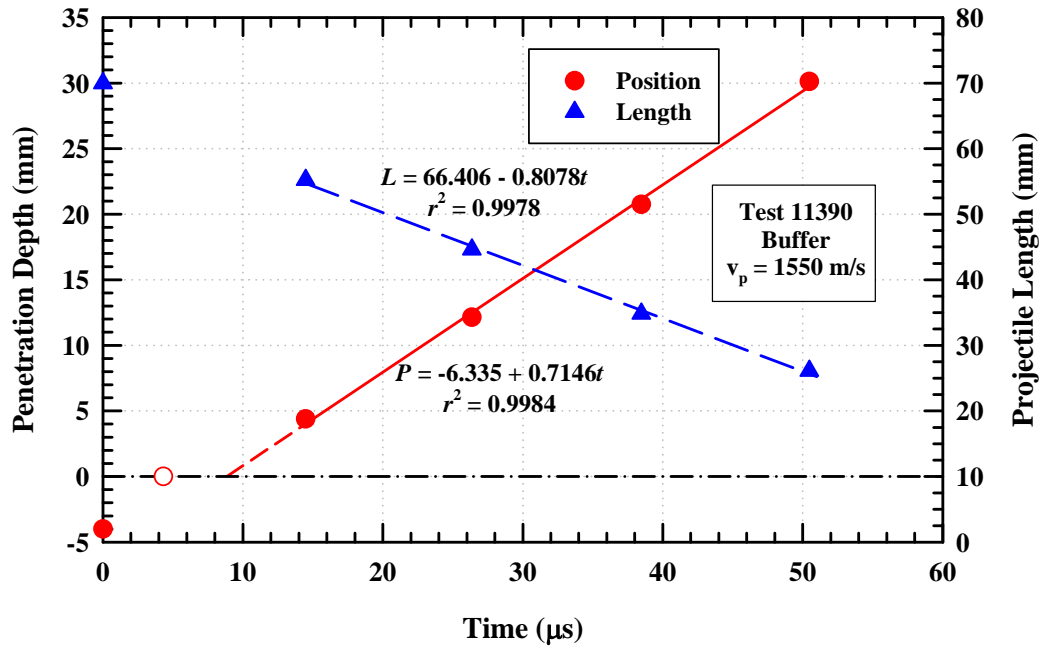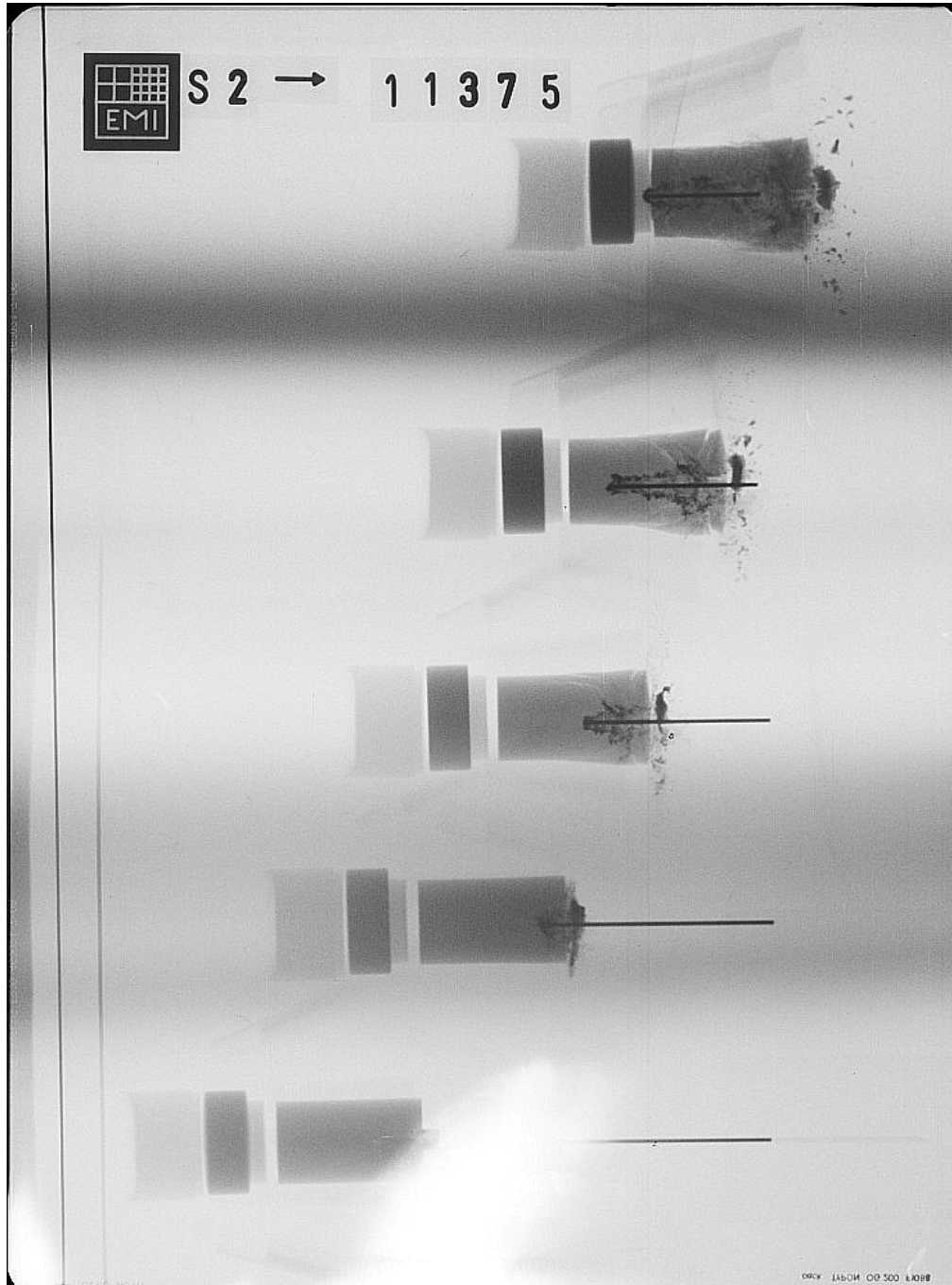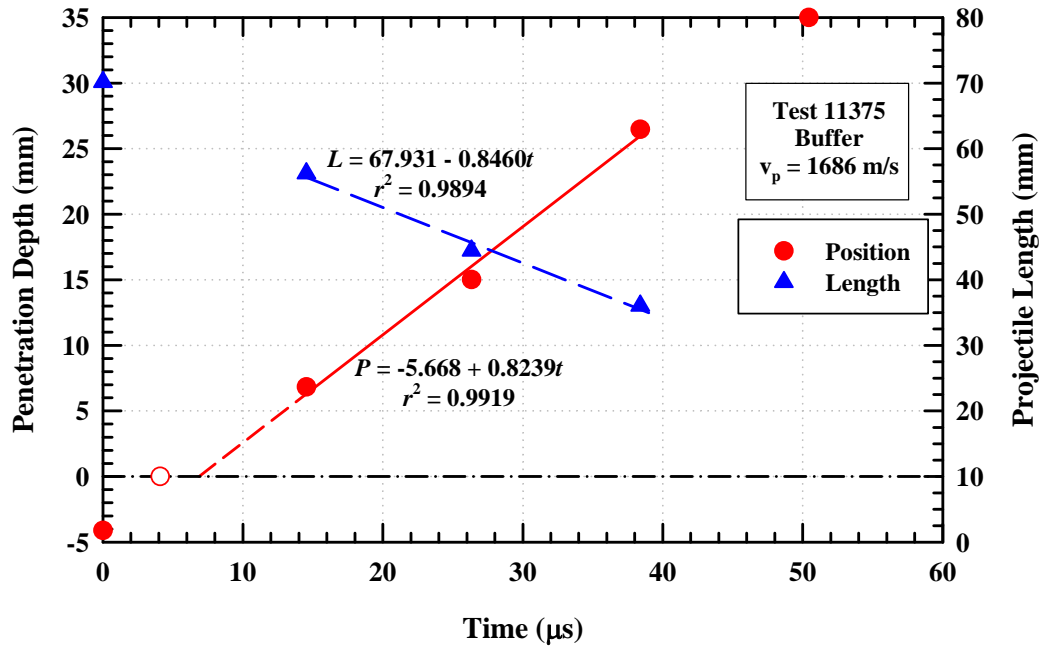**Figure A-7. X-ray picture for Exp. 11358: bare SiC, $v_p = 1381$ m/s.**

Figure A-8. Plot of test data for Exp. 11358.

Figure A-9. X-ray picture for Exp. 11377: buffered SiC, v_p = 1416 m/s.

Figure A-10. Plot of test data for Exp. 11377.

Figure A-11. X-ray picture for Exp. 11393: buffered SiC, v_p = 1484 m/s.

Figure A-12. Plot of test data for Exp. 11393.

Figure A-13. X-ray picture for Exp. 11395: buffered SiC, v_p = 1526 m/s.

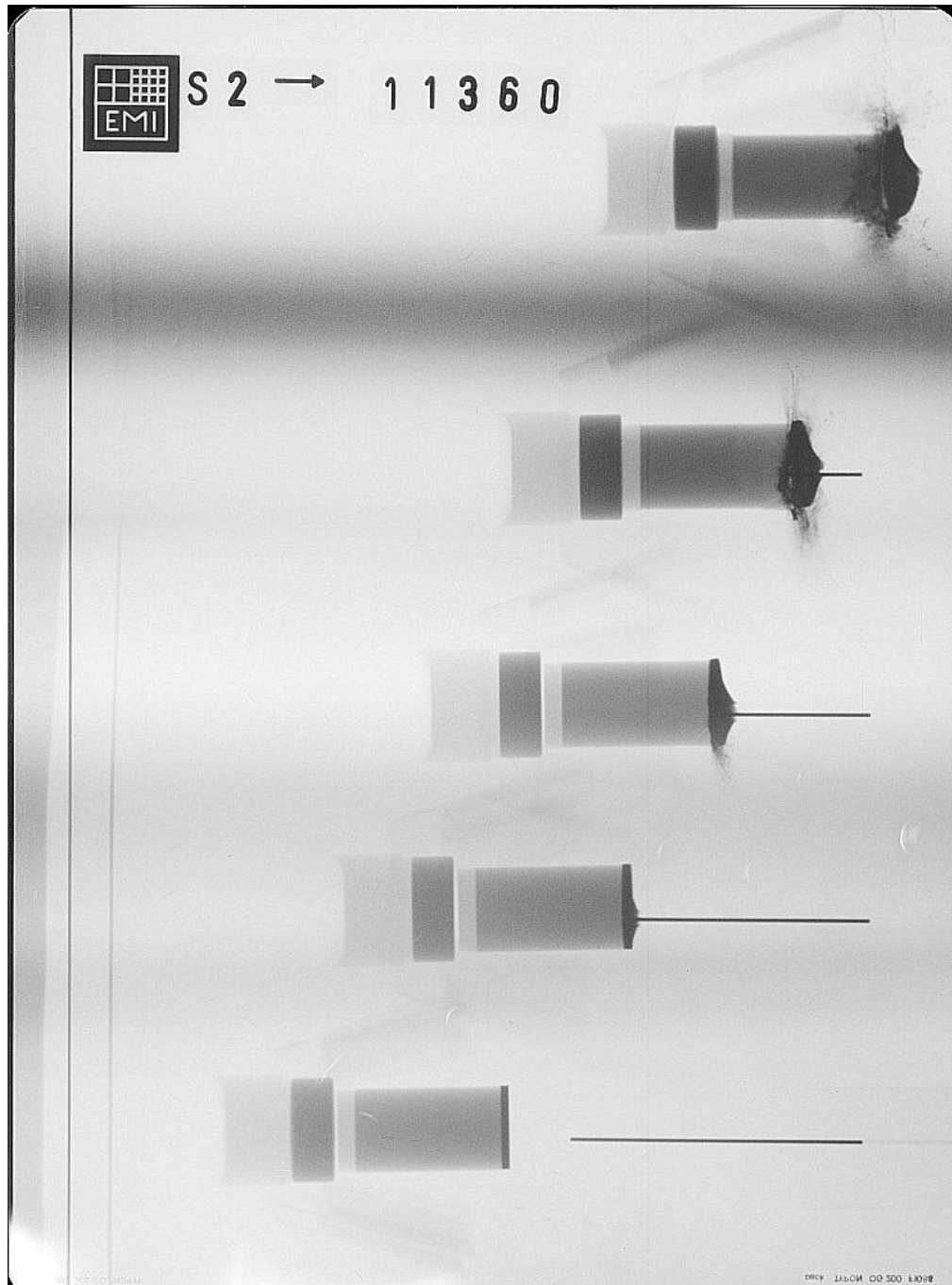**Figure A-14. Plot of test data for Exp. 11395.**

**Figure A-15. X-ray picture for Exp. 11390: buffered SiC, v_p = 1550 m/s.**

Figure A-16. Plot of test data for Exp. 11390.

The figure shows equations:

$$L = 66.406 - 0.8078t$$
$$r^2 = 0.9978$$

$$P = -6.335 + 0.7146t$$
$$r^2 = 0.9984$$

Test 11390
Buffer
$v_p = 1550$ m/s

Figure A-17. X-ray picture for Exp. 11375: buffered SiC, $v_p = 1686$ m/s.

Figure A-18. Plot of test data for Exp. 11375.

$L = 67.931 - 0.8460t$
$r^2 = 0.9894$

$P = -5.668 + 0.8239t$
$r^2 = 0.9919$

Test 11375
Buffer
$v_p = 1686$ m/s

Position
Length

Figure A-19. X-ray picture for Exp. 11360: cover-plate SiC, v_p = 1382 m/s.
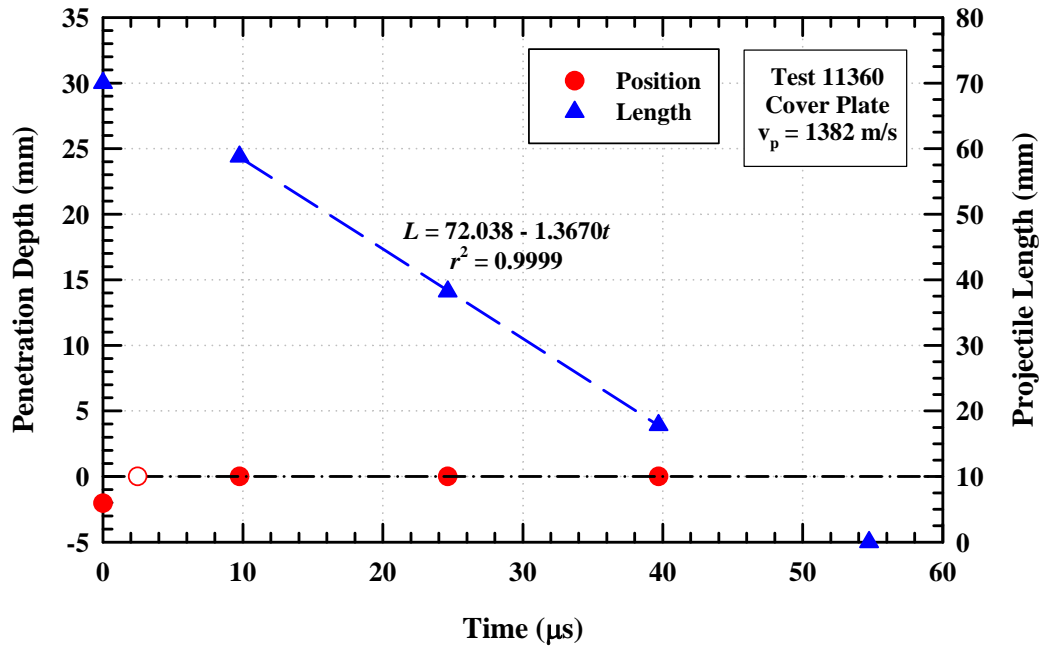
Figure A-20. Plot of test data for Exp. 11360.
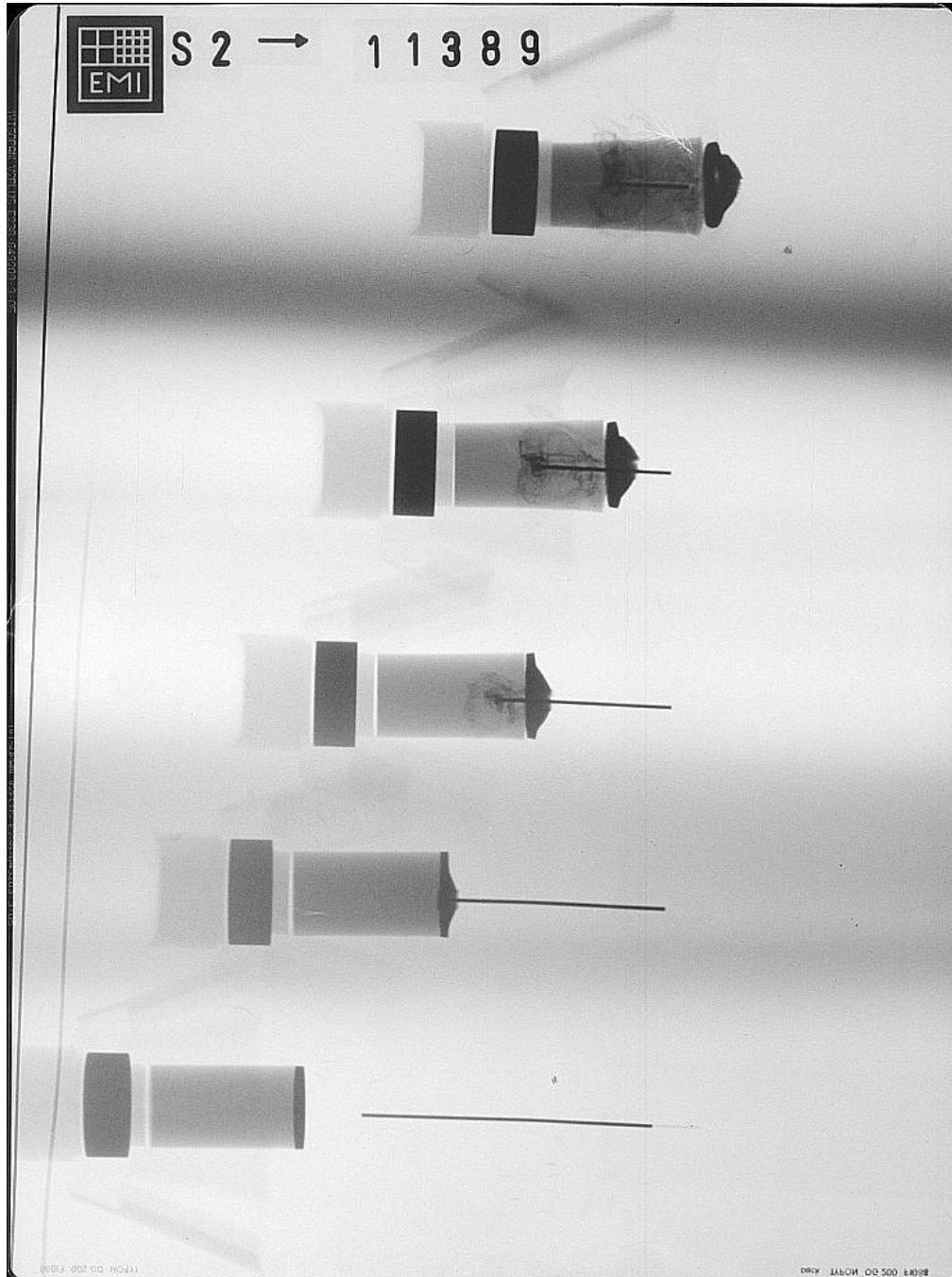
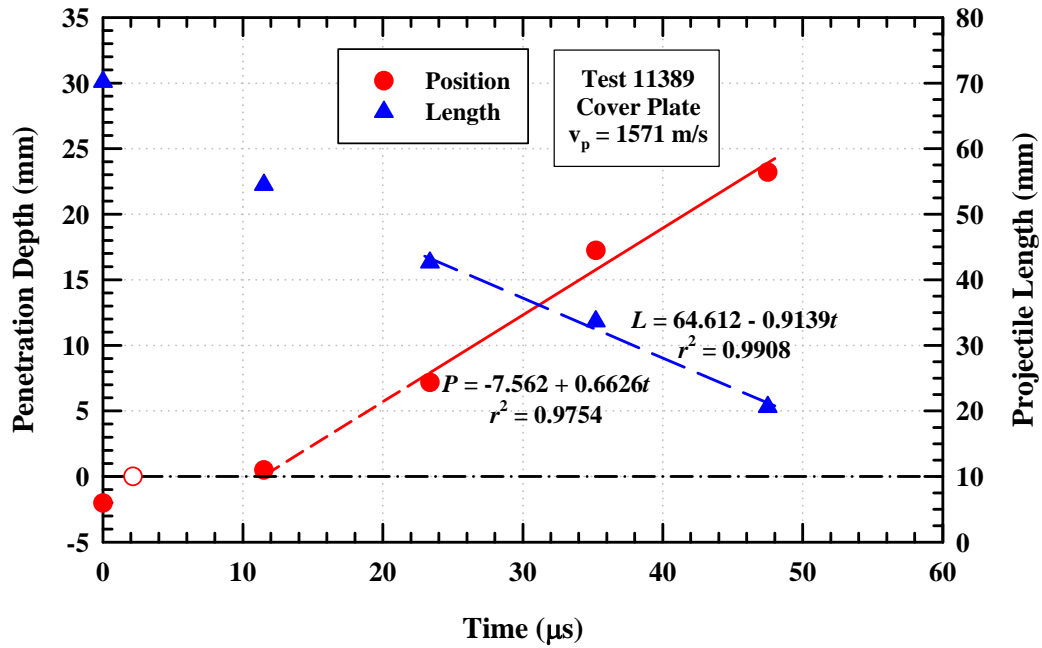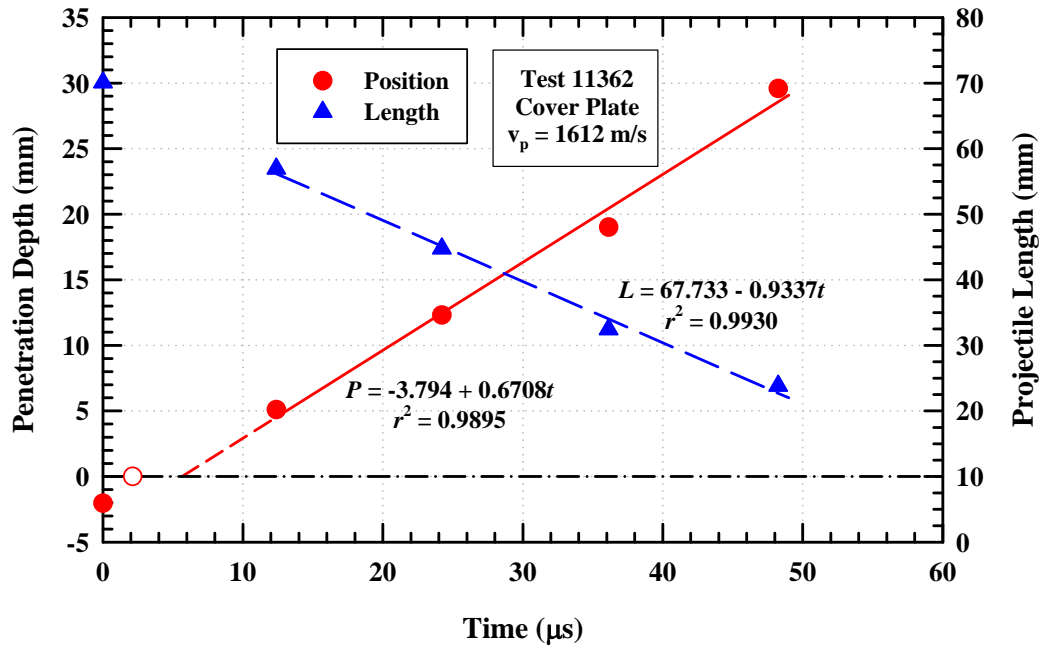**Figure A-21. X-ray picture for Exp. 11389: cover-plate SiC, v_p = 1571 m/s.**
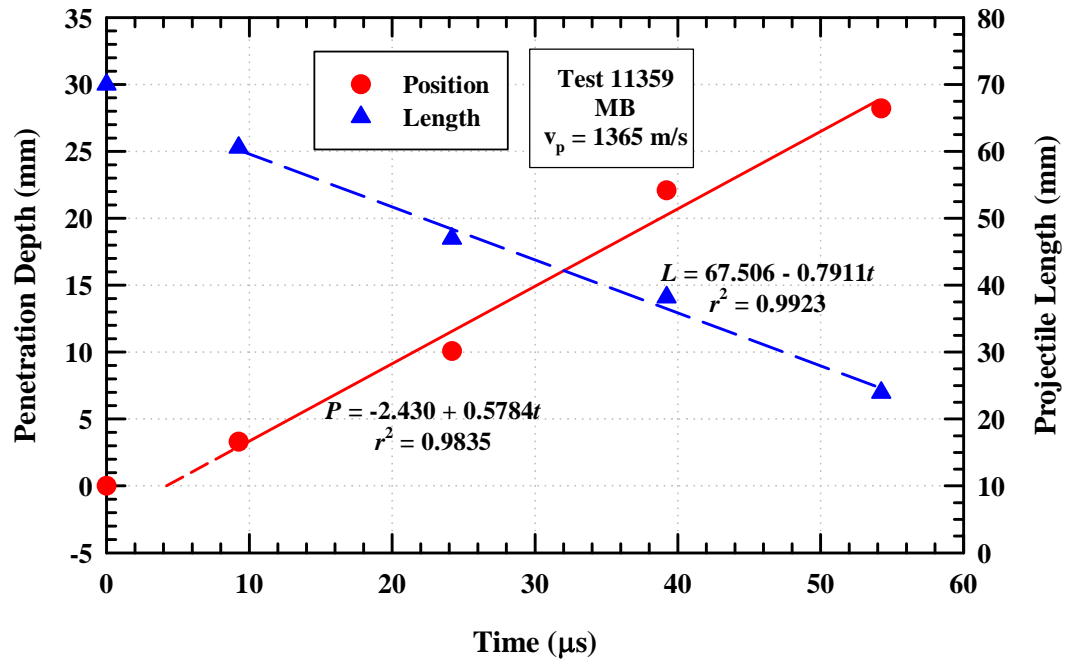
Figure A-22. Plot of test data for Exp. 11389.

The figure shows a plot with Time (μs) on the x-axis (0 to 60), Penetration Depth (mm) on the left y-axis (-5 to 35), and Projectile Length (mm) on the right y-axis (0 to 80). The legend indicates red circles for "Position" and blue triangles for "Length". Annotations within the plot read:

Test 11389
Cover Plate
$v_p = 1571$ m/s

$L = 64.612 - 0.9139t$
$r^2 = 0.9908$

$P = -7.562 + 0.6626t$
$r^2 = 0.9754$

Figure A-23. X-ray picture for Exp. 11362: cover-plate SiC, v_p = 1612 m/s.

Figure A-24. Plot of test data for Exp. 11362.

Figure A-25. X-ray picture for Exp. 11359: bare "missed-buffer" SiC, $v_p = 1356$ m/s.

Figure A-26. Plot of test data for Exp. 11359.

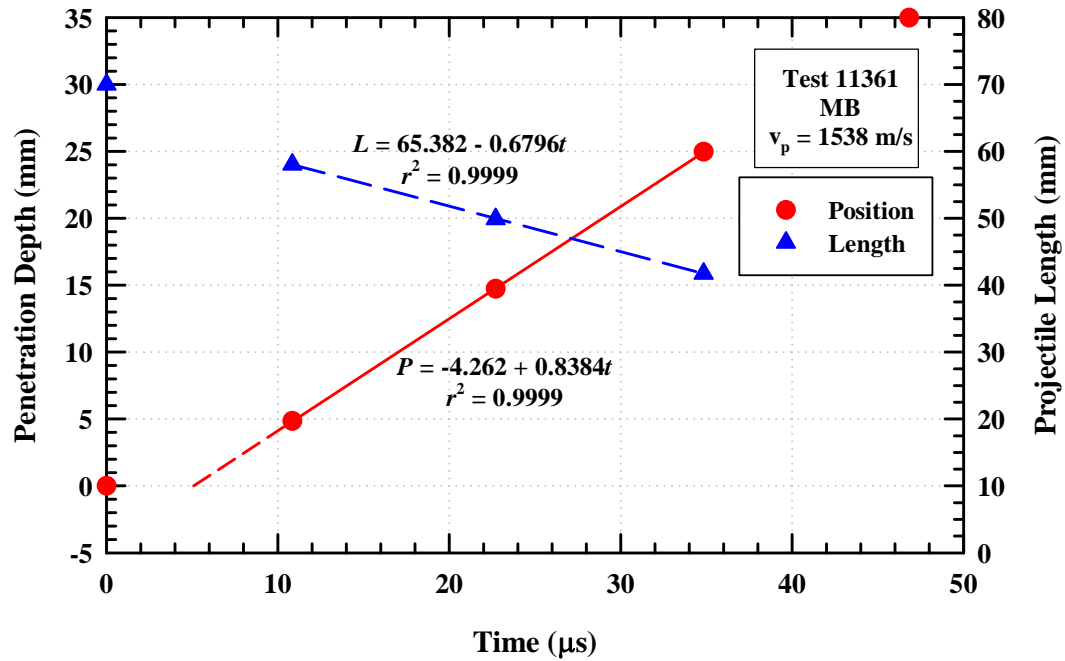**Figure A-27. X-ray picture for Exp. 11361: bare "missed-buffer" SiC, $v_p = 1538$ m/s.**
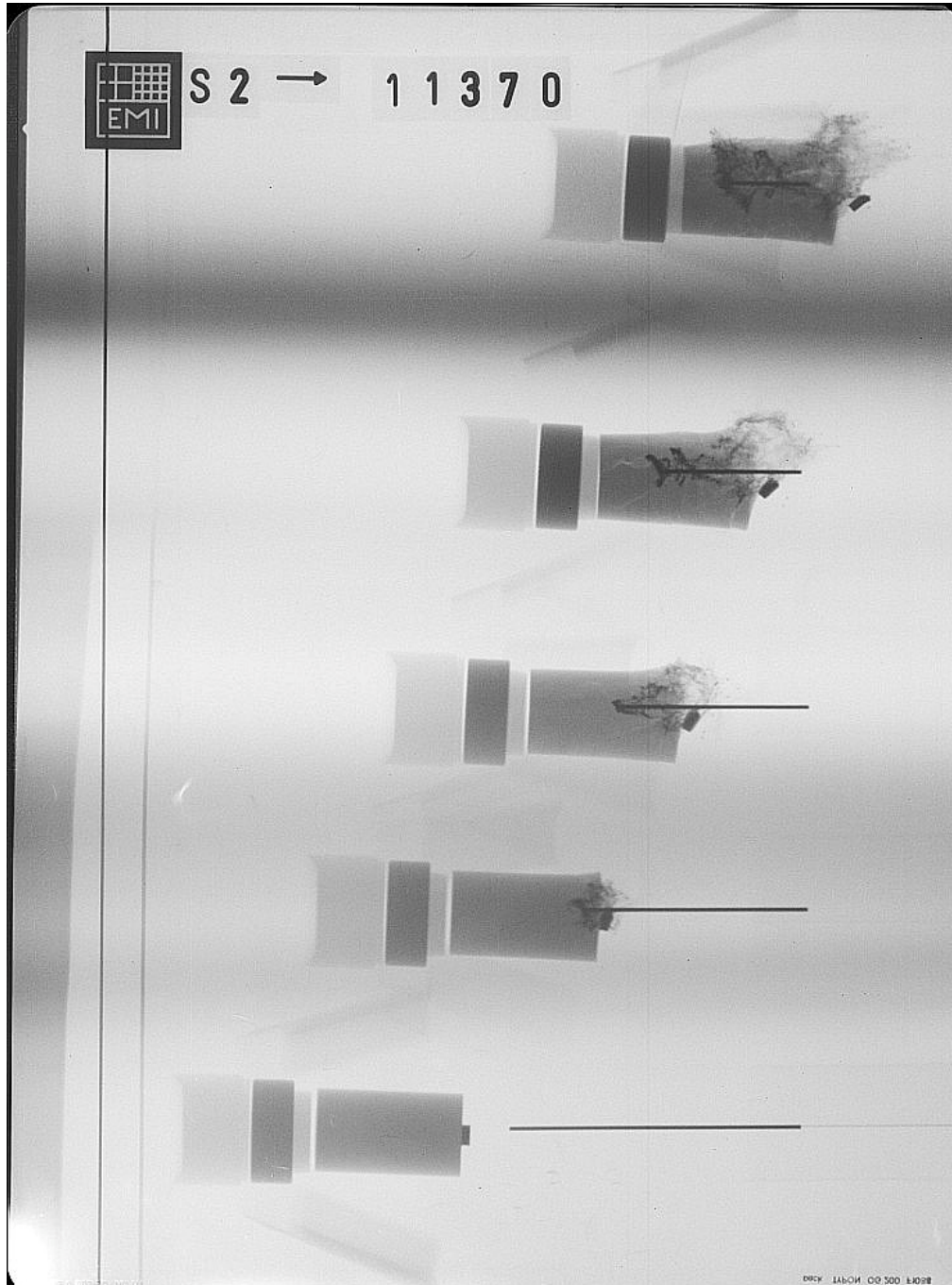
Figure A-28. Plot of test data for Exp. 11361.

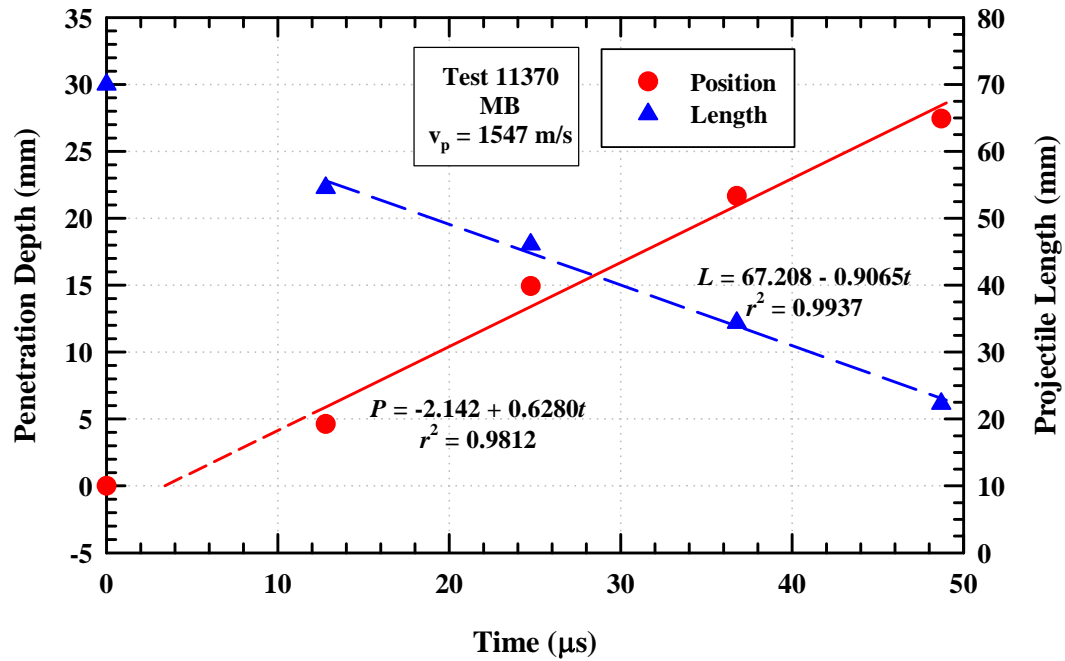**Figure A-29. X-ray picture for Exp. 11370: bare "missed-buffer" SiC, v_p = 1547 m/s.**

Figure A-30. Plot of test data for Exp. 11370.

Figure A-31. X-ray picture for Exp. 11369: bare "missed-buffer" SiC, $v_p = 1611$ m/s.
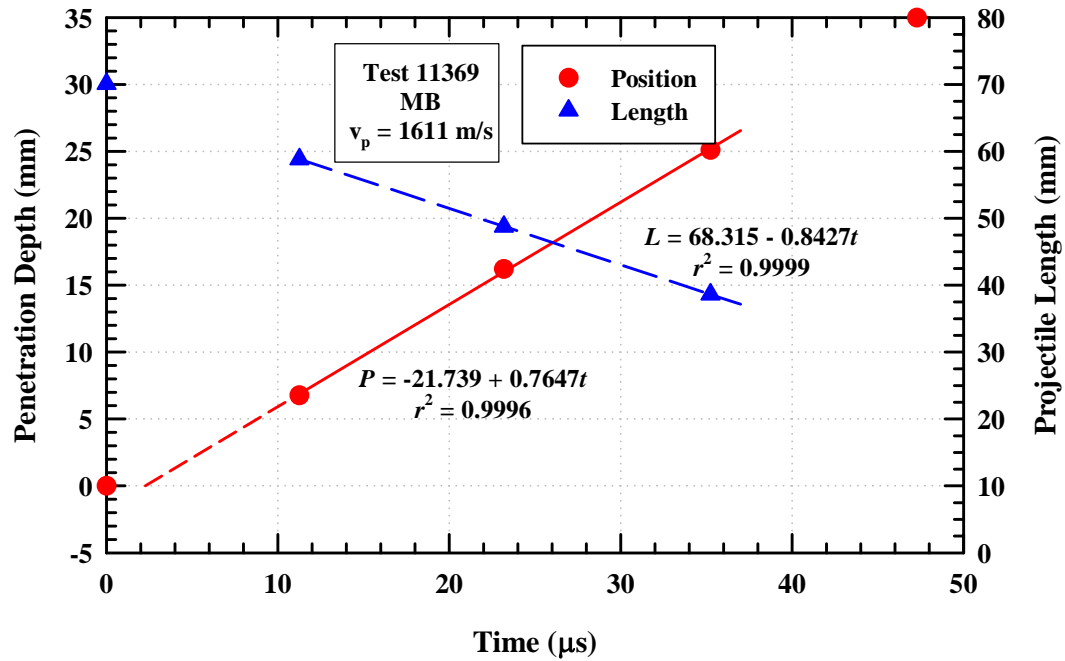
Figure A-32. Plot of test data for Exp. 11369.

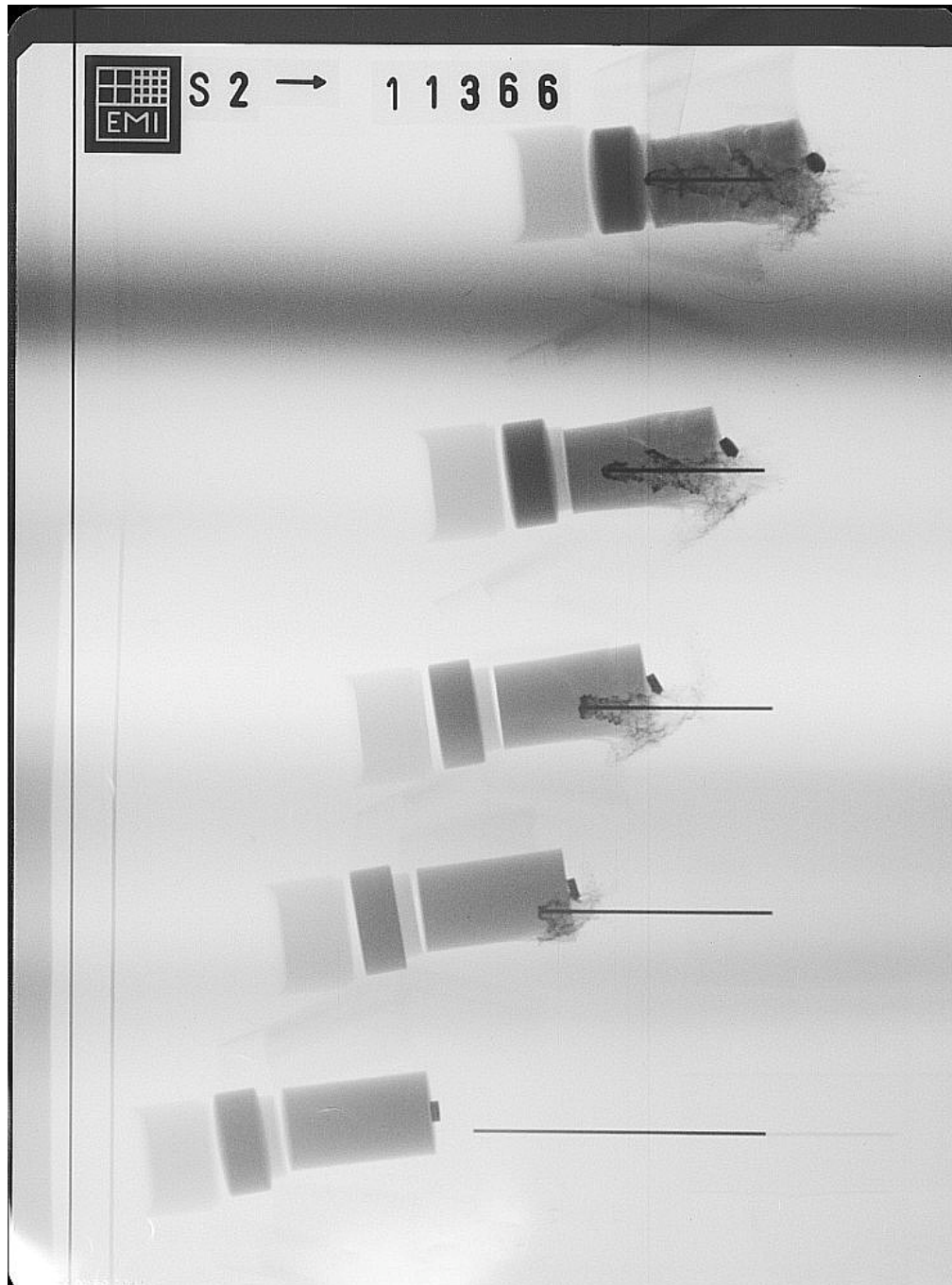**Figure A-33. X-ray picture for Exp. 11391: excessive yaw SiC, v_p = - m/s.**

Figure A-34. X-ray picture for Exp. 11366: excessive yaw SiC, v_p = 1546 m/s.

Figure A-35. X-ray picture for Exp. 11363: excessive yaw SiC, v_p = 1574 m/s.